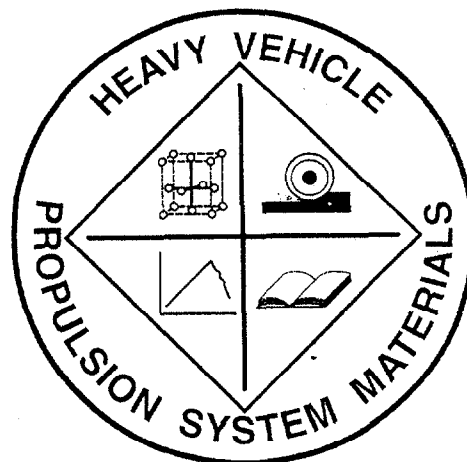


OAK RIDGE
NATIONAL LABORATORY

MANAGED BY UT-BATTELLE
FOR THE DEPARTMENT OF ENERGY

Heavy Vehicle Propulsion System
Materials Program
Semiannual Progress Report for
April 2000 Through September 2000

Prepared for
U.S. Department of Energy
Assistant Secretary for
Energy Efficiency and Renewable Energy
Office of Transportation Technologies



Metals and Ceramics Division

**HEAVY VEHICLE PROPULSION SYSTEM MATERIALS PROGRAM
SEMIANNUAL PROGRESS REPORT FOR
APRIL 2000 THROUGH SEPTEMBER 2000**

**D. R. Johnson
Program Manager**

Date Published: December 2000

NOTICE:

This document contains information of a preliminary nature. It is subject to revision or correction and therefore does not represent a final report.

**Prepared for
U.S. Department of Energy
Assistant Secretary for Energy Efficiency and Renewable Energy
Office of Transportation Technologies
EE 07 01 000**

**Prepared by the
OAK RIDGE NATIONAL LABORATORY
Oak Ridge, Tennessee 37831-6285
managed by
UT-Battelle, LLC
for the
U.S. DEPARTMENT OF ENERGY
under Contract DE-AC05-00OR22725**

REPORTS PREVIOUSLY ISSUED

ORNL/TM-9325	Period March 1983-September 1983
ORNL/TM-9466	Period October 1983-March 1984
ORNL/TM-9497	Period April 1984-September 1984
ORNL/TM-9673	Period October 1984-March 1985
ORNL/IM-9947	Period April 1985-September 1985
ORNL/TM-10079	Period October 1985-March 1986
ORNL/TM-10308	Period April 1986-September 1986
ORNL/TM-10469	Period October 1986-March 1987
ORNL/TM-10705	Period April 1987-September 1987
ORNL/TM-10838	Period October 1987-March 1988
ORNL/TM-11116	Period April 1988-September 1988
ORNL/TM-11239	Period October 1988-March 1989
ORNL/TM-11489	Period April 1989-September 1989
ORNL/TM-11586	Period October 1989-March 1990
ORNL/TM-11719	Period April 1990-September 1990
ORNL/TM-11859	Period October 1990-March 1991
ORNL/TM-11984	Period April 1991-September 1991
ORNL/TM-12133	Period October 1991-March 1992
ORNL/TM-12363	Period April 1992-September 1992
ORNL/TM-12428	Period October 1992-March 1993
ORNL/TM-12674	Period April 1993-September 1993
ORNL/TM-12778	Period October 1993-March 1994
ORNL/TM-12924	Period April 1994-September 1994
ORNL/TM-13046	Period October 1994-March 1995
ORNL/TM-13219	Period April 1995-September 1995
ORNL/TM-13262	Period October 1995-March 1996
ORNL/TM-13395	Period April 1996-September 1996
ORNL/TM-13467	Period October 1996-March 1997
ORNL/TM-13562	Period April 1997-September 1997
ORNL/TM-13648	Period October 1997-March 1998
ORNL/TM-13735	Period April 1998-September 1998
ORNL/TM-1999/95	Period October 1998-March 1999
ORNL/TM-2000/16	Period April 1999-September 1999
ORNL/TM-2000/233	Period October 1999-March 2000

Research sponsored by the U.S. Department of Energy, Assistant Secretary for Energy Efficiency and Renewable Energy, Office of Transportation Technologies, as part of the Heavy Vehicle Propulsion System Materials Program, under contract DE-AC05-00OR22725 with UT-Battelle, LLC.

CONTENTS

SUMMARY AND INTRODUCTION	1
COST EFFECTIVE HIGH PERFORMANCE MATERIALS AND PROCESSING.....	3
<i>Cost-Effective Smart Materials for Diesel Engine Applications (ORNL)</i>	<i>5</i>
<i>Low Cost High Toughness Ceramics (ORNL).....</i>	<i>20</i>
<i>Cost-Effective Sintering of Silicon Nitride Ceramics (SIU-C)</i>	<i>35</i>
ADVANCED MANUFACTURING TECHNOLOGY	53
<i>Durability of Diesel Engine Component Materials (ORNL).....</i>	<i>55</i>
<i>NDE of Ceramic Valves for Diesel Engines (Argonne National Laboratory)</i>	<i>59</i>
<i>Intermetallic -Bonded Cermets (ORNL)</i>	<i>66</i>
TESTING AND CHARACTERIZATION	69
<i>NDE Technology for Fuel Delivery and Insulating Materials (Argonne National Laboratory)</i>	<i>71</i>
<i>Testing and Evaluation of Advanced Ceramics at High Temperature (North Carolina A&T State University)</i>	<i>75</i>
<i>Life Prediction of Ceramic Diesel Engine Components (ORNL)</i>	<i>86</i>
<i>Field Emission Analytical Electron Microscopy for Characterization of Catalyst Microstructures (ORNL)</i>	<i>97</i>
MATERIALS AND TESTING STANDARDS	99
<i>IEA ANNEX II Management (ORNL).....</i>	<i>101</i>
<i>Ceramic Mechanical Property Test Method Development (NIST).....</i>	<i>105</i>

HEAVY VEHICLE PROPULSION SYSTEM MATERIALS PROGRAM
SEMIANNUAL PROGRESS REPORT
FOR APRIL 2000 THROUGH SEPTEMBER 2000

SUMMARY AND INTRODUCTION

The purpose of the Heavy Vehicle Propulsion System Materials Program is the development of materials: ceramics, intermetallics, metal alloys, and metal and ceramic coatings, to support the dieselization of class 1-3 trucks to realize a 35% fuel-economy improvement over current gasoline-fueled trucks and to support commercialization of fuel-flexible LE-55 low-emissions, high-efficiency diesel engines for class 7-8 trucks.

The Office of Transportation Technologies, Office of Heavy Vehicle Technologies (OTT OHVT) has an active program to develop the technology for advanced LE-55 diesel engines with 55% efficiency and low emissions levels of 2.0 g/bhp-h NOx and 0.05 g/bhp-h particulates. The goal is also for the LE-55 engine to run on natural gas with efficiency approaching that of diesel fuel. The LE-55 program is being completed in FY 1997 and, after approximately 10 years of effort, has largely met the program goals of 55% efficiency and low emissions. However, the commercialization of the LE-55 technology requires more durable materials than those that have been used to demonstrate the goals. Heavy Vehicle Propulsion System Materials will, in concert with the heavy duty diesel engine companies, develop the durable materials required to commercialize the LE-55 technologies.

OTT OHVT also recognizes a significant opportunity for reduction in petroleum consumption by dieselization of pickup trucks, vans, and sport utility vehicles. Application of the diesel engine to class 1, 2, and 3 trucks is expected to yield a 35% increase in fuel economy per vehicle. The foremost barrier to diesel use in this market is emission control. Once an engine is made certifiable, subsequent challenges will be in cost; noise, vibration, and harshness (NVH); and performance.

The design of advanced components for high-efficiency diesel engines has, in some cases, pushed the performance envelope for materials of construction past the point of reliable operation. Higher mechanical and tribological stresses and higher temperatures of advanced designs limit the engine designer; advanced materials allow the design of components that may operate reliably at higher stresses and temperatures, thus enabling more efficient engine designs. Advanced materials also offer the opportunity to improve the emissions, NVH, and performance of diesel engines for pickup trucks, vans, and sport utility vehicles.

The principal areas of research are:

Cost Effective High Performance Materials and Processing
Advanced Manufacturing Technology
Testing and Characterization
Materials and Testing Standards

**COST EFFECTIVE HIGH PERFORMANCE
MATERIALS AND PROCESSING**

W.B.S. ELEMENT 1.1.2.4

Cost-Effective Smart Materials for Diesel Engine Applications

J. O. Kiggans, Jr., T. N. Tiegs, F. C. Montgomery, and L. C. Maxey

Michael Matthews, and Alan Steffans

Oak Ridge National Laboratory

Oak Ridge, TN 37831

Objective / Scope

There are two objectives for this project. The first is to evaluate the cost-effectiveness and maturity of various "Smart Materials Technologies," which are under consideration for diesel engine applications, such as fuel injection systems. The second is to develop "Smart Materials," to be incorporated into working actuators and sensors.

Task 1– Fabrication of PZT laminates

This task is directed towards the determination of the optimal conditions for preparing multilayered PZT laminates. The study in this report compares Elvacite 2010 and polyvinyl butyral (PVB) B-98 binders, that are employed in our lab to fabricate PZT tapes. It is an extension of experiments started and discussed in a previous reports.

Experimental Procedure:

Tape cast materials were fabricated using a Mistler Co. TTC-1000 tape casting machine. The preparation of PVB and Elvacite tapes and laminates was discussed in a previous report. Duplicate samples were made for each experiment. After lamination, samples were either not heated (control = C) or heated to 125°, 175°, 225°, or 250 °C prior to the isostatic pressing (isopressed). The 125° and 175 °C heat treatments included a 72 h hold period in air at temperature. An additional set of samples was heated to 175 °C in vacuum and held in vacuum for 72 h. The 225° and 250 °C sample groups were heated at 5°C / min and held at temperature for 1 h. Samples were then: a) isopressed in latex bags on top of a alumina setter at 206 MPa (IPSD206MPa); b) isopressed also at 206 MPa, but without a setter disc (IP206MPa); c) isopressed at 344 MPa without a setter disc (IP344MPa); or d) uniaxially pressed at 69 MPa (DP69MPa). After the final pressing treatment, the samples were heated in a alumina crucible to 600°C to fully remove the binder. Samples were then sintered at 1125°C for 24 h using methods discussed in previous reports. The sintered densities were determined using the Archimedes immersion method. Samples were then ground to approximately 1 mm thickness, polished, and screen printed with silver electrodes. The electrodes were baked on the samples at 600 °C, and then the samples poled at 2.5 kV/mm for 10 min at 120 °C. The

d_{33} values of the samples were measured using a Model 8000 Pennebaker Piezo d_{33} tester (APC Ceramics, Inc.)

Results

Table 1 shows the densities as per cent of theoretical density (with 100 % T. D. = 7.6 g/cm³), and the electromechanical d_{33} values for the sintered laminates processed by the various treatments. The 94.3 % T. D. of the L-225C-DP69 MPa sample was the lowest density value obtained, and the 99.9 % T. D. of the L-225C-IP206MPa sample was the highest density value obtained. It appears that a partial binder burnout step followed by an isopress step is useful for achieving higher sintered densities. Table 1 also shows the d_{33} values of the various samples. All samples had similar d_{33} values, which may indicate that d_{33} values were not totally driven by the sintered densities of the samples.

Task 2 - Multilayer Electroded Laminates

The purpose of this study was to find satisfactory methods for the preparation of PZT laminates with internal electrodes from tape cast materials.

Experimental Procedure:

Methods for the preparation of PZT-4 tapes using PVB-98 binders have been discussed in previous reports. Following the casting of the tapes, a 7.6 X 7.6 cm section of the green PZT tape, still on the mylar on which it was tape cast, was placed on a the vacuum chuck of an Affiliated Manufacturers Inc. (AMI), model No. MSP-053 print apparatus. A small amount of 30% Ag and 70% Pd conducting ink with binders (Ferro Electronics Materials product EL44006) was spread across a 12.7 x 12.7 cm Syscon-Micro Screen (mesh count of 325, a wire diameter of 0.0028 cm, and a screen angle of the mesh to the frame of 45°). Four discs, with connected tab structure, were printed on each piece of the PZT tape. The printed discs were cut from the PZT tape using a 2.85 cm diameter hole punch. Discs were also punched from control PZT tapes lacking electrodes.

Laminates were made from a combination of electroded and non-electroded PZT tape discs. The disc stacking order for the laminate consisted of the following from the bottom to the top of the stack: 1 non-electroded disc, 1 electroded disc, 2 non-electroded discs, 1 electroded disc, 3 non-electroded discs, 1 electroded disc, and 1 non-electroded disc. The electroded discs were stacked with the tab portion of the print at 180 ° orientation for each successive layer. The discs were laminated in a steel die at 80 °C and 10 MPa pressure for 15 min. 6 laminated parts were made using this process.

Laminates were processed by several alternate heat treatment conditions to remove the binders prior to sintering. The first set of laminates was heated in an alumina crucible at 1 °C/ min to

300 °C, held at this temperature for 1 h; heated at 1 °C/ min to 600 °C, held at this temperature for 2 h; and cooled at approximately 10 °C/ min to room temperature. The second set was heated in an alumina crucible at 1 °C/ min to 175 °C and held at this temperature for 2 h; heated at 1 °C/ min to 225 °C and held at this temperature for 2h; heated at 1 °C/ min to 300 °C and held at this temperature for 1 h; heated at 1 °C/ min to 600 °C and held at this temperature for 2 h; and finally cooled at 10 °C/ min to room temperature. The third set of two laminates was heated in an alumina crucible at 1 °C/ min to 175 °C, held at this temperature for 2 h; heated at 1 °C/ min to 225 °C, held at this temperature for 2 h; and cooled at 10 °C/ min to room temperature. The third set of laminates were then isopressed at 206 MPa, and heated at 5 °C/ min to 200 °C, heated at 1 °C/ min to 300 °C, held at this temperature for 1 h; and heated at 1 °C/ min to 600 °C, held at this temperature for 2 h, and cooled at 10 °C/ min to room temperature.

Laminates from sets 2 and 3 were then cut in half. The samples were placed on edge and mounted in a Struers epoxy resin. The epoxy-mounted PZT laminates were ground flat and polished. A portion of each laminate was surface etched using the HCL-HF solution as described in previous reports. The polished and etched samples were examined with both light and scanning electron microscopes.

Results

Although the binder burn-out process used for laminate set 1 samples had been used successfully many times with non-electrode laminated samples, the laminates of set 1 cracked during the binder burn-out process. This suggests that either the binders in the silver-palladium ink caused the cracking, or that the silver-palladium metals catalyzed a more rapid binder volatilization, resulting in the cracks. As a possible solution, set 2 of the electroded laminates was heated by a modified schedule which included additional dwells at lower temperatures. The samples survived the furnace process with no apparent visible cracks. Figure 1 shows photos from the SEM examination of one of the set 2 laminates. Figure 1 a shows the fine grain (1 to 2 micron diameter) of the sample. Figure 1b is representative of the sintered structure, with good densification of the PZT and the metal electrode. However, Figures 1 c and d show some abnormal cracking and electrode delamination. In some cases, a crack propagated from the end of an electrode towards the exterior edge of the part (Fig 1 e). Thus, although the green laminates of set 2 appeared normal, the sintered parts were not satisfactory. To address this problem, an isopress step (as the above section) was inserted into the sample processing following the heat treatment to 225 °C. Fig 2 a shows the microstructure of the grains in this sample. Figure 2 b shows the predominate structure of the sintered parts with very good bonding of the sintered PZT and electrode material. Figure 2 c shows a small area of missing electrode, but this may be an artifact of the polishing method. The only apparent problem in this sample is the crack, which was generated from an electrode surface through the sample. Further samples are being made to address possible solutions to the crack formation in the laminates.

Task 3 – Compositional Alteration of PZT-4

An additional task of this project is the study of cost-effective alternative PZT compositions and processing methods which will allow low temperature (~1125 °C) sintering and grain growth of PZT materials. Various sintering additives and/or grain growth enhancer(s) or inhibitor(s) were selected for this study based on literature references.

Two basic commercial powders were used to make standard (non-doped) samples for this study: 1) APC 840 (American Piezo Ceramics Inc. and 2) TRS 200FG (TRS Ceramics, Inc). The APC 840 is a hard PZT-4 composition that we have used for several studies. The TRS 200FG is a new fine-grained soft PZT powder that was developed by TRS for higher sintered strength due to the fine grain size. Several compositions of APC 840 materials with ceramic dopants were fabricated for this study. Most of the dopants are based on bismuth compositions. Previous studies in our laboratories and others have shown that bismuth oxide additions to APC 840 materials can lower the sintering temperature and in most cases will increase the piezoelectric d_{33} coefficient of the materials. Zirconium tungstate is a special material that has a negative expansion coefficient. It is thought that this material may increase sintered strength of PZT-4 materials.

Methods for sample preparation are described: Binders (usually a combination of PVP K-15 and Carbowax 8000) and the 2 wt. % ceramic additive were added to the base powder, and the mixtures milled in ethyl alcohol for about 24 h. The powders were then dried and ground or ball milled. The fraction of milled powder that passed through a 100 mesh (Tyler) screen was used for sample preparation. Approximately 5 gram portions of each powder were pressed in a 2.85 cm diameter die at pressures from 69 to 83 MPa (pressure depending on the powder type). In addition, some TRS powder was tape cast and a laminated sample made using techniques that have been discussed in previous reports. Pressed and tape cast discs were processed by binder burn-out and sintering using conditions discussed in previous reports. Final sintering temperatures were 893°, 960°, 1025°, and 1125°C. Sintering at 893° and 960°C was conducted without the addition of packing powder, 10 wt % ZrO_2 – 90 wt. %, $PbZrO_3$, since little PbO loss is expected at these temperatures. Following sintering, all samples were weighed, the densities measured, and the electromechanical properties measured.

Table 2 shows that the both weight changes that were observed for various samples. Note that the chemical composition of each ceramic additive is shown as a molar % (total equals to 100). These measurements do not include losses due to binder burn-out. Weight losses represent losses of PbO or other volatile materials present in dopant materials, and weight gains typically represent the incorporation of PbO by equilibration of the packing powder with

a given sample. These calculations are useful in helping understand composition or phase changes that can occur in the materials.

Table 3 and 4 list the sintered densities and d_{33} coefficients for the various sample types fabricated for this study. Several temperatures were chosen to gauge the sintering behavior. It is important to note that materials sintered below 960°C may be able to utilize silver as an electrode material in multilayer devices. However, the higher two temperatures will require electrodes made of silver - palladium mixtures. The first TRS sample in Table 2, a die pressed disc, reached full density at 1125°C. The second TRS sample, a tape cast laminate, reached only 97.6 % theoretical density (T.D.), probably due to a slightly lower green density of the tape cast sample. As noted before, the sintering of piezoelectric materials is very sensitive to small changes in the green density of the starting parts. The d_{33} value for the die pressed TRS part was 0.43, which is considered very good for “soft” PZT materials. The d_{33} value for the tape cast TRS was 0.34, an average value which may reflect the lower sintered density. The second control, the die pressed APC part with no dopant, had a sintered density of 98.0 % T.D, and a d_{33} value of 0.27. These numbers are lower than commercial APC materials, however the commercial materials are normally sintered at 1275°C and only then show d_{33} values of 0.33. Bi_2O_3 was the first bismuth-based additive tested in this experimental series. Note that the Bi_2O_3 addition allows the material to be sintered to full density at 893° C. The d_{33} value of 0.35 is very good and increases only slightly to 0.38 for the materials sintered at 1125°C. The other most promising materials, based on high densities and high d_{33} values, were the APC 840 materials with the 100 $\text{Bi}_2\text{Cu}_{0.1}\text{V}_{0.9}\text{O}_{5.35}$ and the 65 Bi_2O_3 -6 CuO -29 V_2O_5 additions. These materials sintered well at low temperature and also had high d_{33} values. The 100 ZrW_2O_8 sample reached full sintered density at 1125° C and had a good d_{33} value of 0.35. Further work is underway to measure additional electromechanical properties, examine the microstructures, and measure the strengths of these bismuth-based compositions.

Task 4– Fabrication of PZT parts for strength studies and microwave annealing experiments.

A major problem with using PZT materials in actuators is their low strength. A new study has begun to study the effect of microwave anneal heat treatments on the strength of sintered PZT materials. In order to measure the failure stress, samples must be machined to tolerances, such that the thickness variations do not skew the measured failure loads. The main problem in the machining step is to minimize the lead waste generated during this step. Standard Bridgeport Harig Grinders are not acceptable since 1) they generate water borne aerosols that can be released into the working environment, and 2) use a large amount of coolant. A possible solution to minimize machining is to use disc samples, ground and polished with a Stuers RotoForce

Polisher. The disc samples can be tested using biaxial strength measurements, thus eliminating the need to machine bend bars. The first step of the study was to fabricate samples.

Experimental procedure

Three sets of die pressed discs were prepared for this study. Each sample was prepared by pressing 5.5 g of PZT-4 powder (APC Ceramics inc.) at 82 MPa in a 2.87 cm diameter steel die. All samples were heated at 1 °C/min to 300 °C, held at 300 °C for 1 h; heated at 1 °C/min to 600 °C, held at 600 °C for 2 h; and cooled at 10 °C/min. Samples were then loaded in standard sintering crucibles (methods previously described), heated at 10 °C/min to 800 °C; heated at 1.6 °C/min to sintering temperatures of 1125°C (group 1), 1175°C (group 2), or 1325°C (group 3); and cooled at 10 °C/min. Groups 1 and 2 were held at the sintering temperature for 24 h, but group 3 was held for 3 h. All samples were cooled at 5 °C/min to room temperature. Also, two types of control samples (discs), 2.5 cm diameter by 0.10 cm thick, were purchased from APC Ceramics Inc.: 1) sintered, not poled and 2) sintered, electroded, poled PZT-4 discs. Sintered densities were measured as previously described.

Several methods were tested as grinding approaches to obtain suitable ORNL samples for equibiaxial flexural strength measurement. The most successful method employed the following steps. A steel grinding disc, 14 cm diameter by 1.25 cm thick with a flatness to +/- 0.002 cm was fabricated to be used as a sample holder. Glass microscope slides, 1.2 mm thick by 25 mm wide by 37 mm long were glued at 0°, 90°, 270°, and 360° orientations on the edge of the grinding plate using Aremco "Wafer-Mount 562." The thickness of each ORNL sample was measured at 4 points along the outer diameter of each disc, with positions referred to as 0°, 90°, 270°, and 360°. The discs were then glued to the grinding plate in the pattern shown in Figure 3. Samples were weighted to insure minimal glue under the samples. Samples were then ground in successive, 30 sec grinding steps at 60 N and 150 rpm with a water rinse using 320, 500, 1200, 2400, and 4000 mesh SiC abrasive discs. The grinding plate was reheated to remove the samples, and the samples and new glass strips (1 mm thick by 25 mm wide by 37 mm long) remounted with the second opposite surface oriented outward. This second surface was then ground using the grinding sequence described above. Samples were removed and dimensioned in the same manner as prior to grinding. Commercial APC Ceramics samples were not ground in this study.

Monotonic equibiaxial flexural strength testing of the above discs and control APC discs was conducted according to the "not yet released" ASTM method¹ that will replace ASTM F394-78. Figure 4 is a schematic showing the test fixture. Key features of the test fixture include concentric load and support rings fabricated from Delrin plastic; teflon tape above the sample to "minimize the effects of friction" during loading; a rubber layer equal to 1/2 to 1 sample thickness between the sample and the lower support ring "to minimize the effects of load and

support misalignment.” The test requires that “the load rings and test specimen be aligned concentrically to 0.5 % of the support ring diameter.” An Instron 4465 testing machine was used for the strength tests.

Results

Figure 5 shows a plot of the sintered densities of the PZT-4 discs versus the position in the sintering crucible. Samples in groups 2 and 3, sintered at 1175 and 1325 °C were near 100 % T.D. Group 3 samples showed a slight trend of density variation versus position in the crucible. This may be due to lead atmosphere varying somewhat in the crucible. Group 1 samples sintered at 1125 °C had lower densities, as expected and larger variations in densities.

Table 5 shows grinding results for the three groups of ORNL thinned samples. The results show that prior to sintering there was a thickness variation from a low of 0.09 mm to a high of 0.25 mm between the 4 spots on a given sample. After sintering the highest thickness variation on a given sample varied from a high of 0.05 mm to a low of 0.01 mm. Utilizing an F-test to compare the variances of each set before and after grinding demonstrates that the variations in sintered thickness is larger at the 95 % confidence level for the unground samples than the ground samples except for samples 1175-4, 1325-3, and 1325-4.

Table 6 shows results for strength tests on both samples purchased from APC Ceramics and those of the same composition sintered at ORNL. The average strength of the as received unpoled APC samples was 89.1 MPa compared to 111 MPa for the APC poled and electroded sample. It appears the silver electrode and possibly the poling adds strength to the APC samples, but also causes the standard deviation to rise, and the t-test shows that these are the same values statistically. The strengths of the ORNL samples compared favorably to the APC samples. Strengths ranged from 83.5 MPa for the materials sintered at 1125°, to 86.2 MPa for the materials sintered at 1325° C, and to 94.0 MPa for the materials sintered at 1175° C. The comparable strengths of materials sintered at lower temperatures, especially 1125° C, lends confidence to the belief that existing PZT compositions can be sintered using by modified sintering schedules that are compatible with the requirements for using Ag/Pd electrodes.

Reference

- Jon Salem, Jay Wallace, Lynn Powers, and Andy Wereszczak, “Monotonic Equibiaxial Flexural Testing of Advanced Ceramics at Ambient Temperature,” Subcommittee C28.01 on Properties and performance, Rev 4.0, 2000.

Travel

None

Publications

None

Table 1. Densities and d_{33} values for PZT-4 sintered materials.

Sample	PVB Binder		Elvacite Binder	
	Sintered Density (g/cm^3)	d_{33} value (10^{-12} m/V)	Sintered Density (g/cm^3)	d_{33} value (10^{-12} m/V)
L	95.0	0.20	93.2	0.19
L-IPSD206MPa	97.1	0.18	97.8	0.19
L-125C- IP206MPa	99.0	0.18	97.7	0.20
L-175C- IPSD206MPa	99.0	0.19	96.2	ND
L-175CVac- IP206MPa	97.7	0.18	99.2	0.20
L-225C- IP206MPa	99.9	0.21	99.1	0.19
L-225C- IP344MPa	99.4	0.21	98.3	0.19
L-225C- DP69MPa	94.3	0.19	94.0	ND
L-250C- IP206MPa	99.4	0.20	98.0	0.19

L = laminated

IP = isopressed

SD = setter disc used during isopress step

Vac = vacuum

DP = uniaxial die press

Table 2. Weight changes for PZT compositions sintered at various temperatures

Base Powder	Additive - 2 Wt%	weight loss during sintering 24 hr at temp			
		893 °C no atm. Powder	960 °C no atm. Powder	1025 °C	1125 °C
TRS200FG*	none	-0.66%	-0.64%	0.01%	-0.05%
TRS200FG**	none				0.38%
APC840	none				-0.82%
APC840	100 ZrW ₂ O ₈			1.14%	1.49%
APC840	100 Bi ₄ Ti ₃ O ₁₂				-0.77%
APC840	100 Bi ₂ O ₃	-1.91%			-2.18%
APC840	58Bi ₂ O ₃ -42SrO	-1.86%	-2.37%		-2.35%
APC840	31Bi ₂ O ₃ -44SrO-25CuO	-1.82%	-1.94%		-2.15%
APC840	72Bi ₂ O ₃ -21CaO-7CuO	-1.73%	-2.15%		-2.26%
APC840	100 Bi ₂ Cu _{0.1} V _{0.9} O _{5.35}	-0.67%	-1.64%	0.12%	0.13%
APC840	65Bi ₂ O ₃ -6CuO-29V ₂ O ₅	-1.47%	-2.34%		0.86%

*die pressed powder

**tape cast powder

Table 3. Density values for PZT compositions sintered at various temperatures

Base Powder	Additive - 2 Wt%	Density after sintering 24 hr at temp			
		893 °C no atm. powder	960 °C no atm. powder	1025 °C	1125 °C
TRS200FG*	none	64.8%	78.6%	91.7%	100.8%
TRS200FG**	none				97.6%
APC840	none				98.0%
APC840	100 ZrW ₂ O ₈			88.6%	101.4%
APC840	100 Bi ₄ Ti ₃ O ₁₂				99.3%
APC840	100 Bi ₂ O ₃	100.5%			100.9%
APC840	58Bi ₂ O ₃ -42SrO	97.5%	100.1%		98.5%
APC840	31Bi ₂ O ₃ -44SrO-25CuO	99.0%	100.2%		98.5%
APC840	72Bi ₂ O ₃ -21CaO-7CuO	96.7%	95.9%		99.1%
APC840	100 Bi ₂ Cu _{0.1} V _{0.9} O _{5.35}	96.8%	99.6%	99.3%	98.4%
APC840	65Bi ₂ O ₃ -6CuO-29V ₂ O ₅	100.3%	101.0%		99.1%

*die pressed powder

**tape cast powder

Table 4. d_{33} values for PZT compositions sintered at various temperatures

Base Powder	Additive - 2 Wt%	d_{33} *** after sintering 24 hr at temp			
		893 °C no atm. powder	960 °C no atm. powder	1025 °C	1125 °C
TRS200FG*	none	n.m	0.19	0.26	0.43
TRS200FG**	none				0.34
APC840	none				0.27
APC840	100 ZrW ₂ O ₈			0.05	0.35
APC840	100 Bi ₄ Ti ₃ O ₁₂				0.32
APC840	100 Bi ₂ O ₃	0.35			0.38
APC840	58Bi ₂ O ₃ -42SrO	0.16	0.33		0.36
APC840	31Bi ₂ O ₃ -44SrO- 25CuO	0.32	0.12		0.25
APC840	72Bi ₂ O ₃ -21CaO- 7CuO	0.24	0.24		0.35
APC840	100 Bi ₂ Cu _{0.1} V _{0.9} O _{5.35}	0.28	0.40	0.32	0.36
APC840	65Bi ₂ O ₃ -6CuO- 29V ₂ O ₅	0.32	0.41		0.22

n.m.= not measured

*die pressed powder

**tape cast powder

***X 10⁻¹² m/V

Table 5. Thickness of samples ground using Struers fixture with glass leveling plates

Sample	Initial Thickness (mm)				Final Thickness (mm)			
	0°	90°	180°	270°	0°	90°	120°	270°
1125-1	1.48	1.45	1.58	1.64	1.22	1.17	1.19	1.20
1125-2	1.48	1.64	1.54	1.39	1.20	1.20	1.19	1.19
1125-3	1.41	1.50	1.59	1.46	1.14	1.15	1.18	1.19
1125-4	1.61	1.68	1.50	1.47	1.26	1.27	1.25	1.25
1175-1	1.46	1.50	1.55	1.47	1.22	1.20	1.21	1.20
1175-2	1.37	1.55	1.50	1.32	1.25	1.26	1.26	1.25
1175-3	1.55	1.60	1.48	1.46	1.20	1.23	1.24	1.24
1175-4	1.40	1.47	1.54	1.55	1.25	1.21	1.20	1.20
1325-1	1.33	1.40	1.54	1.42	1.24	1.23	1.25	1.25
1325-2	1.48	1.55	1.48	1.39	1.28	1.27	1.28	1.28
1325-3	1.37	1.44	1.49	1.43	1.24	1.20	1.22	1.27
1325-4	1.47	1.52	1.56	1.61	*	1.23	1.20	1.22

*chipped edge – no measurement

Table 6. Strengths of as received and ORNL fabricated PZT-4 materials

Sample Type	Strength (MPa)	Standard Deviation (MPa)
As Received APC Unpoled	89.1	3.3
As Received APC Poled and Electroded	111.0	25.3
ORNL 1125° C – 24 h	83.5	4.2
ORNL 1175° C – 24 h	94.0	6.4
ORNL 1325° C – 3 h	86.2	0.7

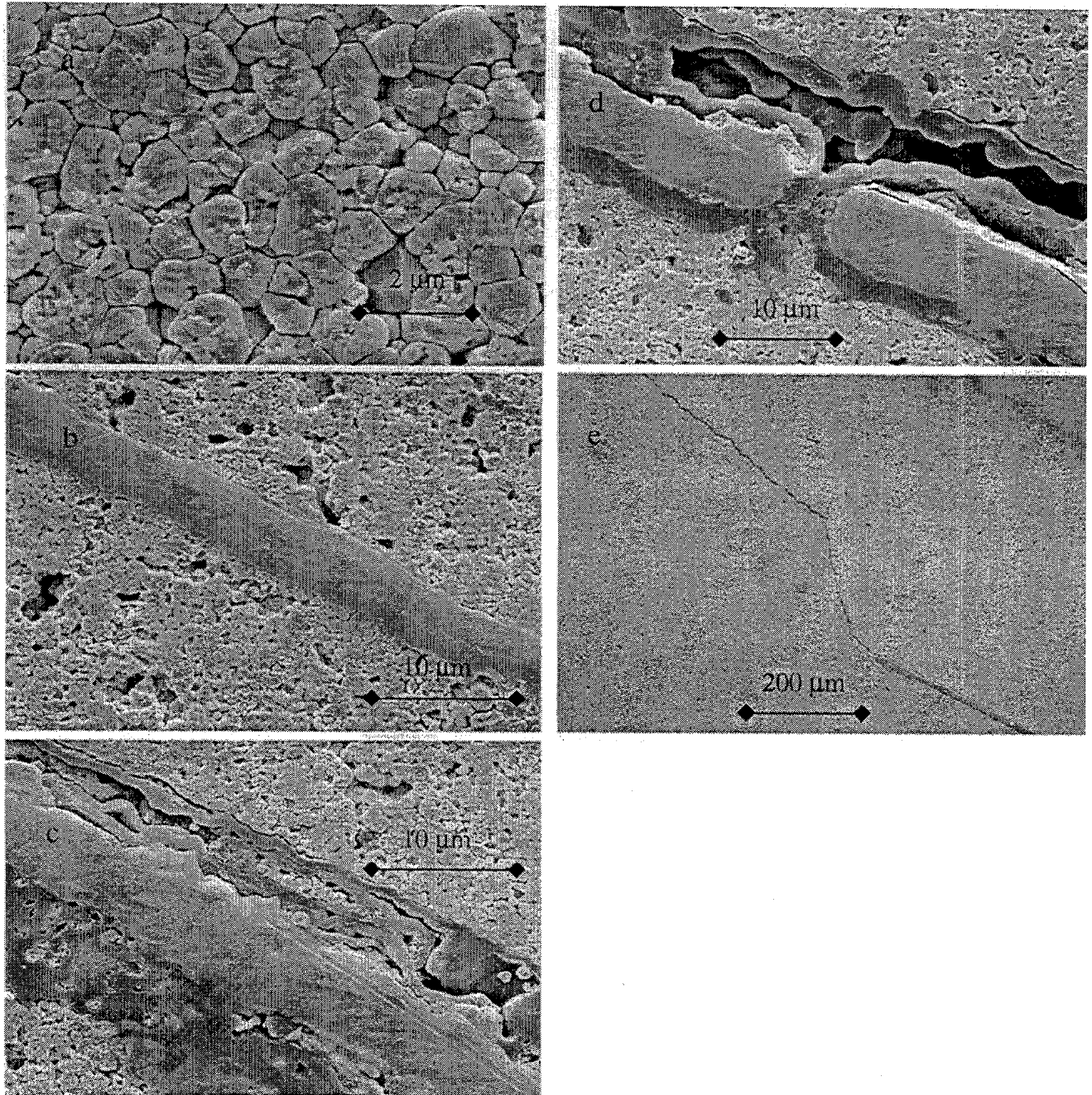


Figure 1. SEM photos(a-e) of a representative sample from set 2 of the laminated and sintered PZT-4 material in containing internal electrodes.

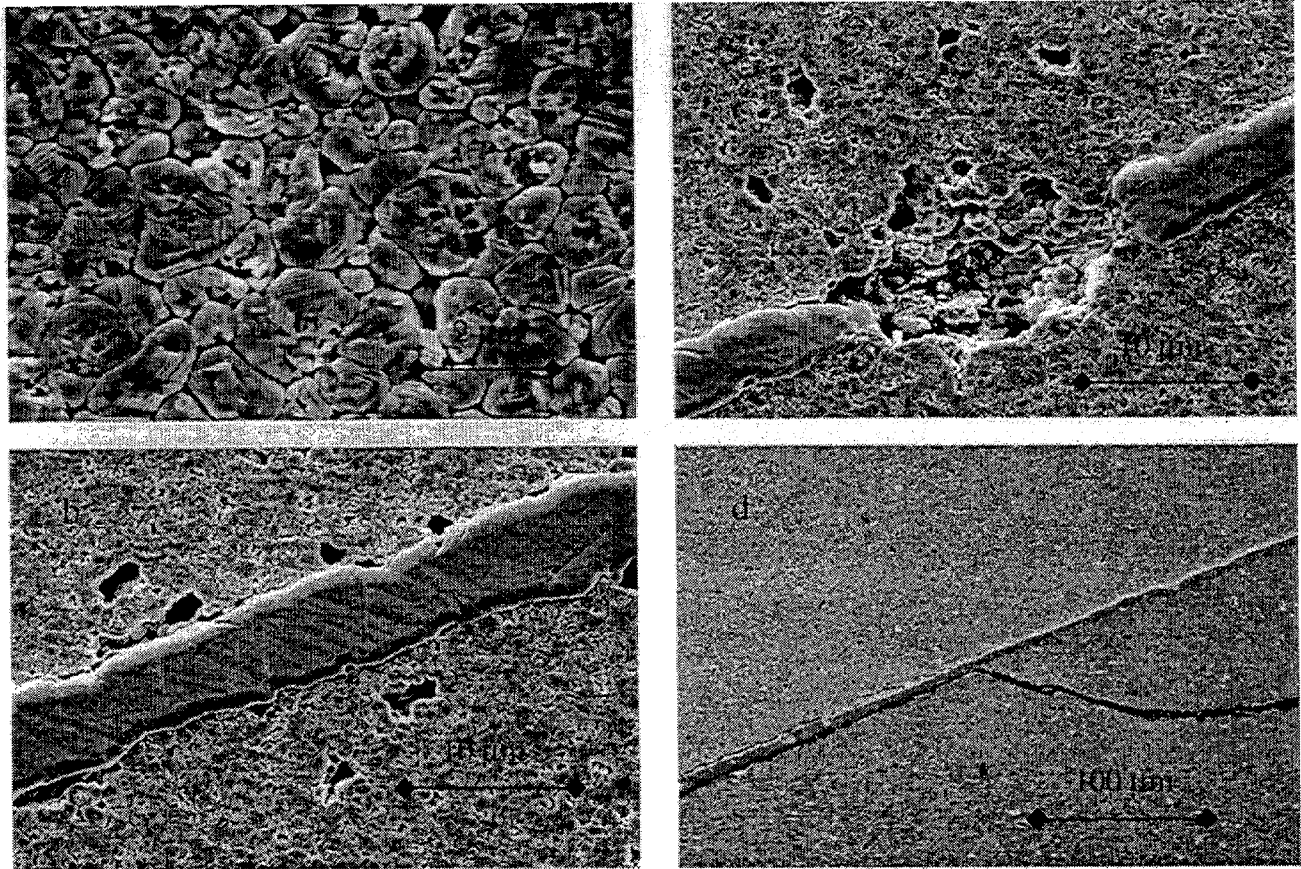


Figure 2. SEM photos(a-d) of a representative sample from set 3 of the laminated and sintered PZT-4 material in containing internal electrodes.

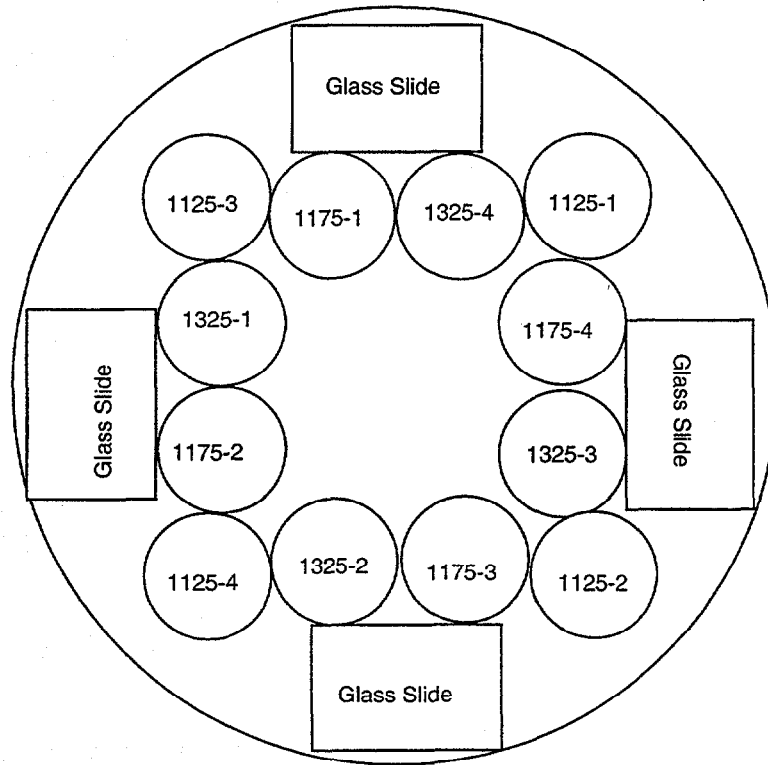


Figure 3. Fixture for grinding PZT-4 samples for strength measurements.

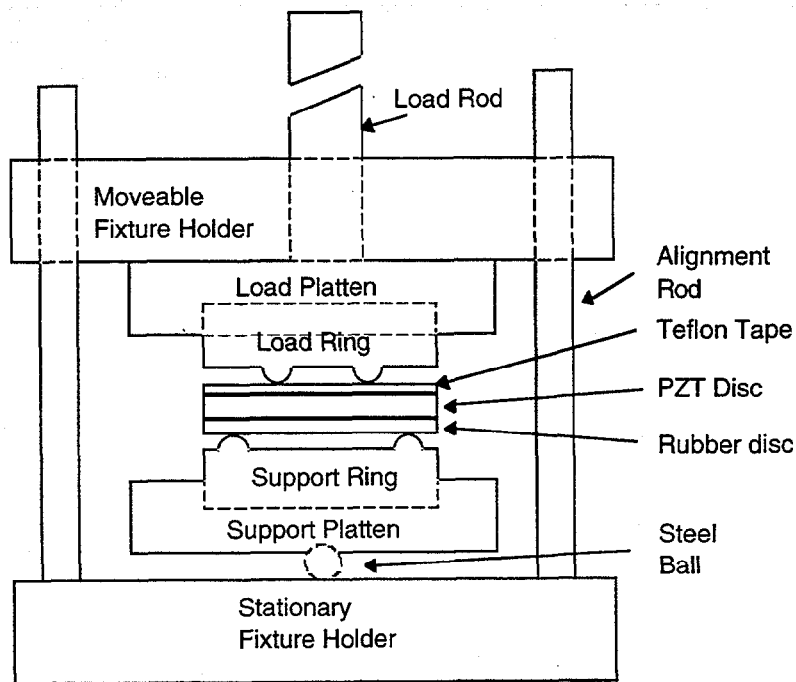


Figure 4. Mechanical fixture with sample for equibiaxial flexure strength measurement

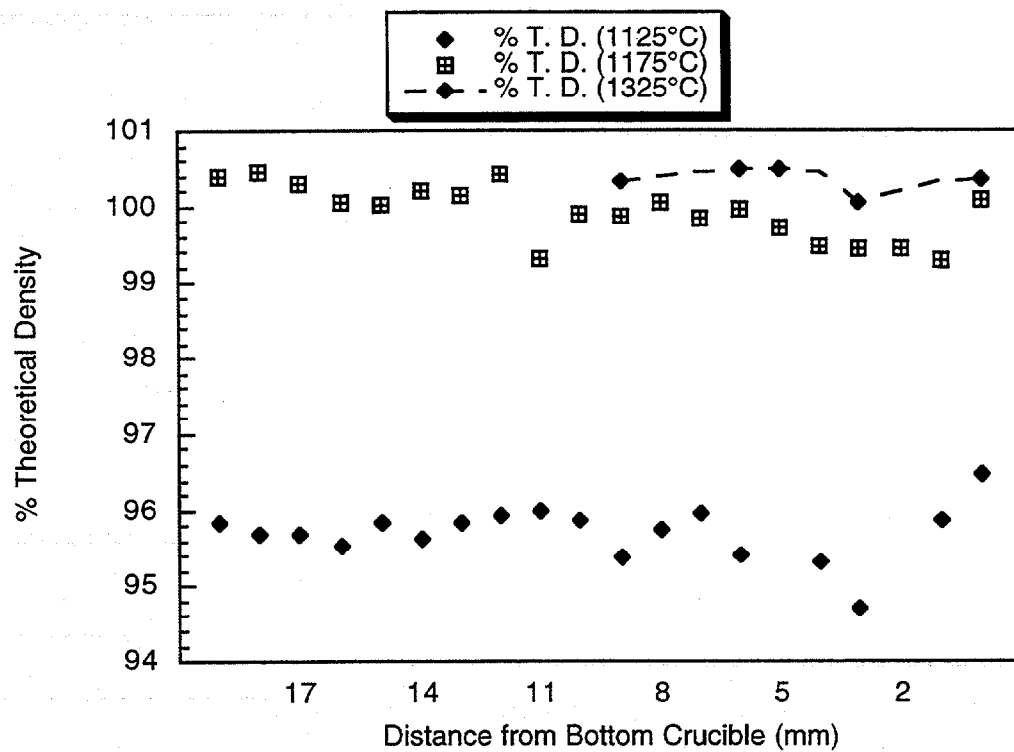


Figure 5. Densities of PZT-4 discs

W.B.S. ELEMENT 1.2.3.1
LOW COST-HIGH TOUGHNESS CERAMICS

T. N. Tiegs, F. C. Montgomery, P. A. Menchhofer, D. L. Barker, and A. Woods

Oak Ridge National Laboratory
Oak Ridge, TN 37831

Objective/Scope

Significant improvement in the reliability of structural ceramics for advanced diesel engine applications could be attained if the critical fracture toughness (K_{Ic}) were increased without strength degradation. Currently, the project is examining toughening of ceramics by two methods: microstructure development in oxide-based ceramics, and incorporation of ductile intermetallic phases.

Technical Highlights

Previous studies have shown that the properties of the aluminide-bonded ceramics (ABC) are attractive for diesel engine applications and consequently, development of these materials was started. At the present time, TiC-40 vol. % Ni_3Al composites are being developed because they have expansion characteristics very close to those for steel. Preliminary wear testing indicated that improved wear resistance could be achieved by decreasing the grain size of the TiC. Achieving fine grain size with the high binder contents is difficult because of the large inter-grain distances. In addition, it was thought that changing the TiC grain shape from a highly faceted one to a more rounded equiaxed grain would reduce localized stress at sharp corners. This, in turn, would improve abrasion resistance from any wear debris. Consequently, grain size refinement is presently being studied. Several approaches can be used to control the final TiC grain size. The methods studied in the present report include: (1) use of additives to change the interface behavior of the growing TiC grains, and (2) reduction of the initial TiC particle size.

Grain Refinement by Use of Additives

Conventional TiC-based cermet processing uses other carbide additions to aid in densification and also to maintain small grain size. For example, VC is typically added to WC-Co hardmetals and Mo_2C is a common additive to TiC-Ni cermets. An earlier study had shown that Mo, W, and Cr additions to the Ni_3Al binder resulted in grain refinement and rounding of the TiC grains. However, in that study, the samples were fabricated by reaction sintering of mixtures of Ni and NiAl to form the Ni_3Al in-situ with the TiC. However, for these TiC- Ni_3Al composites, another study showed superior properties are obtained from samples fabricated with prealloyed Ni_3Al . Consequently, a study was done to examine grain refinement and grain shape modifications in Ni_3Al composites utilizing prealloyed Ni_3Al powders. A few approaches were examined to inhibit TiC grain growth and change the final grain shape. These included, use of additives to change the interface behavior of the growing TiC grains; use of secondary particles to physically inhibit grain growth, and rapid sintering to minimize high temperature exposure. The grain growth inhibitors studied were TaC, VC, $Cr_{23}C_6$, and Mo_2C . Both TaC and VC form complete solid solutions with TiC whereas, $Cr_{23}C_6$ and Mo_2C are only partially soluble. During sintering,

these additives can influence the interface properties during solution-precipitation and grain growth. The extent of the interface interaction would affect the final grain size and grain shape.

TiN has a low solubility in molten Ni₃Al and was selected as an additive to physically impede grain growth. Earlier results on rapid sintering of silicon nitride and Ni₃Al cermets using a continuous belt furnace had showed excellent densification and properties for these materials. Consequently, continuous belt furnace sintering with high heating rates was examined to minimize grain size in conjunction with the use of grain growth inhibitors.

Several carbide additions were tested as shown in Table 1. The substitution was made on the basis of a 10 vol. % replacement of the TiC. The TiC* and Ni₃Al† powders used in fabrication were the same for all the composites. Note the large size of the prealloyed Ni₃Al powder produced by inert gas atomization. The Ni₃Al content for all the composites in the study was 40 vol. %. This composition was chosen because the thermal expansion is similar to that of steel. Sintering was done in either of two furnaces: (1) a graphite element furnace utilizing a vacuum/low pressure hot-isostatic pressure cycle (V-LPHIP), or (2) a continuous belt furnace with graphite elements at one atmosphere argon flow.

Densification – Additives are well known to inhibit grain growth in several metal carbide systems. The effect of the grain growth inhibitors on densification is shown in Fig. 1. As indicated, the various additives had only a minor effect on the densification compared to the baseline alloy composition. High densities were achieved at temperatures $\geq 1450^\circ\text{C}$. The results on the continuous belt sintering are shown in Fig. 2. In general, lower densities were obtained for the continuous sintered samples compared to the V-LPHIP processed ones. Previous work had found roughly equivalent densification between the two methods. However, in the present study, no definitive explanation has been found for the differences. The continuous sintering did not have a degassing hold step at 1200°C , nor a pressurization step at the end of the firing schedule. Further work is being done to determine the reasons for the discrepancies.

Microstructure – The qualitative effects of the various grain growth inhibitors on the microstructures can be seen in Fig. 3. As expected, the TiC grains exhibit a core-rim structure, which is formed by the solution-precipitation process that occurs during liquid phase sintering.

The TaC addition to the composites appeared to have little effect on the grain size and grain shape compared to the baseline microstructure. EDAX revealed that the white cores observed in the backscattered electron image are TaC. Evidently, the TaC is very stable and does not go into solution readily in the Ni₃Al liquid phase during sintering. As such, it can act as nucleation sites for heterogeneous precipitation of TiC much like the larger TiC particles do in the baseline composition. In addition, TaC can also preferentially precipitate at the core-rim interface on TiC grains as evidenced by the white regions observed on the TiC cores. Apparently, any TaC that does go into solution will precipitate first, followed by precipitation of the secondary TiC. Because Ta does not stay in the liquid phase, it has little effect on changing the grain growth behavior. No observable Ta concentration (by EDAX) was found in the Ni₃Al phase. The VC addition resulted in a bimodal grain size distribution and qualitatively, an overall reduction in

* Kennametal, Grade 2000, average particle size 1.2-1.3 μm (Latrobe, PA)

† Homogeneous Metals, Cohoes, NY, Alloy IC-50 (Ni-11.3 w/o Al-0.6 w/o Zr-0.02 w/o B), average particle size $\leq 75 \mu\text{m}$

grain size. No rounding of the grains was observed and the TiC grains remained quite faceted with sharp corners. Vanadium was observed by EDAX throughout the rim structure, but did not appear to preferentially precipitate at the core-rim interface. No V was observed to remain in the Ni₃Al phase. Vanadium evidently acts as a grain growth inhibitor because it precipitates from solution along with the secondary TiC onto the remnant cores and alters the interface characteristics during precipitation process.

In contrast to TaC and VC, the Cr₂₃C₆ additions resulted in both grain size refinement and rounding of the TiC grains. Cr was observed to be predominantly located in the rim structure, but smaller concentrations were also found in both the TiC cores themselves and remaining in the Ni₃Al binder. The ability of TiN additions to physically inhibit grain growth was apparent in the microstructure. As expected, no change in the grain shape resulted from the TiN additions.

Mechanical Properties – The mechanical properties were determined for composites that achieved a density $\geq 95\%$ T. D. and sintered by V-LPHIP at 1450°C. The flexural strength, fracture toughness and hardness are summarized in Fig. 4. As shown, the TaC and Mo₂C additions had strength values very similar to baseline composition. On the other hand, the VC addition decreased the strength slightly and a significant decrease was associated with the TiN addition. A very similar trend was seen with the fracture toughness measurements. The toughnesses were very good in most cases, which is attributable to the ductile nature of the Ni₃Al binder phase. The carbide additions all showed increased hardness compared to the baseline composition. The hardness increase are related to the solid solutions these carbides form with the TiC.

Grain Refinement by Reduction of Initial TiC Particle Size

One of the most obvious ways to improve grain refinement is to reduce the initial TiC particle size prior to sintering. In conjunction with Coors (under a CRADA), a milling study was done to examine the milling behavior of several commercial grade TiC powders and the effect of particle size reduction on the densification behavior and properties. Numerous milling trials were performed and are summarized in Table 2.

Milling Study - The TiC particle size reduction behavior as a function of milling time is shown in Figs.5 and 6. For the test conditions used in the experiments, the WC and ZrO₂ mill media types (with 4.9 and 3 mm diameters, respectively) had similar behavior. It would be expected WC would result in higher milling efficiency because of its higher specific density. However, the larger media size results in fewer media-media contacts and less efficient particle size reduction. Going to a smaller WC media size (1.1 mm diameter) resulted in a substantial increase in milling rate. Because the TiC powders had essentially bimodal size distributions, one of the important parameters was the D₉₀ value, which is a measurement of the larger particle sizes in the distribution. The D₉₀ results, in Fig. 6, show the effectiveness of the small WC media in reducing the particle sizes for the larger grains.

As indicated in Table 2, because of the very high hardness of TiC, significant mill media wear was introduced into the batch compositions. While the zirconia is expected to be non-reactive in the TiC-Ni₃Al system, the WC is believed to take part in the solution-reprecipitation of the TiC grains during liquid phase sintering and is incorporated into the microstructure. In addition to mill media wear, oxygen contents of the TiC powder are also increased with milling. This leads

to other processing problems as will be discussed below. The milling results illustrate the need to use TiC-based milling media in processing to minimize batch compositional changes.

Several of the milled TiC powders were subsequently used to fabricate composites with 40 vol. % Ni₃Al (IC-50) as indicated in Table 2. Because of the small particle sizes, high surface areas, and high oxygen content of these powders, off-gassing of volatile species during high temperature sintering was anticipated. Thermal gravimetric analysis (TGA) was performed to evaluate the weight loss behavior. The samples underwent binder burnout up to 400°C in argon prior to the TGA tests. The results are shown in Fig. 7. (The instrument had an anomaly at ~1050°C to 1150°C, which also was present in the Al₂O₃ standard sample.) Significant weight losses are observed for the fine TiC milled with the small WC media. Also a comparison between the two media types indicates that for comparable milling conditions, the WC-milled materials exhibited larger weight losses. This suggests that, in addition to TiC oxidation, WC from the wear debris may also contribute to oxygen pickup in the batch composition.

Sintering Study - Several of the milled TiC powders were subsequently used to fabricate composites with 40 vol. % Ni₃Al (IC-50) as indicated in Table 3. Several parameters were studied using statistically designed orthogonal arrays for the experimental variables (Taguchi Method) as shown in Table 4. The summary of the densification results from the Taguchi study are shown in Table 3. To analyze the effects of the different sintering parameters, the densities of all of the compositions for the various runs were averaged together. The level effects and the calculated percent contributions to the densification were analyzed by an ANOVA treatment of the data and the results are shown in Table 4. As indicated, the major overwhelming influence on the densification behavior was the use of vacuum. Apparently, the off-gassing of the specimens during sintering is necessary to achieve high densities and is improved by the use of vacuum. The other factors that had any significance were the sintering temperature and the use of pressurization at the sintering temperature. The sintering time and the 800°C post-sinter hold had minor effects. The 1200°C pre-sinter hold and the heating rate had no perceptible effects in the study.

Comparisons of the different parameters are shown in Figs. 8 through 14. As indicated in Fig. 8, longer sintering times improve the densification. However, it is well known that extended high temperature exposure increase grain size because of Ostwald ripening. Thus, while densities are improved, longer hold times are not desirable for grain refinement. The same is true for the sintering temperature. As illustrated in Fig.9, the higher sintering temperature increases density, but is not a way to keep grain size small.

Little effect of the 1200°C hold on densification is evident from Fig. 10. In fact, the no hold at 1200°C exhibited slightly higher densities. The 1200°C hold was used in previous studies to aid in degassing samples prior to densification. Previous work had shown that even at 1200°C (before the appearance of a liquid phase), solid state reactions do occur between the TiC and the Ni₃Al. These reactions may actually be non-beneficial to the sintering process. This is reinforced when only the DC-70 samples are analyzed. This sample would have the minimum amount of off-gassing (since no extensive TiC milling was done) and it showed significantly better densification with no 1200°C hold (95 versus 89 % T. D.).

The effect of the heating rate (Fig. 11) indicates the slower rate is better for densification. This result may also be a consequence of the off-gassing behavior, which would be more efficient at

the slower ramp speeds prior to the formation of the liquid phase (and the subsequent closing of the pores). In fact, for the DC-70 sample (with minimal off-gassing), no effect of the heating rate was evident. As expected, the vacuum sintering was definitely the single most important variable as indicated in Fig. 12.

The 800°C hold was examined as a variable because in conventional processing of Ni₃Al alloys, the intermediate temperature anneal is employed to develop secondary phases in the microstructure and improve properties. Thus, it was desirable to determine if it would have any desirable benefits for the composites. It was believed that the hold may affect the properties, but not the density since this temperature is well below any liquidus temperature for this system. Fig. 13 shows that the 800°C hold actually had a detrimental effect on densification. A closer look at the data reveals that the hold is more of a problem when used in conjunction with the pressurization step. Fig. 15 compares the different sets of data. These results suggest that the high pressure argon used in the pressurization step may be incorporated into the liquid phase during sintering and that during the 800°C hold it may come out of solution. The pressurization step does improve densities (Fig. 14), however, the exact parameters (time, pressure, release point, etc.) may have to be modified to minimize any detrimental effects.

Microstructure Characterization – The effect of milling conditions on the microstructure of the TiC-Ni₃Al composites is shown in Fig. 16. As expected, as the milling intensity increased (and the initial TiC particle size decreased), the final TiC grain size becomes finer. The DC-70 sample used as-received TiC and was milled only in the secondary ball-milling operation. Smaller grain sizes were observed for the attritor milled samples (DC-74, -75, -78, and -79). Very fine grain sizes were associated with the TiC milled with the 1.1 mm WC media (DC-90 and -91). Microstructure characterization at relatively low magnification showed poor wetting behavior between the Ni₃Al and the milled TiC. Fig. 17 shows that as the TiC particle size becomes smaller (and the oxygen content increased), decreased wetting occurs. This results in regions without liquid infiltration and is the reason for decreased densities.

Status of Milestones

On schedule.

Communications/Visits/Travel

Travel by T. N. Tiegs to St. Louis, MO, May 1-May 3, 2000 to attend the American Ceramic Society Annual Meeting and present a paper entitled, "Grain Growth Inhibitors In Intermetallic-Bonded TiC Composites."

Travel by T. N. Tiegs to New York, NY, May 30-June 3, 2000 to attend the International Conference on Powder Metallurgy and Particulate Materials and present a paper entitled, "Grain Refinement in TiC-Ni₃Al Composites."

Problems Encountered

None.

Publications

T. N. Tiegs, F. Montgomery, P. A. Menchhofer, D. L. Barker, F. L. Goranson, and D. Wittmer, "Grain Refinement in TiC-Ni₃Al Composites," to be published in Proceedings of International Conference on Powder Metallurgy and Particulate Materials, New York, NY(2000).

T. N. Tiegs, J. L. Schroeder, P. A. Menchhofer, F. C. Montgomery, D. L. Barker, F. L. Goranson, and D. Wittmer, "Processing and Properties of TiC-Ni₃Al Composites," to be published in Proceedings of 7th International Symposium on Ceramic Materials and Components for Engines, Goslar, Germany (2000).

T. N. Tiegs, M. L. Santella, C. A. Blue, F. Goranson, and P. A. Menchhofer, "FGM Fabrication by Surface Thermal Treatment of TiC-Ni₃Al," to be published in Proceedings of 6th International Symposium on Functionally Graded Materials, Ceramic Transactions, American Ceramic Society, Westerville, OH (2000).

Table 1. Samples of aluminide-bonded TiC ceramics fabricated to determine the effect of different carbide substitutions on the sintering behavior and properties of the aluminide-bonded TiC. All samples fabricated with 40 vol. % of the Ni₃Al binder phase by sintering of prealloyed powders. The different carbides were substituted on the basis of 10 vol. % of the TiC.

Sample ID	Carbide Substitution
DC-43B	--
DC-50	TaC
DC-51	VC
DC-52	Cr ₂₃ C ₆
DC-57	Mo ₂ C
DC-58	TiN

Table 2. Results of milling study on commercial TiC powders.

Run No.	TiC Type	Total Mill Time (h)	Mill Speed (RPM)	Media Type	Media/Charge Ratio (wt.)	Media Wt. Loss (%)	Media Addition to TiC (wt. %)	Mean Particle Size (μm)	Particle Size, D_{90} (μm)	Oxygen Content (wt. %)
1	Jet-Mill	15	250	ZrO ₂ -3 mm	10:1	0.52	4.9	0.66±0.20	1.4	
2	Jet-Mill	7	275	WC-4.9 mm	20:1	0.27	5.1	0.74±0.24	1.6	
3	Jet-Mill	6	300	ZrO ₂ -3 mm	9.9:1	0.48	4.6	0.55±0.18	1.2	1.94
4	Jet-Mill	12	300	WC-4.9 mm	23.3:1	0.30	6.5	0.47±0.14	0.9	2.21
5	2000	12	300	ZrO ₂ -3 mm	9.9:1	0.78	7.2	0.61±0.32	1.3	
6	2000	12	300	WC-4.9 mm	23:1	0.39	8.2	0.70±0.23	1.5	
7	1000	12	300	WC-4.9 mm	22.9:1	0.24	5.1	0.77*	2.4*	1.19
8	1000	12	300/500	ZrO ₂ -3 mm	9.8:1	0.94	8.5	0.20*	0.63*	3.02
9	1000	8	300	WC-4.9 mm	22.9:1	0.25	5.5	0.50*	1.53*	1.19
10	2000	12	300	ZrO ₂ -3 mm	9.7:1	1.51	12.8			
11	1000	8	400	WC-1.1 mm	23:1	0.36	7.6	0.32±0.09	0.5	3.36
12	1000	3	400	WC-1.1 mm	23:1	0.19	4.1	0.18*	0.52*	2.34
13	2000	3	400	WC-1.1 mm	20.6:1	0.47	8.8			
--	Jet-Mill	0	N.A.	N.A.	N.A.	N.A.	N.A.	1.00±0.32	2.1	1.43
--	1000	0	N.A.	N.A.	N.A.	N.A.	N.A.	1.31±0.42	2.7	
--	2000	0	N.A.	N.A.	N.A.	N.A.	N.A.	3.16±0.9	5.8	0.51

Table 3. TiC-Ni₃Al composites fabricated from milled TiC powders.

Sample No.	Mill Run No.	TiC Type	Mean Particle Size (μm)*	Oxygen Content (wt. %)
DC-70	None	2000	3.16 \pm 0.9	
DC-72	None	2000	3.16 \pm 0.9	
DC-74	4	Jet-Mill	0.47 \pm 0.14	2.21
DC-75	3	Jet-Mill	0.55 \pm 0.18	1.94
DC-78	5	2000	0.61 \pm 0.32	
DC-79	6	2000	0.70 \pm 0.23	
DC-87	8	1000	0.20**	3.02
DC-88	7	1000	0.77**	1.19
DC-89	9	1000	0.50**	1.19
DC-90	11	1000	0.32 \pm 0.09	3.36
DC-91	12	1000	0.18**	2.34

*Prior to ball milling step with Ni₃Al powder.

** Measurements made at Coors Tek, all others made at ORNL.

Table 4. Optimization of sintering schedule for TiC-Ni₃Al composites to achieve grain refinement. The matrix is a L₈ (2⁷) orthogonal array.

Test No.	Sinter Time (min)	Sinter Temperature ($^{\circ}\text{C}$)	1200 $^{\circ}\text{C}$ Hold During Heating ^a	Heating Rate ($^{\circ}\text{C}/\text{min}$)	Sinter Atmosphere	800 $^{\circ}\text{C}$ Hold During Cooling ^b	1 MPa Pressurization Step ^c
1	40	1425	Yes	10	Vacuum	No	Yes
2	40	1425	Yes	20	Argon	Yes	No
3	40	1475	No	10	Vacuum	Yes	No
4	40	1475	No	20	Argon	No	Yes
5	20	1425	No	10	Argon	No	No
6	20	1425	No	20	Vacuum	Yes	Yes
7	20	1475	Yes	10	Argon	Yes	Yes
8	20	1475	Yes	20	Vacuum	No	No

^a 1200 $^{\circ}\text{C}$ hold for 30 min. during heating

^b 800 $^{\circ}\text{C}$ hold for 30 min. during cooling

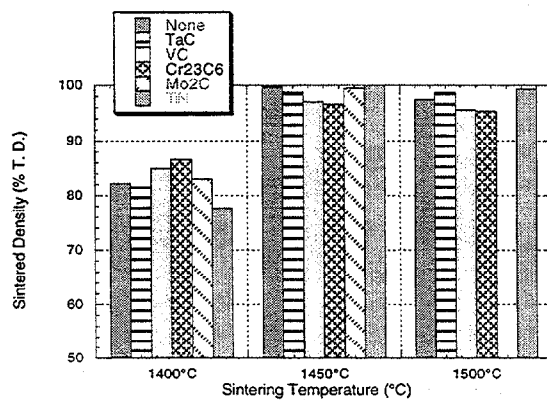
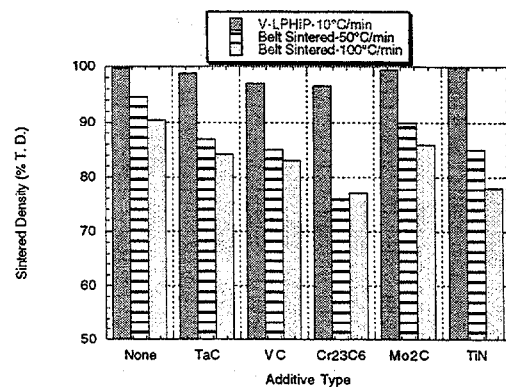
^c Pressurization step occurs during last half of the sintering time (i.e. either 20 or 10 min.)

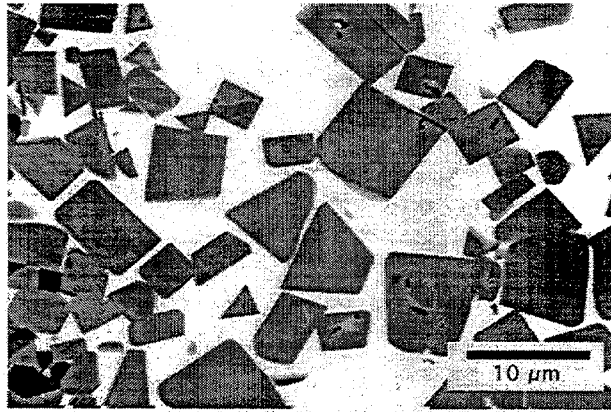
Table 5. Summary of densification results from sintering study.

Run No.	DC-70	DC-72	DC-74	DC-75	DC78	DC-79	DC-81	Ave.
1	99.2	99.5	99.9	100	93.1	98.9	80.5	95.9
2	74.2	73.9	70.7	76.8	85.0	88.6	80.2	76.9
3	98.0	96.9	91.3	91.3	95.6	100	88.1	94.5
4	97.1	89.9	87.9	91.5	92.2	95.2	83.3	91.0
5	85.8	72.3	74.9	80.2	81.7	84.6	77.1	79.5
6	99.6	90.3	90.5	82.9	78.7	94.0	84.0	88.6
7	95.2	80.6	80.5	83.0	84.9	89.2	81.1	84.9
8	97.1	94.1	96.0	89.0	89.0	93.0	82.8	91.7

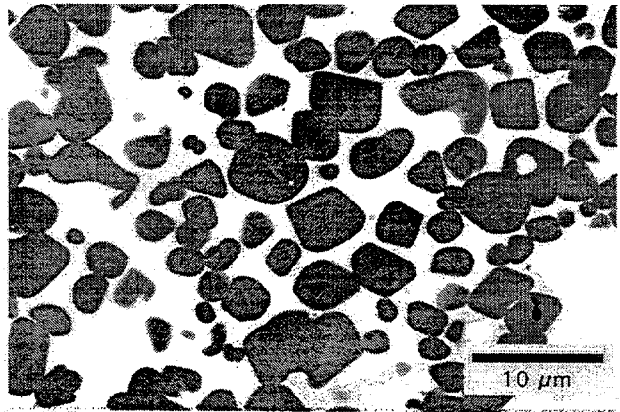
Table 6. Level effects and percent contributions to densification from the different parameters.

Variable	Level Effect	Percent Contribution
Sinter Time	3.40	5
Sinter Temp	5.30	15
1200°C Hold	1.05	0
Heating Rate	1.65	0
Sinter Atmosphere	9.56	53
800°C Hold	3.31	5
Pressurization Step	4.45	10
Error		12

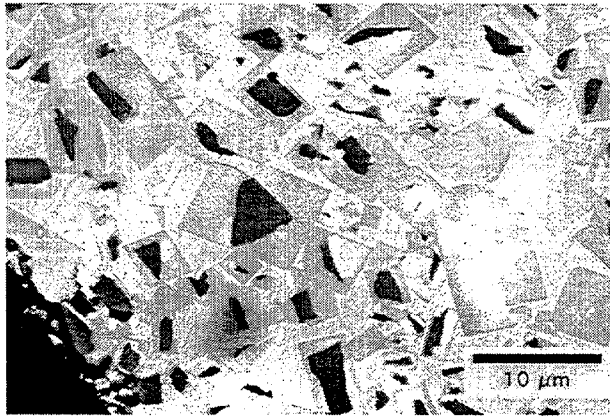
Fig. 1. Densification of composites fabricated with various grain growth inhibitors. Composites contained 40 vol. % Ni_3Al and sintered by V-LPHIP process.Fig. 2. Densification of composites fabricated with various grain growth inhibitors and sintered by V-LPHIP process or by continuous belt furnace. Composites contained 40 vol. % Ni_3Al and sintered at 1450°C.



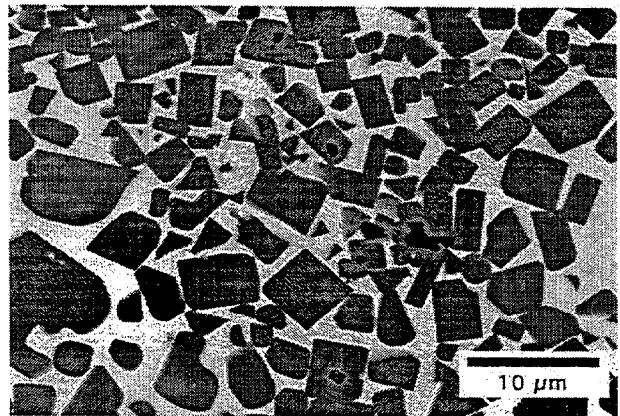
(a)



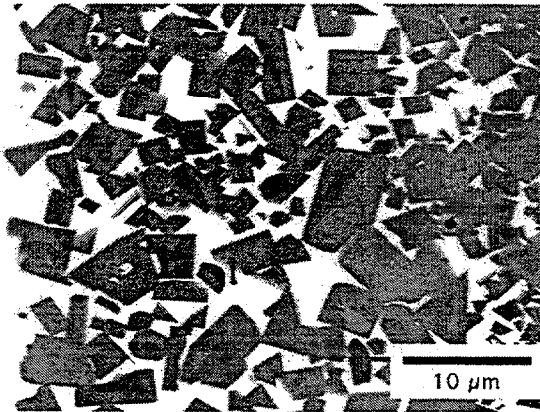
(d)



(b)

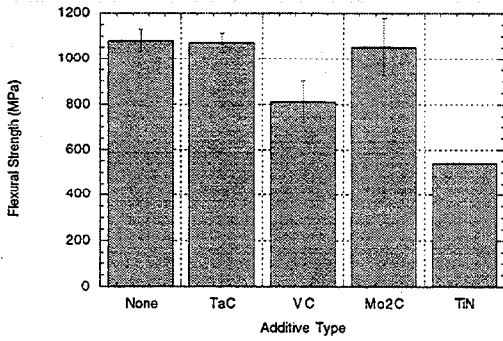


(e)

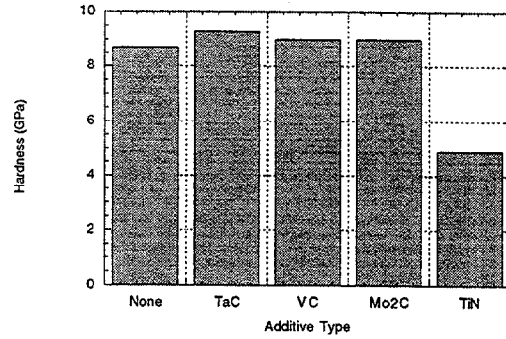


(c)

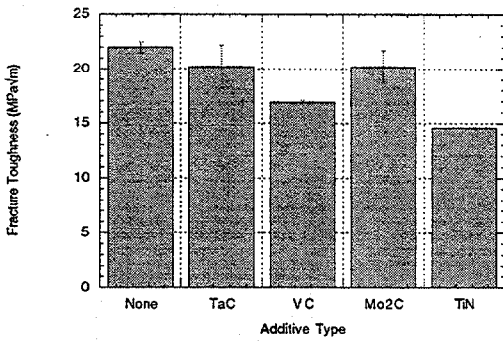
Fig. 3. Microstructures of (a) Baseline alloy; (b) TaC addition; (c) VC addition, and (d) Cr₂₃C₆ addition, (e) TiN addition. Samples sintered at 1500°C by V-LPHIP process.



(a)



(c)



(b)

Fig. 4 Flexural strength, fracture toughness and hardness of composites fabricated with various grain growth inhibitors. Composites contained 40 vol. % Ni_3Al and sintered by V-LPHIP process at 1450°C .

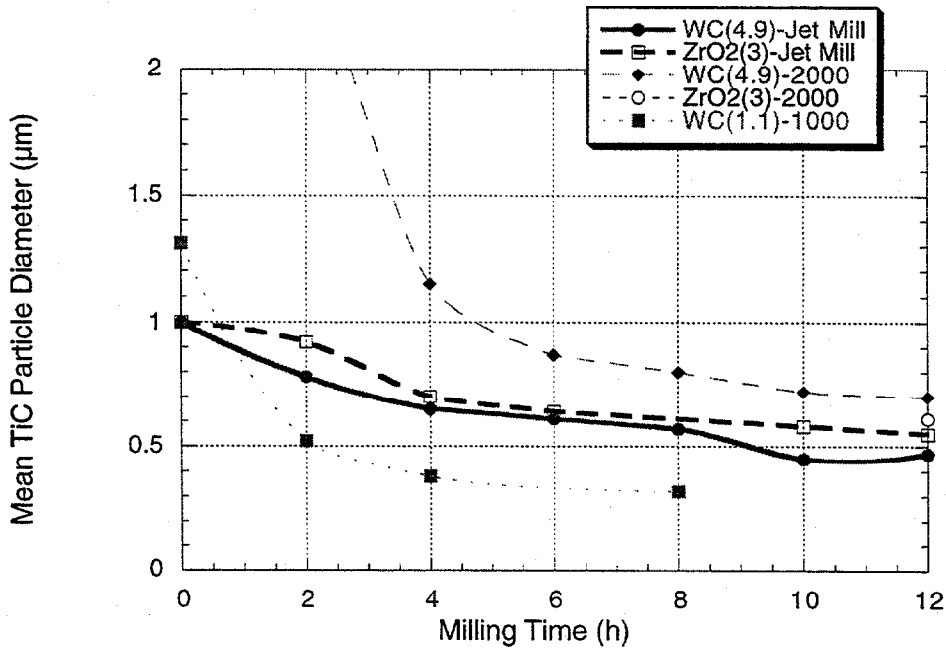


Fig. 5. Mean TiC particle size reduction during milling.

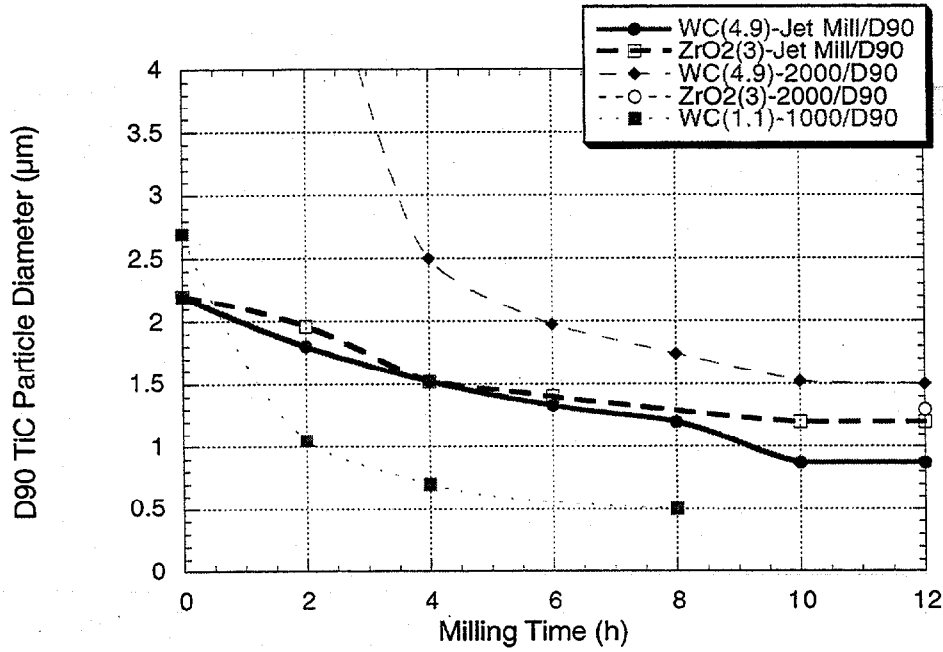


Fig. 6. D₉₀ TiC particle size reduction during milling.

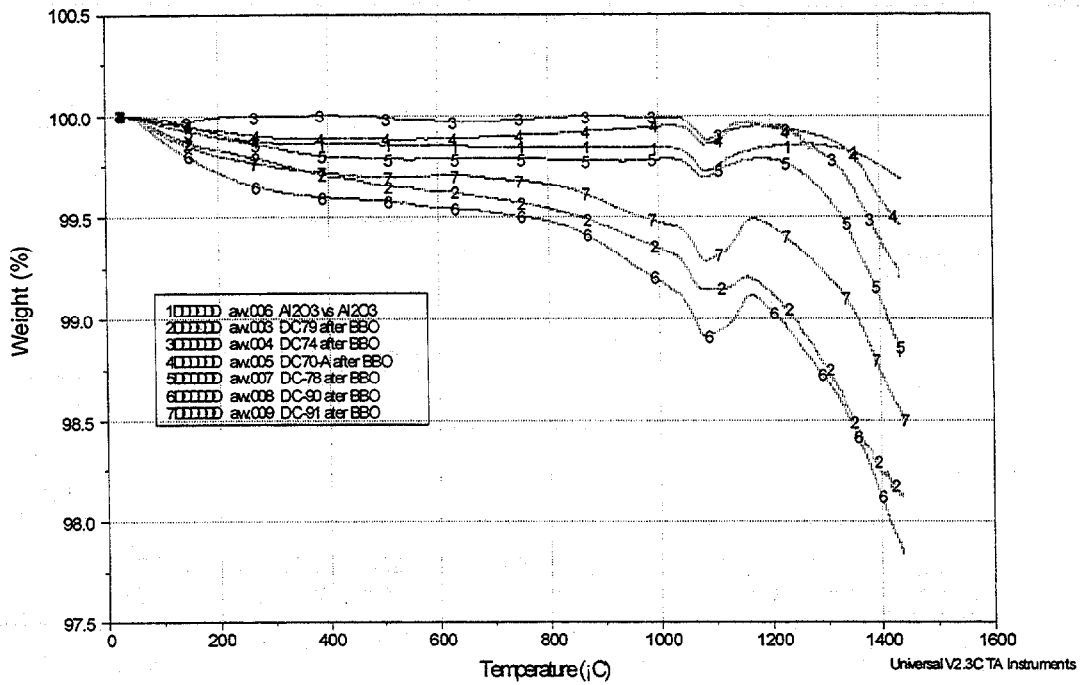


Fig.7. Thermal gravimetric analysis (TGA) results on composite powders after binder burnout. (The instrument had an anomaly at ~1050°C to 1150°C, which also was present in the Al₂O₃ standard sample.)

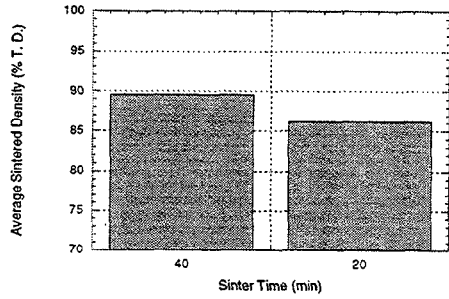


Fig. 8. Effect of sintering time on average density of TiC-Ni₃Al composites.

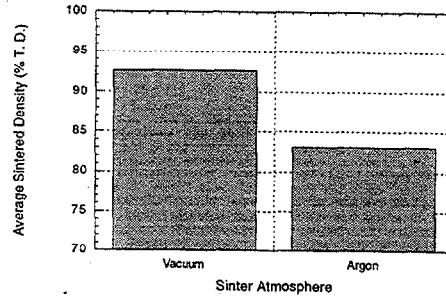


Fig. 12. Effect of sintering atmosphere on average density of TiC-Ni₃Al composites.

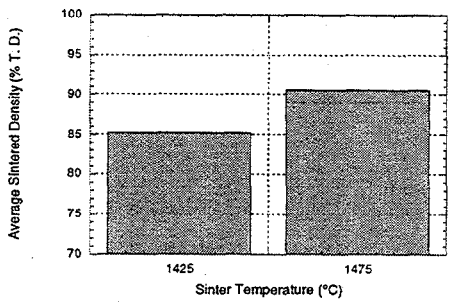


Fig. 9. Effect of sintering temperature on average density of TiC-Ni₃Al composites.

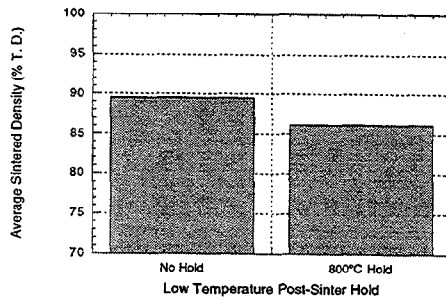


Fig. 13. Effect of 800°C post-sinter hold on average density of TiC-Ni₃Al composites.

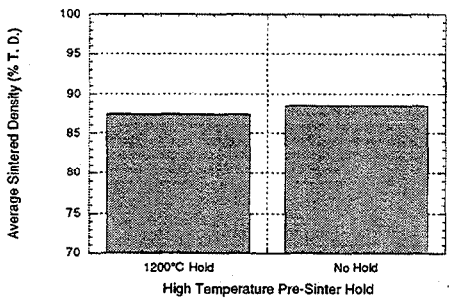


Fig. 10. Effect of 1200°C pre-sinter hold on average density of TiC-Ni₃Al composites.

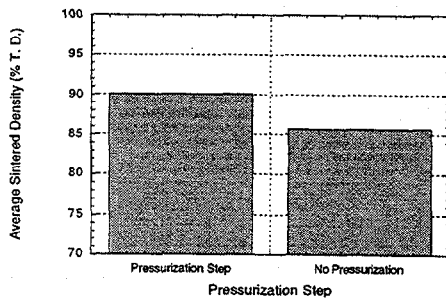


Fig. 14. Effect of 1 MPa pressurization step on density of TiC-Ni₃Al composites.

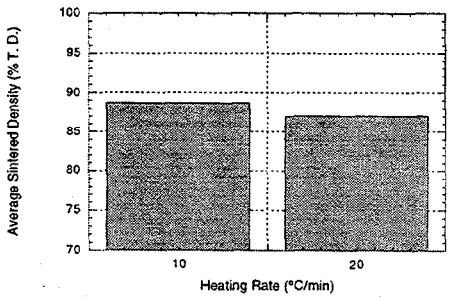


Fig. 11. Effect of heating rate on average density of TiC-Ni₃Al composites.

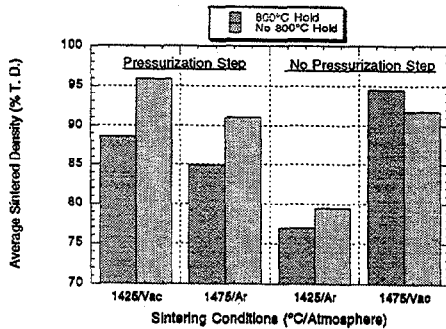
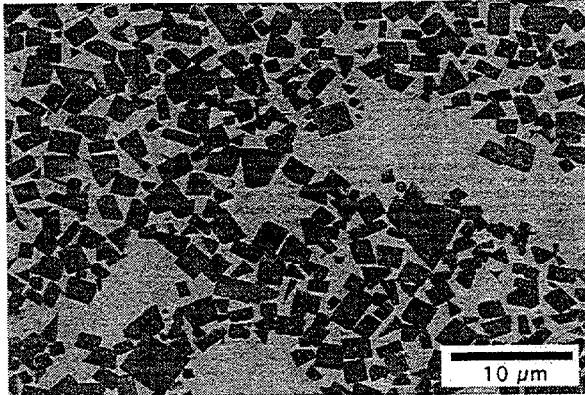
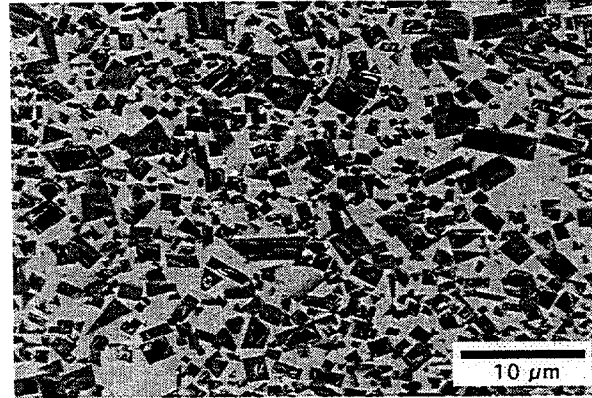


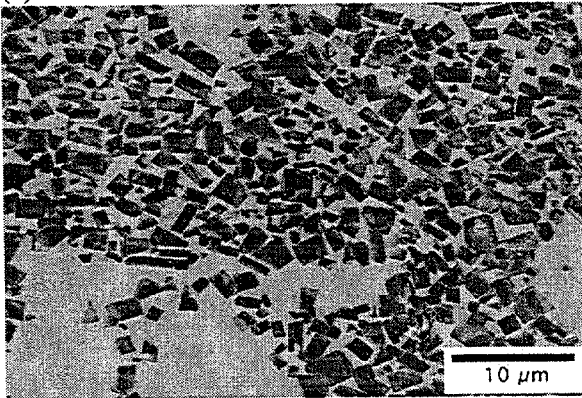
Fig. 15. Comparison of sintered densities for 800°C hold at different conditions.



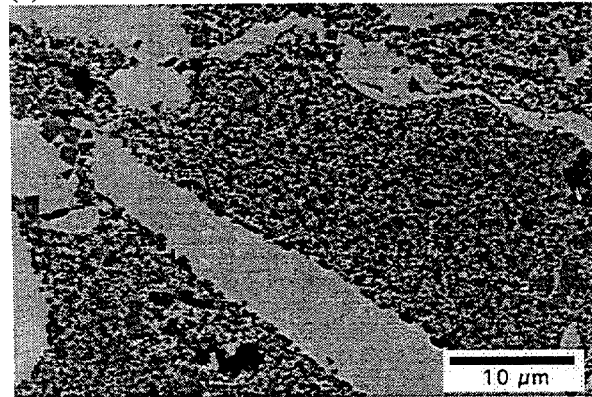
(a) DC-70-1



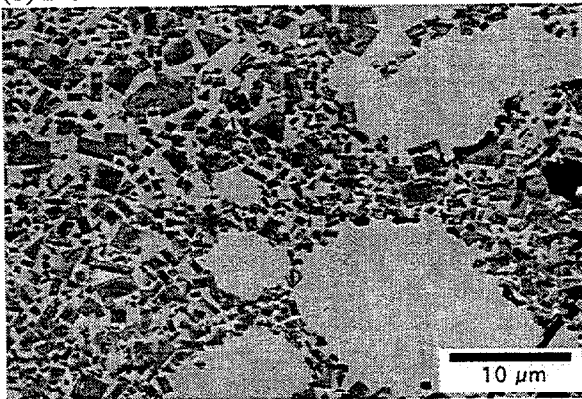
(e) DC-79-1



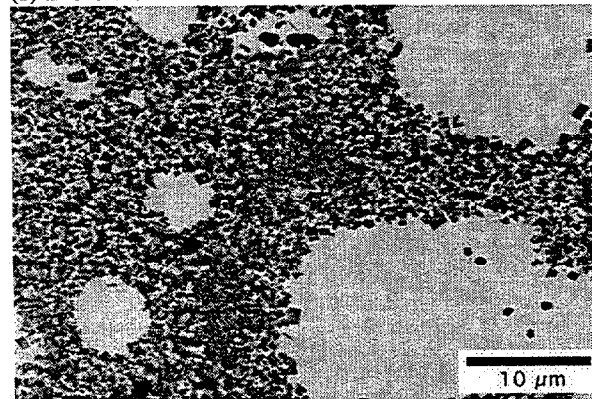
(b) DC-74-1



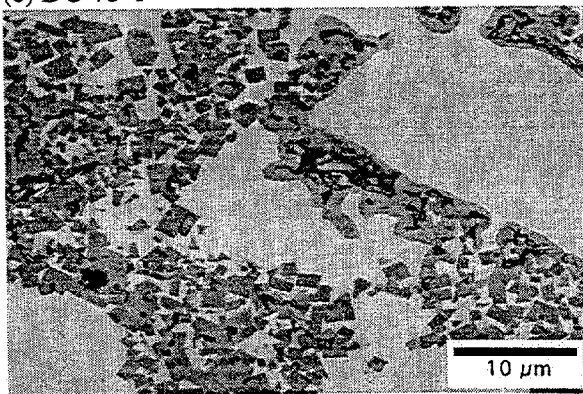
(f) DC-90-9



(c) DC-75-1

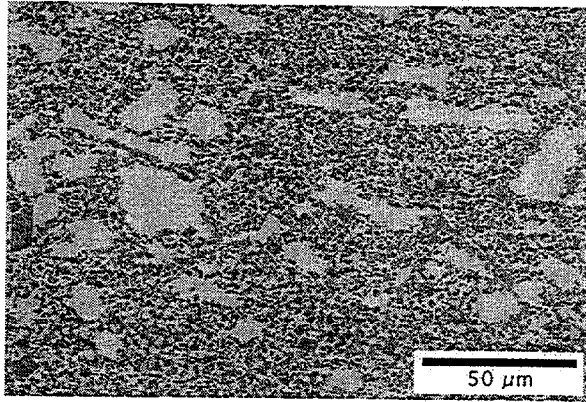


(g) DC-91-9

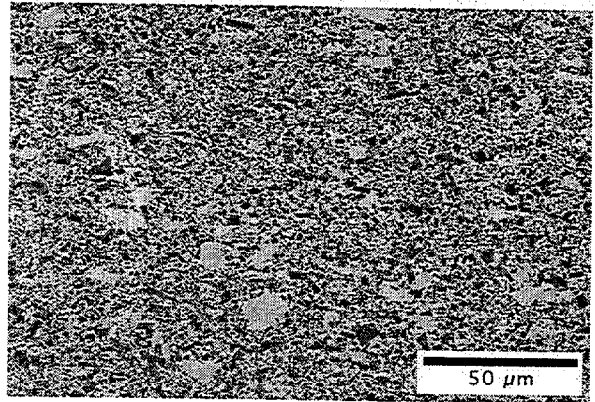


(d) DC-78-1

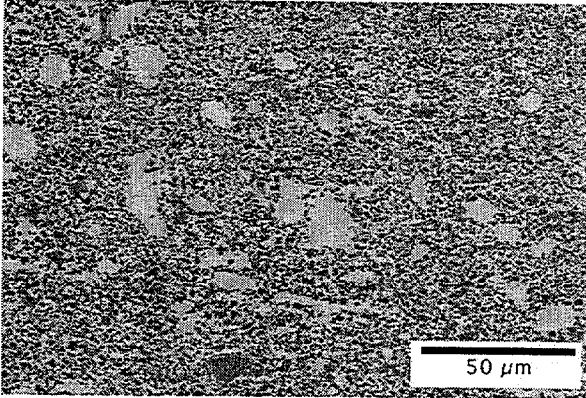
Fig. 16 Microstructures of TiC-40 vol. % Ni₃Al (IC-50) fabricated using different milling conditions: (a) DC-70; (b) DC-74, (c) DC-75, (d) DC-78, (e) DC-79, (f) DC-90, and (g) DC-91.



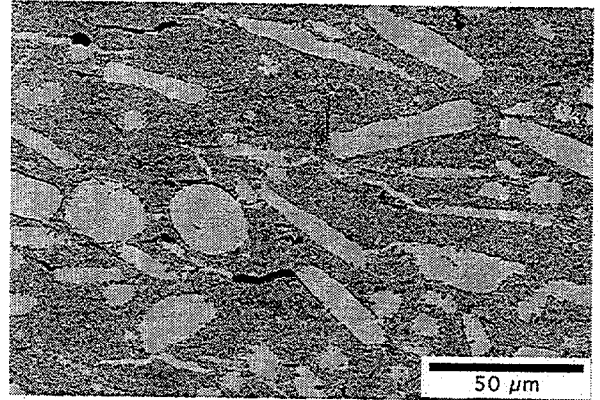
(a) DC-70-1



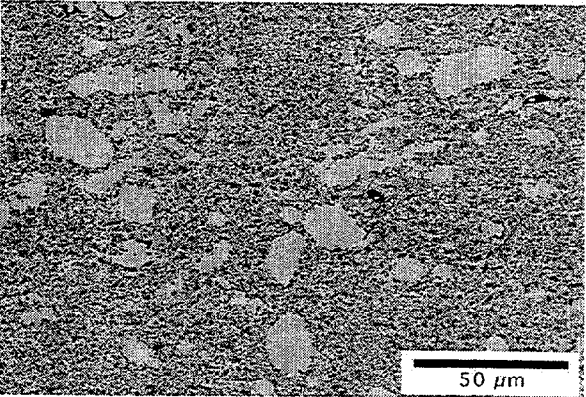
(e) DC-79-1



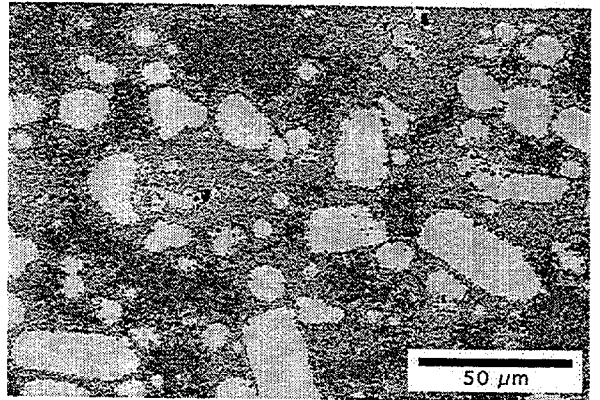
(b) DC-74-1



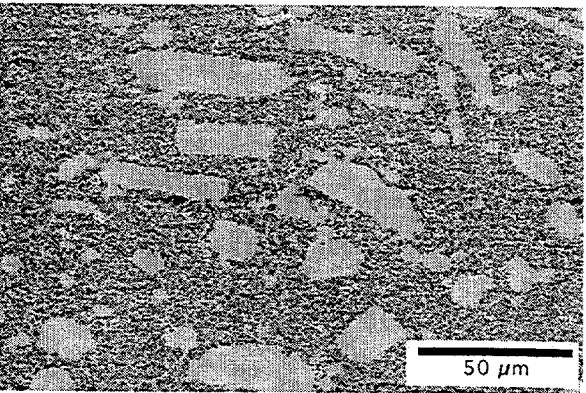
(f) DC-90-9



(c) DC-75-1



(g) DC-91-9



(d) DC-78-1

Fig. 17. Microstructures of TiC-40 vol. % Ni₃Al (IC-50) fabricated using different milling conditions: (a) DC-70; (b) DC-74, (c) DC-75, (d) DC-78, (e) DC-79, (f) DC-90, and (g) DC-91.

Cost Effective Sintering of Silicon Nitride Ceramics (SIU-C)-

D. E. Wittmer, Southern Illinois University, Carbondale, IL 62901

Objective/Scope

The purpose of this work is to investigate the potential of cost effective sintering of Si_3N_4 and inter-metallic bonded carbides through the development of continuous sintering techniques.

Technical Highlights

Task 1. Refine Economic Model and Design for Chosen Furnace Configuration

This task was completed as reported in a previous semiannual report.

Task 2. Continue evaluation of sintering parameters on properties of selected Si_3N_4 compositions

1. Prototype Belt Furnace

The furnace continues to operate efficiently without problem. Additional graphite boats have been designed, ordered and received which will allow for full load operation.

2. Collaboration with Industrial Partners and Affiliates

Work continues according to plan to develop collaborations with industrial partners. Due to the proprietary/confidential relationships established, the results of these collaborations will be reported as part of their individual programs.

3. Evaluation of Continuous Sintering of Silicon Nitride-Titanium Carbide

This task has been completed.

Task 3. Continue Evaluation of Low Cost Si_3N_4 Powders

This task has been completed.

Task 4. Design and Construct Prototype Belt Furnace

This task has been completed.

Task 5. Continuous Sintering of Intermetallic Bonded Carbides

Current plans are to pursue the proposed activities . More specifically:

- Prepare larger samples of TiC bonded with 40 vol.% IC-50, IC-218, NiCr and NiCrFe in order to be able to machine test bars for strength and fracture toughness measurements.
- Use turbomilling in order to investigate the possibilities to reduce the carbide and intermetallic grain size efficiently without increasing oxygen contamination.
- Prepare samples with higher binder content, possibly 40-60 vol.% to increase the strength, toughness and the thermal expansion.
- Investigate the high-temperature properties of the above-mentioned compositions.
- Optimize the continuous sintering parameters for the NiCr and NiCrFe bonded TiC.
- Investigate the corrosion resistance further, for longer times and at elevated temperatures.

During this reporting period, work was initiated to investigate turbomilling of TiC in non-aqueous solvents. A glove box was designed, constructed and installed on the turbomill at SIUC to allow turbomilling in a slight overpressure of Ar. All turbomilling trials used isopropanol as the solvent. YTZ media was used in the 6 in. diameter turbomilling chamber at about a 2:1 ratio to the TiC and milling was for 4-6 hours, depending on the particle size obtained. Particle size analyses were conducted at 1 hour intervals. Following milling of the TiC, the media was removed and the NiCrFe or other intermetallic was added to the mill. Milling continued for 30 min to homogenize the mixture. These mixtures were then air dried and granulated. Following drying some of the mixture was dry pressed and some was batched for low pressure injection molding.

Also during this reporting period the Blue-M oven was installed and tested for binder removal from both the pressed and injection molded parts. The injection molded parts were about 1cm square by about 6 cm long or cylinders 1.25 and 1.8 cm in diameter by 8 cm long. A three stage binder removal step was developed to allow debinding of these test bars without warpage or cracking.

Aaron Woods, graduate student, completed his internship at ORNL working on the same formulations but with conventional processing methods. Several disks of the conventionally processed formulations were recently sintering in the batch furnace at ORNL using the vacuum-LPHIP (Ar) techniques developed at ORNL. Disks of these formulations were also sintered in flowing Ar in the continuous furnace at SIUC at 1400°C and 1450°C and a belt speeds of 0.75"/min and 1.5"/min (soak time of about 30 min.). The density and hardness results are given in Figures 1-12. Microstructural result for these formulations will be determined during the next reporting period.

Effects of Milling and Sintering Methods

As part of this work, batches have been ball milled and attritor milled at ORNL and processed in the turbomill at SIU. For ball milling, 13 mm YTZ media were used and milling took place for 24 hours in alcohol. For attritor milling, 1.1 mm WC media were used and milling took place in alcohol at 550 rpm for 4 hours. For turbomilling the TiC was turbomilled for 5.5 hours in isopropanol at 1200 rpm, the intermetallic powders were then added and milling continued for 0.5 hours.

Figures 1 and 2 compare the densities and hardness values obtained for NiCr-TiC composites processed by the three milling methods and then sintered in a batch furnace at ORNL. The sintering process is the same as used in the past where a vacuum is held at low temperatures, followed by low pressure Ar sintering. As seen in these figures, turbomilling produced the highest densities and the lowest hardness, which is contrary to expectations, based on density alone. The microstructures are presently being investigated to determine a plausible explanation.

For the NiCrFe-TiC composites, the results for densities and hardness values for the three milling methods (Figures 3 and 4, respectively), show that once again the turbomilling appeared to produce higher densities. In this case, the hardness values were generally higher for the composites produced by turbomilling, but about the same for the 40 vol% composite which is of greatest interest.

Figures 5 and 6 compare the density results and hardness obtained for the NiCr-TiC composites processed by ball milling and sintered by either batch or continuous (belt furnace) methods. For the composites containing the higher volume of binder phase the continuous furnace produce equivalent or higher densities, while producing significantly lower hardness. The microstructures are presently being investigated to determine plausible causes for these results.

The results for the NiCrFe-TiC composites produced by ball milling and sintered by the two different methods are given in Figures 7 and 8. These figures show that once again the belt furnace produced nearly equivalent or slightly higher density than the same formulation sintered in the batch furnace. The hardness values were measurably lower for all three volume loadings of binder processed by ball milling for the continuous sintered composites, compared to the batch sintered ones.

The behavior observed for the ball milled composites was even more noticeable for the the turbomilled composites sintered in the batch furnace (Figures 9 through 12). The only exception was the 50 vol% NiCr-TiC composite sintered in the belt furnace. More work is needed to determine the effects of the high heating and cooling rates obtainable in the continuous furnace.

Low Pressure Injection Molding

During this reporting period, several batches were made and injected using the Peltzman MIGL-28 unit. During previous runs, the major problems were pitting and voids in the parts caused by mixing in the injection unit and binder removal problems. The injection process was modified in an attempt to reduce/eliminate the defects previously observed. The recent results are given in Table I.

Sample ID	Sample Volume (cc)	Average # of Visible Defects	Surface Appearance After Binder Removal
IM-14	6	6	Moderate surface pitting
IM-15	6	1	Very slight surface pitting
IM-16	10	4	Heavy surface pitting
IM-17	10	1	Moderate surface pitting
IM-18	10	0	Slight surface pitting

All of the mixtures were process as follows: binders were melted in the pre-heated well, the ceramic and metallic powders were then added, mixed with a spatula until the powders were coated (~10 min), the cover was placed on the unit, the mixture was then mixed under vacuum for 60 min. IM-18 produced the best results to date. IM-18 is a 40:60 intermetallic-TiC composite. The intermetallic phase consisted of Fe, NiAl, Ni. The binder was petroleum jelly, paraffin, and stearic acid at a ratio of 55:43:2 by volume. These parts were 10 cc rods formed in a steel die at 50 psi with the injection well at 71 °C, the pipe at 71 °C and orifice at 63 °C. For this run the mixer was turned off and the vacuum removed just prior to injecting each part. Each 10 cc bar was injected in 30 seconds and removed immediately after the pressure was completely released. The vacuum was then reapplied and the mixer turned on during the cooling of the mold. The part was then removed from the mold and the process repeated. The binders were removed in flowing Ar by packing the parts in sand in graphite boats and removing the binder according to the standard schedule. The green density for IM-18 was 63.7% of the calculated theoretical density.

Status of Milestones

- | | | |
|----|--|-------------|
| 1. | Refine Economic Model and Design for Chosen Furnace Configuration | Completed |
| 2. | Continue Evaluation of Sintering Parameters on Properties of Selected Si_3N_4 Compositions | Completed |
| 3. | Continue Evaluation of Low Cost Si_3N_4 Powders | Completed |
| 4. | Design and Construct Prototype Belt Furnace | Completed |
| 5. | Continuous Sintering of Inter-Metallic Bonded Carbides | On Schedule |

Communications/Visits/Travel

D. E. Wittmer to ORNL to discuss progress with Ray Johnson and Terry Tiegs and attended two progress review meetings.

Aaron Woods to ORNL for internship with Terry Tiegs for summer/fall term.

Problems Encountered

None

Publications and Presentations

"Continuous Sintering of NiCr and NiCrFe-TiC Intermetallics," D. E. Wittmer, A. Woods, F. Goransson, T. Tiegs, and P. Menchhofer. Abstract submitted to 2001 International Conference on Powder Metallurgy and Particulate Materials, PMTec 2001, May 3-17, New Orleans, LA

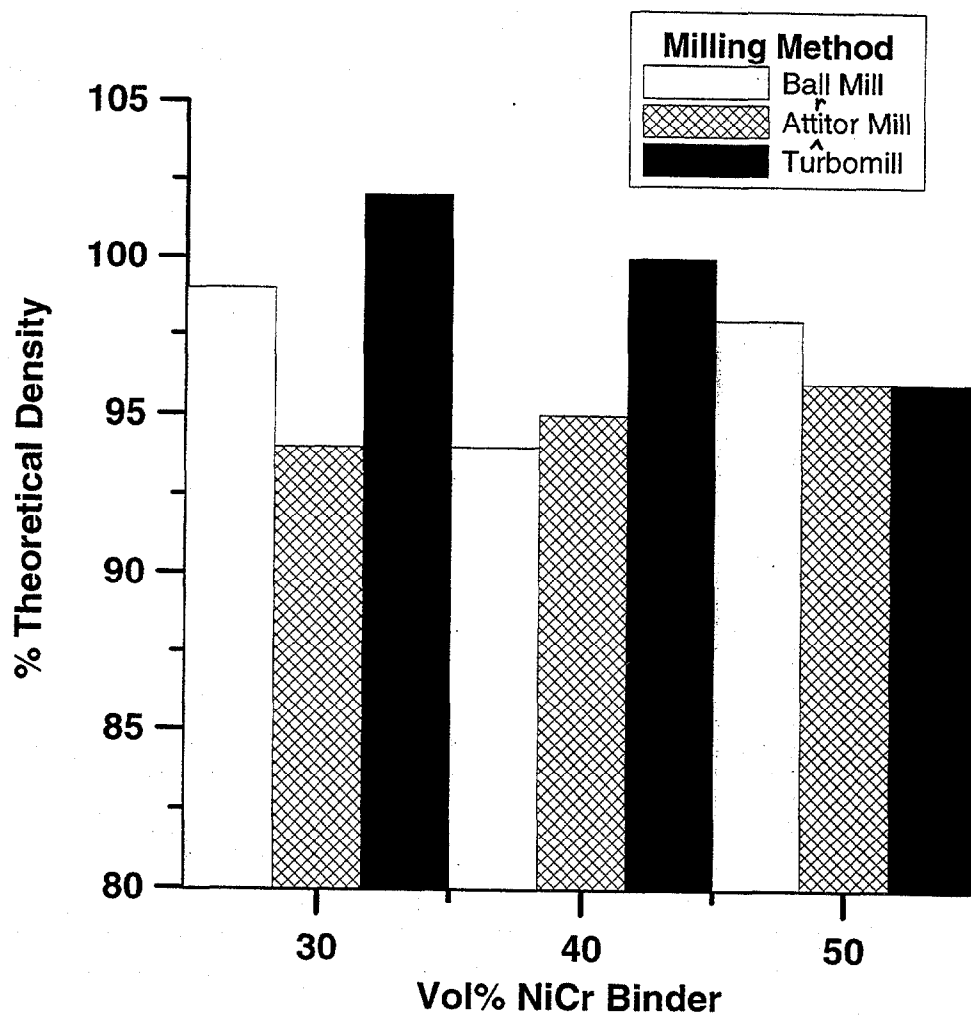


Figure 1. Densification behavior of NiCr-TiC composites obtained by three milling methods and batch sintered in Ar.

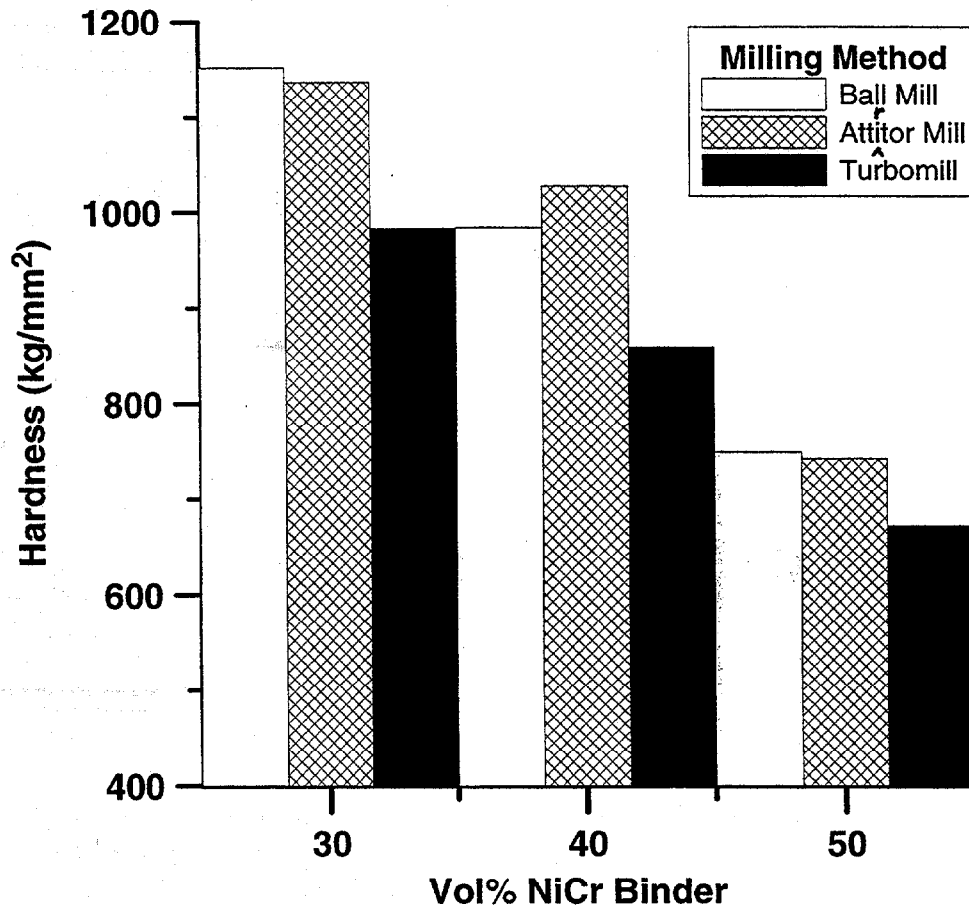


Figure 2. Comparison of Vicker's hardness results for three different milling methods for NiCr-TiC composites sintered in Ar in a batch furnace.

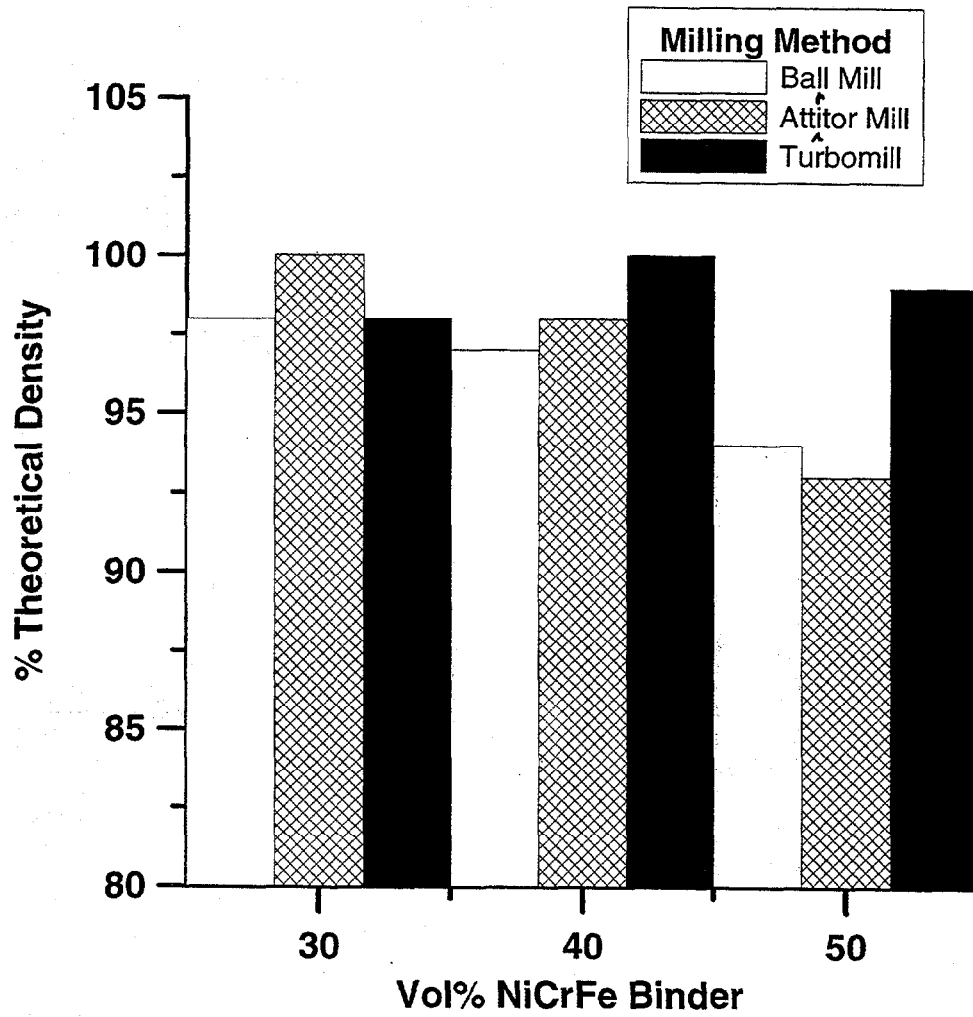


Figure 3. Densification behavior of NiCrFe-TiC composites obtained by three milling methods, batch sintered in Ar.

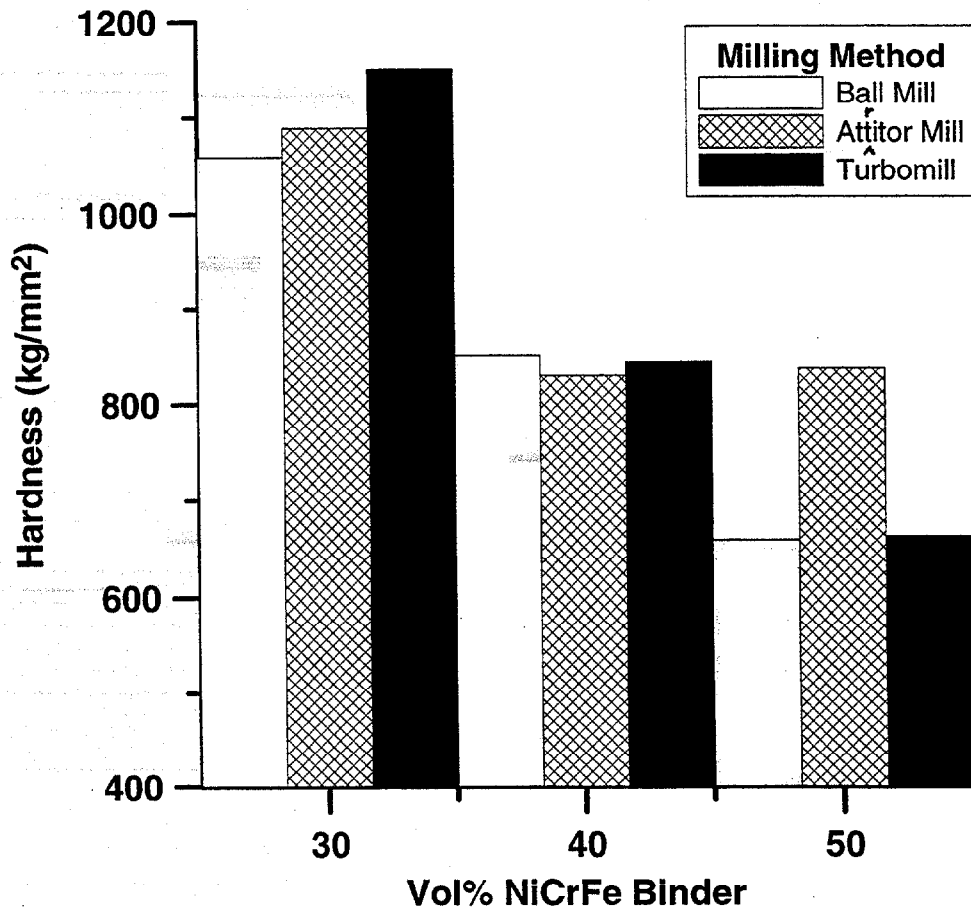


Figure 4. Comparison of Vicker's hardness results for three milling methods for NiCrFe-TiC composites sintering in Ar in a batch furnace.

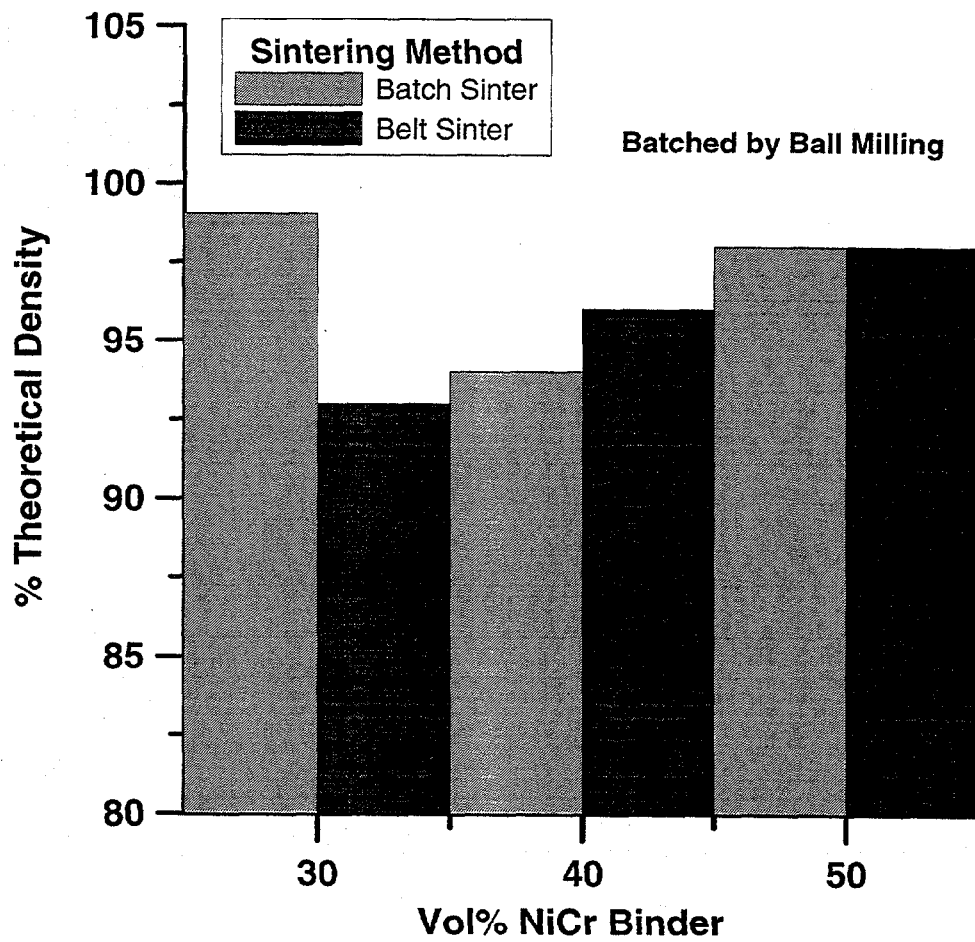


Figure 5. Comparison of densification behavior for NiCr-TiC composites processed by ball milling and sintered by two methods in Ar.

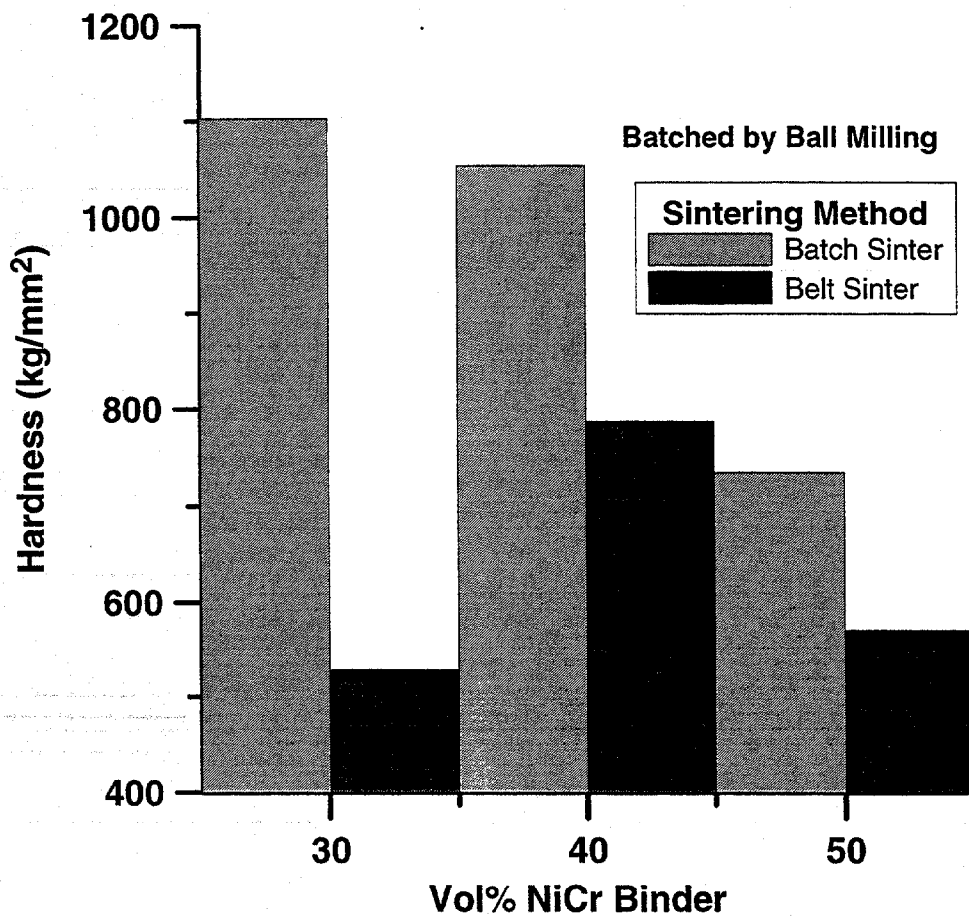


Figure 6. Comparison of Vicker's hardness for NiCr-TiC composites processed by ball milling and sintered by two methods in Ar.

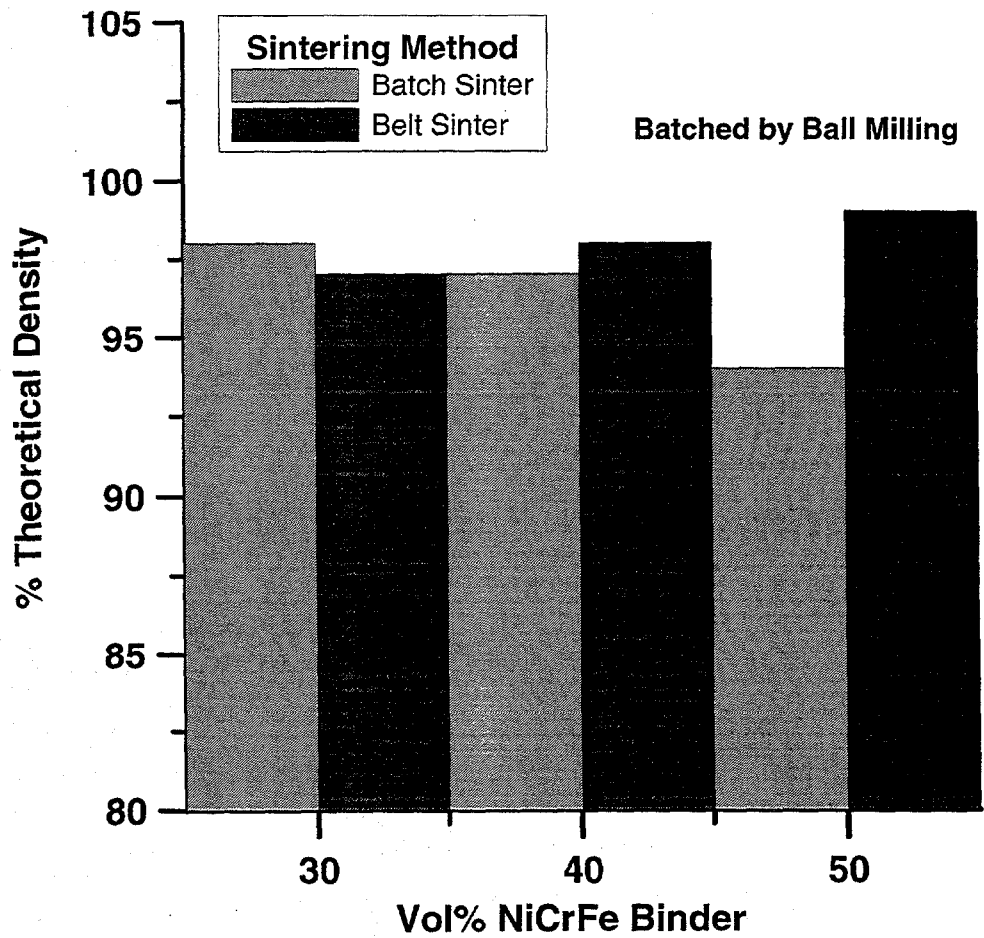


Figure 7. Comparison of densification behavior for NiCrFe-TiC composites processed by ball milling and sintered by two methods in Ar.

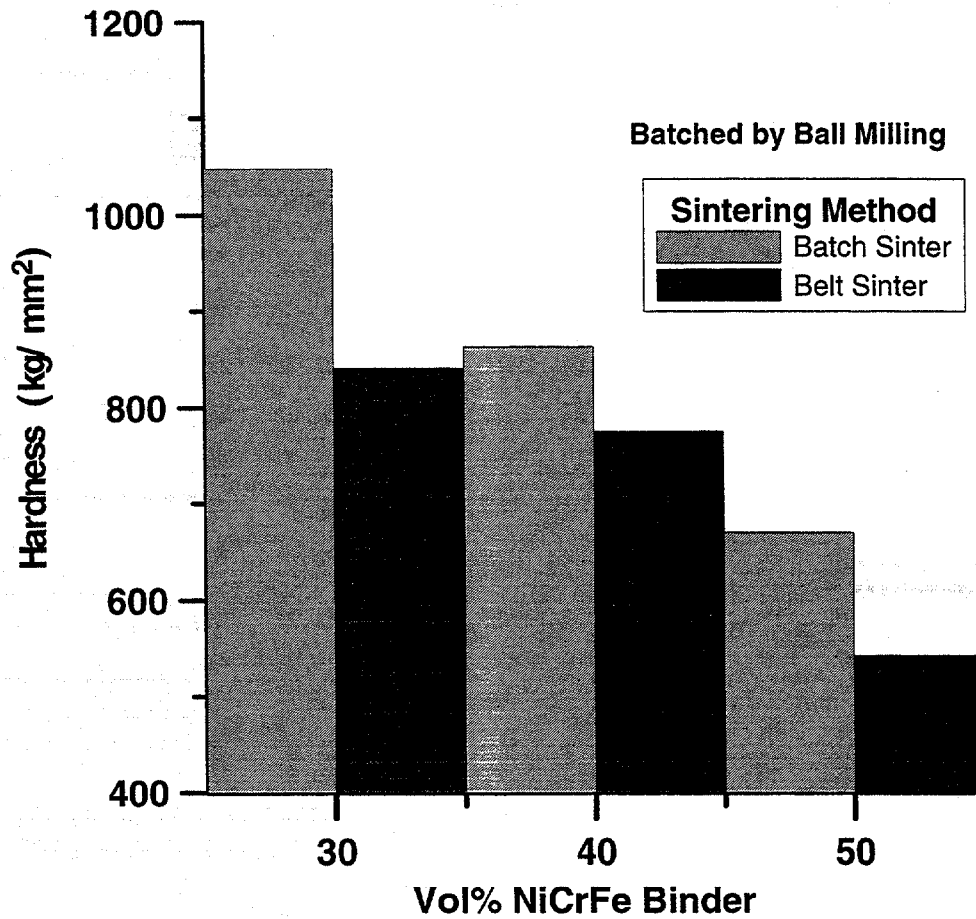


Figure 8. Comparison of Vicker's hardness for NiCrFe-TiC composites processed by ball milling and sintered by two methods in Ar.

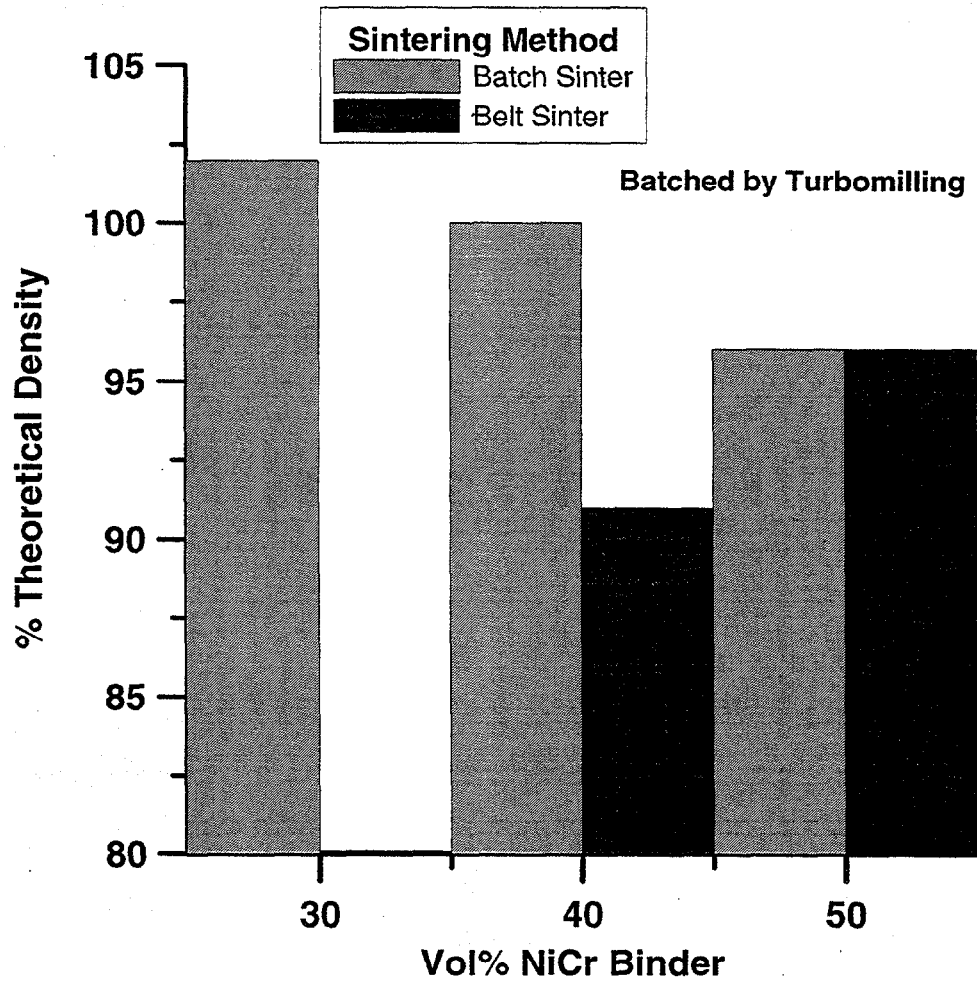


Figure 9. Comparison of densification behavior of NiCr-TiC processed by turbomilling and sintered by two methods in Ar.

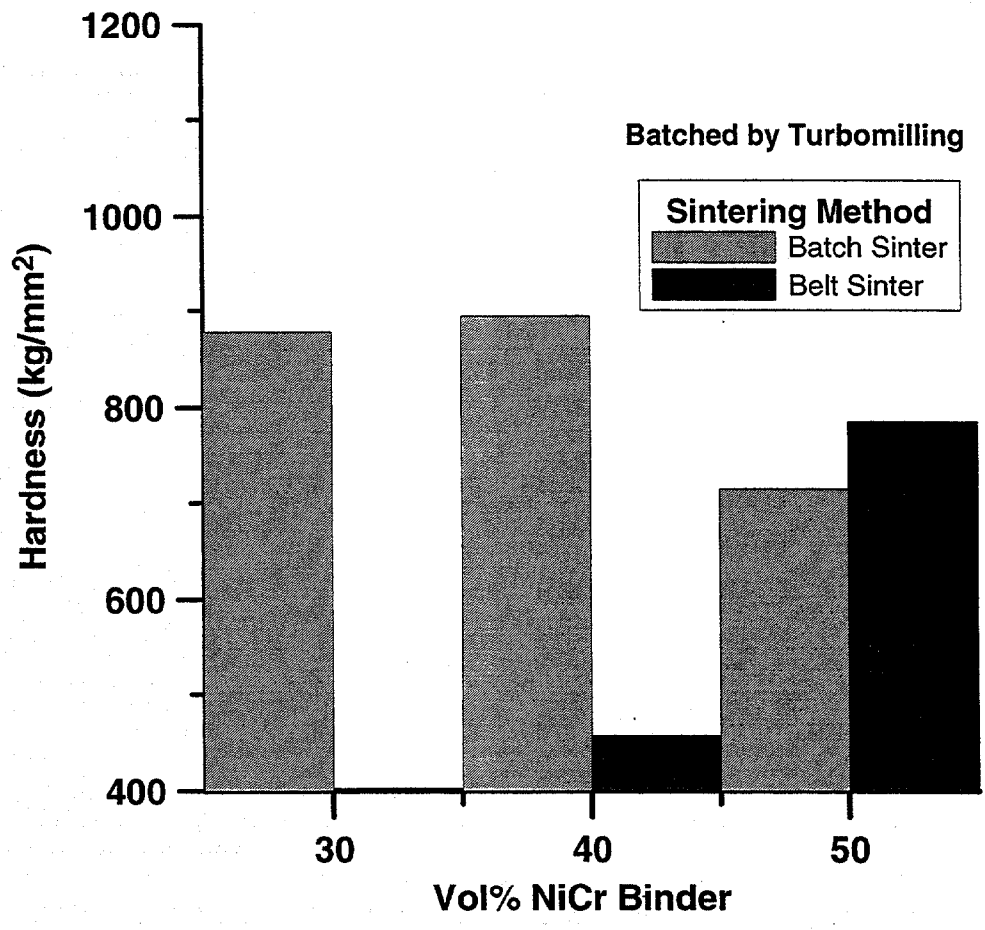


Figure 10. Comparison of Vicker's hardness results for NiCr-TiC composites processed by turbomilling and sintered by two methods in Ar.

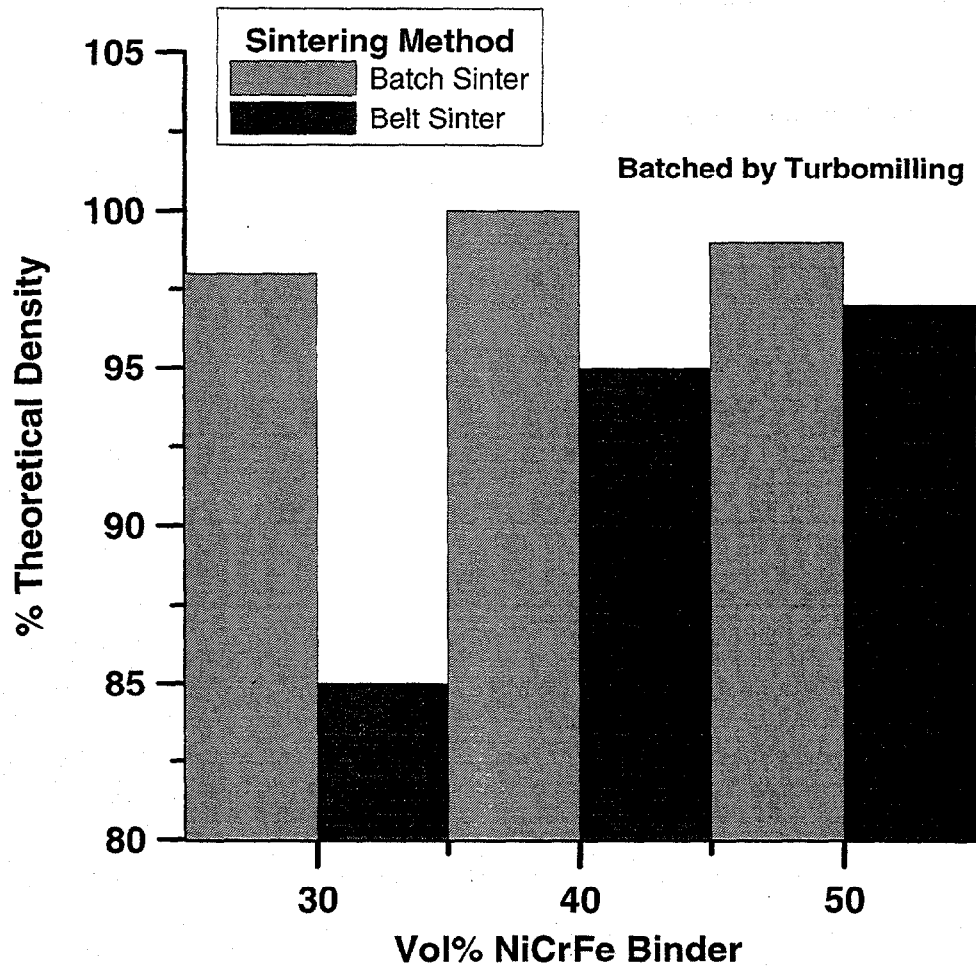


Figure 11. Comparison of densification behavior for NiCrFe-TiC composites processed by turbomilling and sintered by two methods in Ar.

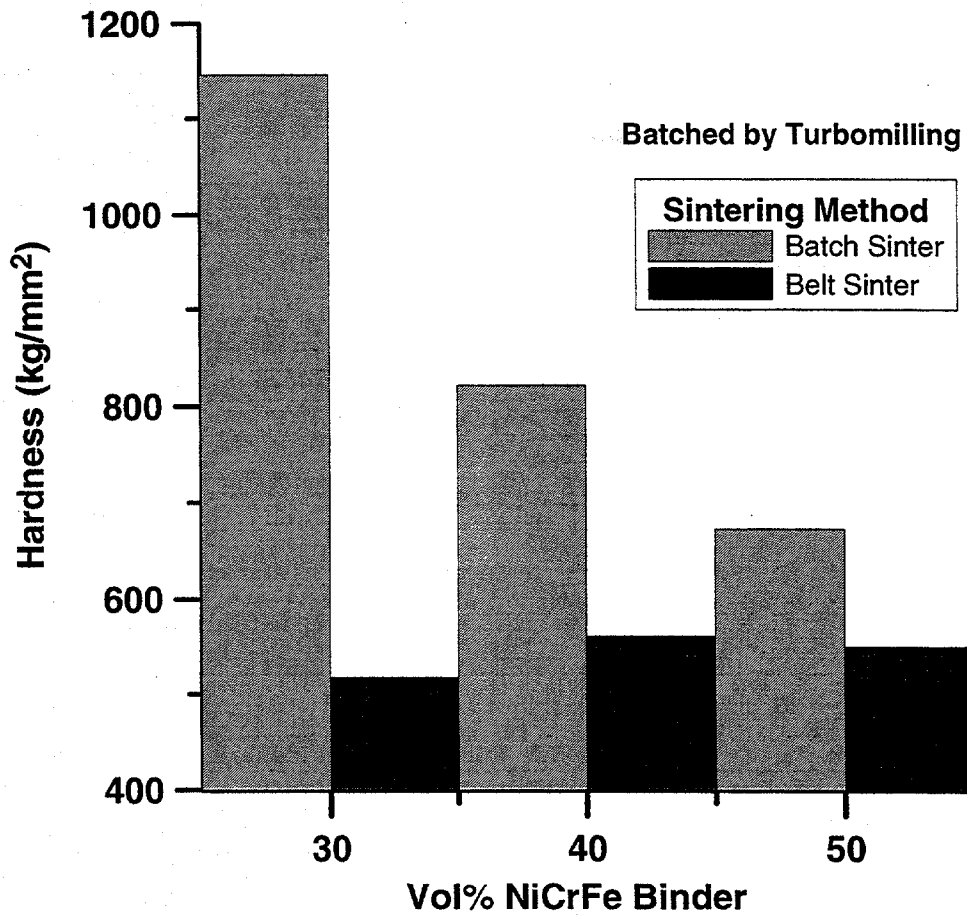


Figure 12. Comparison of Vicker's hardness for NiCrFe-TiC composites processed by turbomilling and sintered by two methods in Ar.

ADVANCED MANUFACTURING TECHNOLOGY

Durability of Diesel Engine Component Materials

Peter J. Blau and Ronald D. Ott
Oak Ridge National Laboratory

Objective/Scope

The objective of this effort is to enable the development of more durable, low-friction moving parts in diesel engines for heavy vehicle propulsion systems by conducting friction, lubrication, and wear analyses of advanced materials, surface treatments, and coatings. The scope of materials and coatings is broad and includes any metallic alloy, intermetallic compound, ceramic, or composite material which is likely to be best-suited for the given application. Parts of current interest include valves, valve guides, and scuffing-critical components, like fuel injector plungers. Hot scuffing is a primary surface damage mode of interest. Bench-scale simulations of the rubbing conditions in diesel engine environments are used to study the accumulation of surface damage, and to correlate this behavior with the properties and compositions of the surface species. The effects of mechanical, thermal, and chemical factors on scuffing and reciprocating sliding wear are being determined, and the results will be used to refine material selection strategies for durability-critical engine components.

Technical Highlights

In FY 2000, the primary effort was focused on developing a capability to evaluate the scuffing resistance of various material combinations for use in unlubricated, high-temperature service in diesel engines. A second FY 2000 project examined the sliding friction and wear of Zr-based amorphous metals under lubricated conditions to determine whether these unique materials have attractive tribological properties. The following paragraphs summarize these efforts.

Project work was temporarily suspended during the summer of 2000; therefore, progress was limited during the second half of FY 2000. A revised series of project milestones was developed to take into consideration special needs in the area for fuel injector materials. The revised milestones for FY 2001 are listed later in this report

(a) *High-Temperature Scuffing of Diesel Engine Components.* The redesign and construction of a new, high-temperature scuffing test system was completed in early summer 2000. Basic characteristics of the machine are:

Contact geometry: pivoting cylinder on flat (see Figure 1)

Drive: variable speed, linear-to-rotary drive train

Loads: variable, dead-weight (minimum 20 N)

Torque sensing: load cell in the upper drive train linkage

Temperatures: room temperature up to at least 750° C

Atmosphere: air

Possible lubricants: liquid, solid, or none

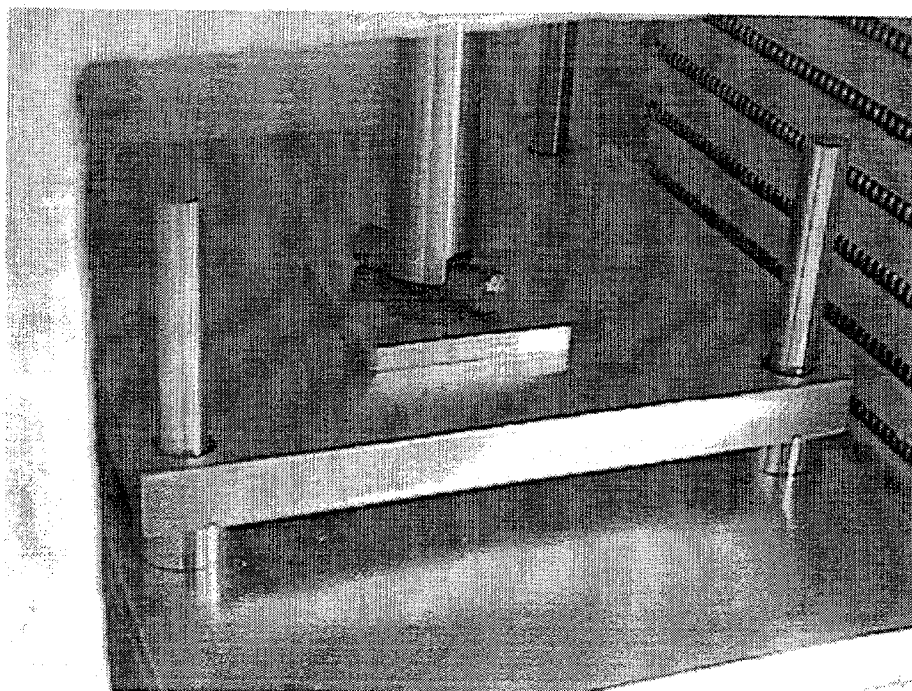


Figure 1. Interior view of the furnace chamber showing the pivoting cylinder-on-flat arrangement of the high-temperature scuffing test system. Fixtures are fabricated from temperature-resistant stainless steel alloy. A dead-weight load is applied from above and the twisting torque is continuously measured.

(b) *Friction and Wear of Metallic Glasses.* Specimens of a Zr-based, multi-component metallic glass were specially prepared for this study by Dr. C. T. Liu's group at ORNL. Pin-on-disk tests were conducted in accordance with ASTM standard G-99 to compare the friction and wear behavior of the metallic glass with that of two, commercial metallic alloys (Stainless steel 303, and Ni-200) tested under the same conditions, all sliding against polished 52100 steel disks. The amorphous alloy's composition (in at%) was 17.9 Cu, 14.6 Ni, 5.0 Ti, and 10.0 Al, with the balance, Zr. The Vickers microindentation hardness numbers of the test specimen materials are given in Table 1. Friction and wear results are summarized in Tables 2(a) and (b).

Table 1. Comparison of Vickers Microindentation Hardness Numbers

Material	HV, GPa* [indentation load 0.98 N]
Amorphous alloy, Zr-Cu-Ni-Ti-Al	5.77
Steel, AISI 52100, annealed (disk test specimen)	3.67
Steel, AISI 303 Stainless	3.46
Nickel, Ni-200	2.31

* kg/mm^2 (previously-used HV units) = $101.9 \times \text{GPa}$

Table 2(a). Friction and Wear Data from Unlubricated Tests
(4.95 N load, 0.26 ± 0.02 m/s sliding speed, sliding distance 100 m, room temp.)

Pin Material	Steady State Friction Coeff.	Pin Wear Rate ($\text{mm}^3/\text{N}\cdot\text{m}$)	Disk Wear Rate ($\text{mm}^3/\text{N}\cdot\text{m}$)	Ratio of Pin to Disk Wear
303 St. Steel	0.94	4.99×10^{-4}	5.91×10^{-4}	0.84
Ni-200	1.11	1.07×10^{-3}	9.82×10^{-4}	1.09
Amorphous alloy	0.74	4.68×10^{-4}	4.54×10^{-4}	1.03

Table 2(b). Friction and Wear Data from Lubricated Tests
(as above but lubricated with 15W40 diesel oil)

Pin Material	Steady State Friction Coeff.	Pin Wear Rate ($\text{mm}^3/\text{N}\cdot\text{m}$)	Pin Wear Ratio (dry/lubricated)	Disk Wear Observations
303 St. Steel	0.17	4.73×10^{-9}	1.1×10^5	fine scratch
Ni-200	0.17	1.39×10^{-8}	7.3×10^4	fine scratch
Amorphous alloy	0.20	8.01×10^{-7}	5.8×10^2	roughened track*

* Material was displaced above and below the plane of the disk surface. This was substantiated by profilometry, but there was no clearly measurable wear groove cross-sectional area, and therefore no wear rate could be obtained.

The amorphous alloy's hardness was greater than that of the other two pin materials, and layman's wisdom would suggest it has better wear resistance, but hardness alone does not determine a material's sliding wear behavior. Under unlubricated conditions, both the wear and average sliding friction coefficient of the amorphous alloy were slightly lower than the other two materials, but this was not the case under lubricated conditions. Despite its higher hardness, the amorphous alloy's wear behavior was worse than the two other combinations when tested in oil. Traditional engine oil additives react with ferrous materials to form anti-friction and anti-wear films. They were not designed for non-ferrous alloys, like the Zr alloy tested here.

X-ray analysis by T. Watkins of ORNL indicated that sliding conditions did not induce a transformation from the amorphous to crystalline state, as has been reported in past studies of other amorphous alloys. It is likely that the relatively low contact pressures and speeds used here did not produce high enough temperatures to induce such structural transformations.

While not encouraging, these preliminary pin-on-disk results should not rule out the use of Zr-based amorphous alloys in other types of tribosystems. Rather they suggest that more research is needed in order to establish both the potential and the limitations of amorphous alloys being considered for wear applications. At the present time, however, no further studies of amorphous metal alloys are planned under this project. A more complete description of this work will be presented and published in 2001 (see 'Publications and Presentations,' below).

Future Plans

- a) Complete room-temperature baseline tests in the scuffing apparatus and prepare for elevated temperature baseline tests.

Status of MilestonesFY 2000 Milestones

- 1) Complete preliminary evaluation of the friction and wear of amorphous alloys and submit report. (June 30, 2000) Status – completed.
- 2) Complete design and construction of high-temperature scuffing test system. (June 30, 2000) Status – completed.

FY 2001 Milestones

- 1) Complete baseline scuffing tests at room and elevated temperature. Submit report. (Previous milestone date changed from September 30, 2000 to December 31, 2000)
- 2) Complete elevated temperature scuffing tests of leading candidate materials and coatings. Submit report. (March 31, 2001)
- 3) Complete design and construction of a computer-controlled fuel injector materials testing system capable of studying the effects of varying injector motions and loading cycles on material response. (September 30, 2001)

Communications/Visitors/Travel

None

Problems Encountered

None.

Publications and Presentations

P. J. Blau (2001) "Friction and Wear of a Zr-Based Amorphous Metal Alloy under Dry and Lubricated Conditions," accepted for presentation at Wear of Materials 2001, April 23-26, and publication in *Wear* journal, expected in the fall of 2001.

NDE of Ceramic Valves for Diesel Engines – Jiangang Sun, William A. Ellingson, (Argonne National Laboratory), and Seung-Kun Lee (Caterpillar Inc.)

Objective/Scope

Emission reduction in diesel engines designated to burn fuels from several sources has lead to the need to assess ceramic valves to reduce corrosion and emission. The objective of this work is to evaluate several nondestructive evaluation (NDE) methods to detect defect/damage in structural ceramics valves for diesel engines. There are three tasks to be carried out in this work: (1) Finalize correlation of NDE to machining damage. This limited effort will conclude the earlier work to correlate NDE data with mechanical properties of machining-damaged Si_3N_4 ceramics. Elastic optical scatter method will be used to examine these specimens and the NDE data will be correlated with flexural strength. (2) Correlate NDE data with mechanical properties for fatigue/wear damaged samples. These include rotary fatigue, dynamic fatigue, impact/sliding wear, and possible thermal shock testing. The induced damage will be assessed using various NDE methods including dye penetrant, optical scatter, impact acoustic resonance (IAR), X-ray CT, thermal imaging, and others. NDE data will be correlated with those from characterization tests including mechanical strength, SEM, and others. (3) Conduct NDE studies of full-size engine valves. In this part of the work, full sized ceramic valves will be produced for testing in a single cylinder test engine. These valves will be examined using NDE techniques developed at Argonne.

Technical Progress

1. Elastic Optical Scattering NDE for Machining Damage

During this period we studied fifteen AS800 and SN235 and thirteen CFI Si_3N_4 ceramic specimens that were obtained from Caterpillar Inc. The samples were machined into flexure bars having the dimensions shown in Fig. 1.

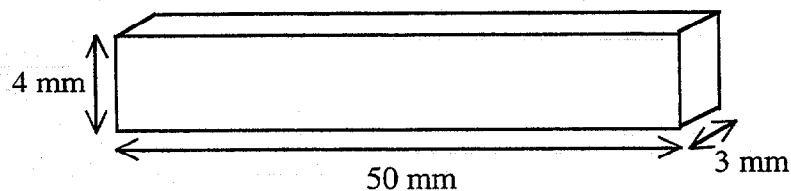


Figure 1. Schematic diagram of a Si_3N_4 ceramic flexure bar.

The objective of this study is to correlate the optical laser scattering data to the flexure strength of the ceramic bars. The optical laser scattering data will be correlated to strength data from four-point-bend tests. The four-point-bend test will apply tensile stress and compression stress to the broad sides (50 mm x 4 mm) of the bar. The maximum stress in the material will occur at and near the surface of the bar on broad sides. Hence, the greatest probability of fracture will come from defects that exist on the surface and near subsurface of the bar.

In order to increase data acquisition speed, five flexure bars were stacked with the broader surfaces exposed for scans. Optical scatter data were collected over a 30-mm x 19-mm region at a resolution of 10 μm . Figure 2 shows typical laser scatter sum and ratio image data for

AS800, CFI, and SN235 ceramics. Based on the theory of optical scattering for the laser scatter system, defect and damage should appear brighter in sum images and darker in ratio images. It is seen that suspected spot defects are evident over the entire surfaces of AS800 and SN235 specimens. Suspected machining-damage lines are also found on the SN235 and AS800 specimens. For the CFI material, the scatter images in Fig. 2 do not show clear defect/damage features.

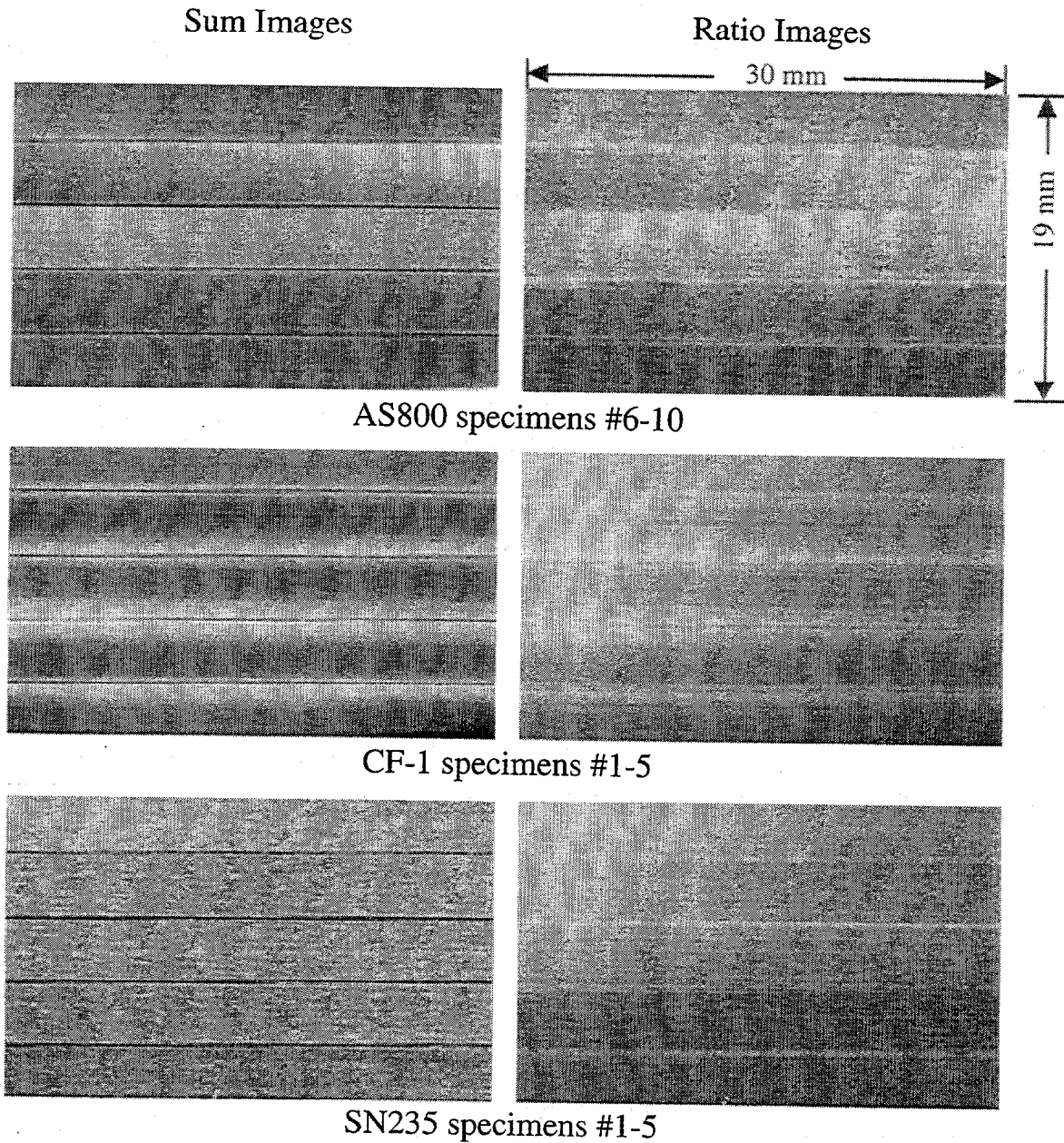


Figure 2. Optical scattering sum and ratio image data of AS800 specimens #6-10, CFI specimens #1-5, and SN235 specimens #1-5.

Previous studies on limited specimens showed that statistical parameters of the optical scattering image data can be correlated with machining conditions and mechanical properties for

a variety of machined Si_3N_4 specimens. The relevant statistical parameters are the coefficient of variance C_v (standard-deviation/mean) and skewness C_s (skew/mean). Figures 3-5 show plots of C_v and C_s for all specimens of AS800, CFI, and SN235, respectively. The error bars represent the values for each side of the bar with the average between the two values represented as the data point. The large spread of data for some specimens is due to a color variation in the material. Figure 6 shows the optical scattering sum images obtained on the two broad sides of AS800 specimen #6. It is evident that the optical scatter intensity is strongly affected by the color variation in the material. However, a close examination of the image data reveals that all defect features are still present in the data provided that the image can be properly scaled to eliminate the mean intensity variation. Furthermore, it is understood that the color variation in specimen is due to material processing and it may not affect the strength. Therefore, a filtering scheme is being derived which accounts for the local color variation into a local mean intensity image instead of using a constant mean intensity value for the entire image. Statistical parameters will then be calculated based on the local deviation from the mean intensity image. It is expected that this scheme will effectively eliminate the scatter intensity variation due to specimen color change or presence of surface contamination, so that a reliable correlation of optical scatter data (e.g., C_v or C_s) with specimen strength may be established that is not affected by specimen size.

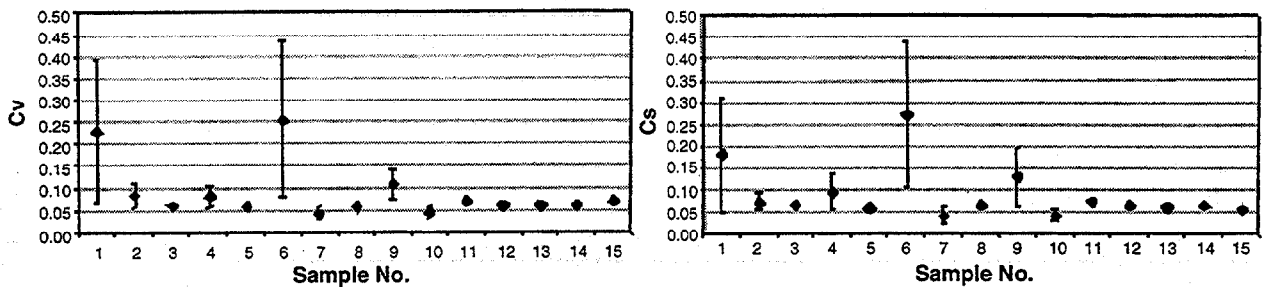


Figure 3. Statistical parameters C_v and C_s for fifteen AS800 samples

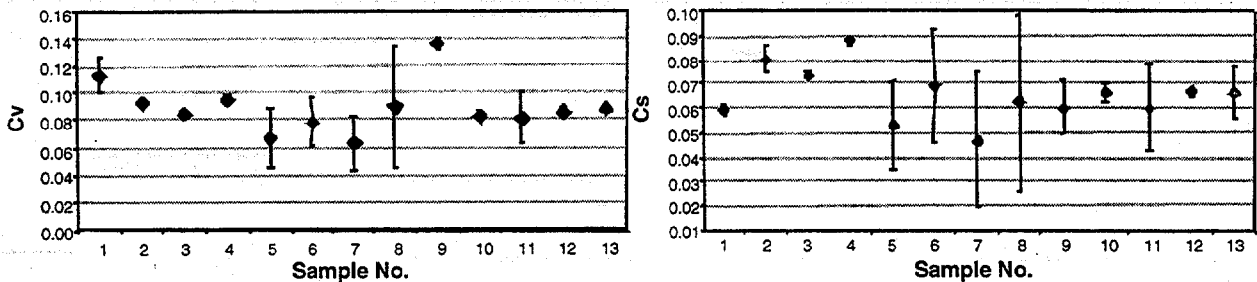


Figure 4. Statistical parameters C_v and C_s for thirteen CFI samples

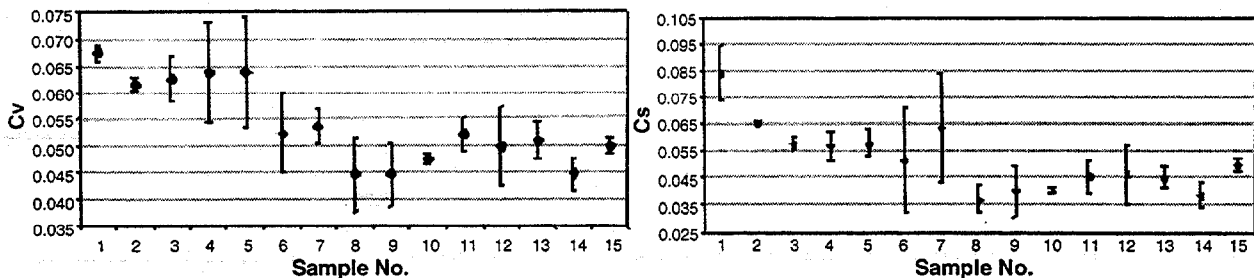


Figure 5. Statistical parameters C_v and C_s for fifteen SN235 samples

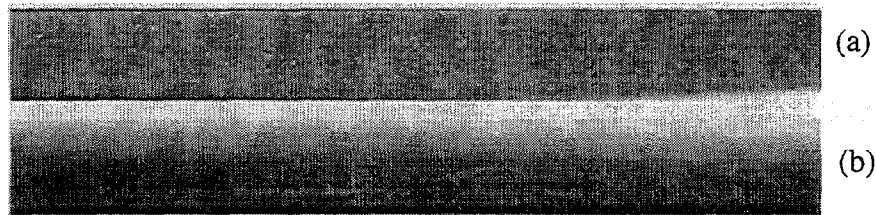


Figure 6. Optical scattering sum image data obtained on (a) side 1 and (b) side 2 of AS800 specimen #6.

During this period we have received from Caterpillar all GS44, AS800, CFI, and SN235 flexure-bar specimens that have been tested by four-point bending to determine their strength. Figure 7 shows a photograph of three broken GS44 specimens. It is seen that fracture occurs at one or two locations on the bending surface. Examination of these fracture surfaces and its comparison with previously obtained optical scatter data is being conducted to determine if there is a correlation between the fracture location and features detected by optical scattering.

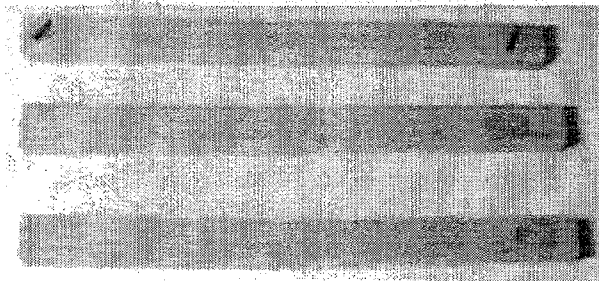


Figure 7. Photograph of broken GS44 bars from four-point bending test.

2. NDE Study of Silicon Nitride-Steel Joints

During this period we received two sets of silicon nitride-steel-joint tensile-rod specimens from Caterpillar, with a total of nine small joints as shown in Fig. 8 and ten large joints as shown in Fig. 9. The joints were made by Honeywell using a brazing method with Ag-Cu as a brazing agent. Mo and Ni were used as insert materials for accommodating thermal expansion mismatch between ceramic and steel. There are two Ni inserts and one Mo insert in the joint, and each layer has brazing agent as shown in Fig. 10. The small joint specimen is 76-mm (3") long, 6.3-mm (1/4") in diameter, and the joint region is located in a reduced-diameter gauge section of 3.2-mm (1/8") in diameter. The large joint specimen is 156-mm (6 1/8") long, 14-mm in diameter, and contains two joint sections at both ends of an 18.5-mm long ceramic section at the middle of

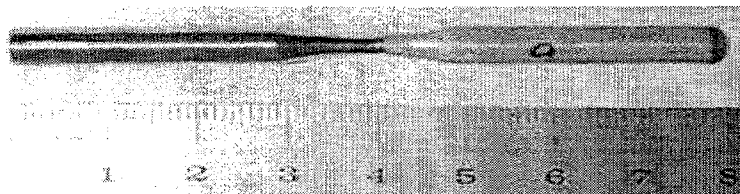


Figure 8. Photo of a small joint from Caterpillar, Inc.

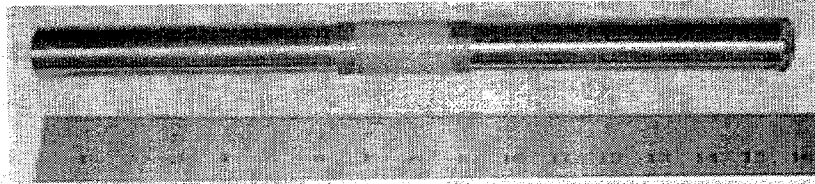


Figure 9. Photo of a large joint from Caterpillar, Inc.

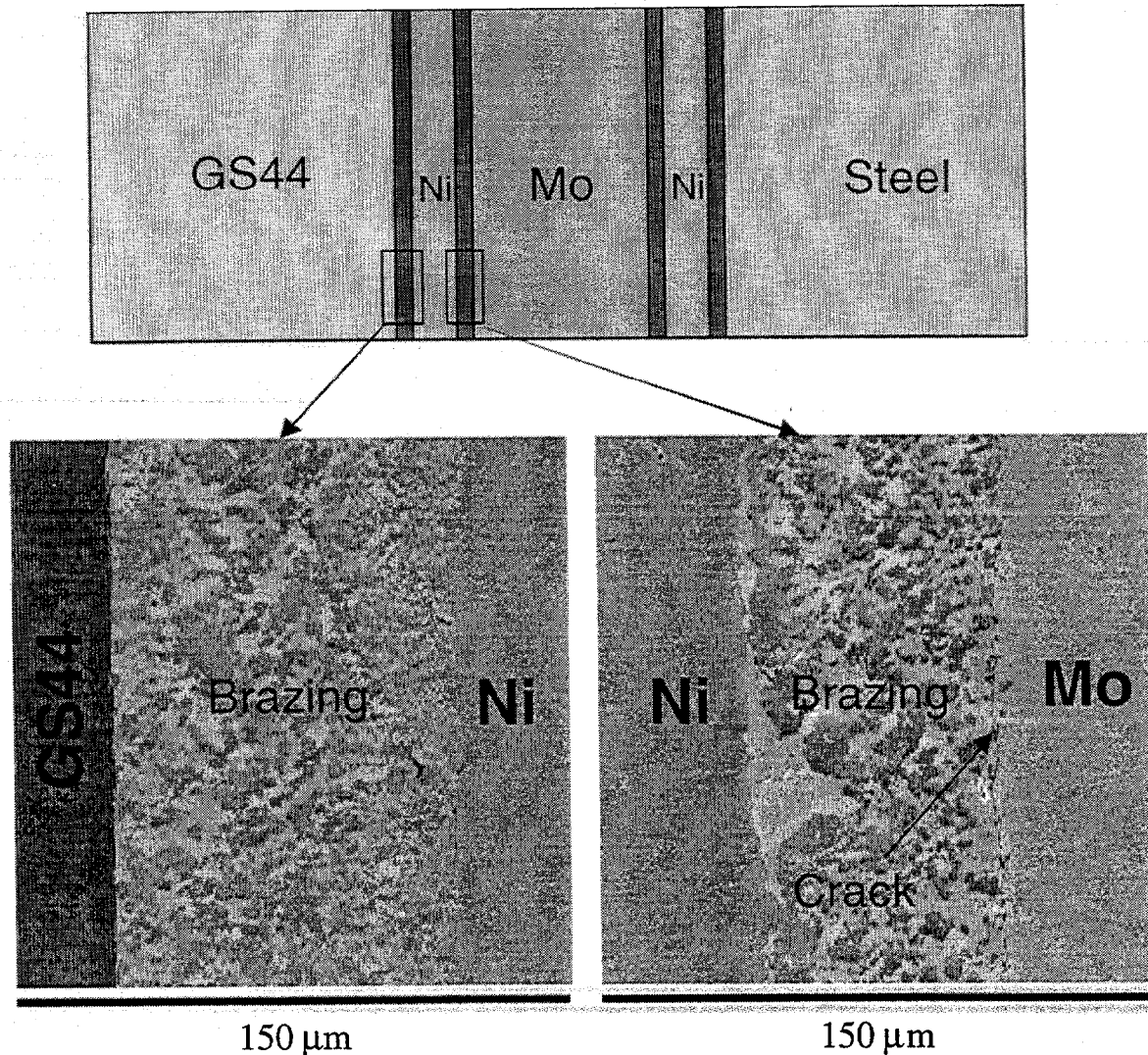


Figure 10. Schematics of joint section and SEM images of joint interfaces showing a crack between Mo and brazing material.

the specimen. Microstructural analysis of the silicon nitride-steel joint was conducted by Caterpillar, Inc. It was found (see Fig. 10) that there is a composition gradient in the brazing material (Ag versus Cu) between silicon nitride and Ni. Note that a delamination (cracking) was found in the interface between brazing and Mo. It could be the weakest point in this joint.

NDE techniques capable for characterizing these joint specimens have been evaluated. These techniques include impact acoustic resonance, thermal imaging of transient heat conduction through interfaces, immersion ultrasonic scanning, and X-ray CT imaging.

The impact acoustic resonance technique may determine characteristic resonance frequencies and damping capacities of a joint. Previous studies on other samples (not joints) showed that characteristic frequency and damping capacity were affected by cracking in a sample. It is expected that same phenomenon should be found for these joints.

Initial test with thermal imaging technique was conducted to determine the heat transfer rate across the interfaces. By inserting the steel end into boiling water, transient heat conduction is generated from the steel section to the insert materials and eventually to the ceramic section. An infrared digital camera is focussed on the joint region to examine the heat transfer for possible resistance variation at various interfaces. The camera has a very high sensitivity with a temperature resolution of better than 0.01°C . Current issue of using this technique is to find a suitable coating material that can increase the emissivity of the metal surfaces.

Many studies using oblique ultrasonic scanning on joints have been reported in the literature. It was shown that this technique has sensitivity on detecting distributed porosities and cracks. We are currently applying this technique for the joints. We use an immersion oblique pitch-catch setup that can scan the joint interfaces. Because cracking between the Mo and Ni is of major concern, the study is focussed on this interface. However, there are many issues that affect the data sensitivity and accuracy, such as geometry effect, signals from interface reflection against transmission, and selection of various mode-converted beams within the sample.

X-ray CT for the joint is being evaluated. Because the crack gap is very narrow, estimated to be $0.4\ \mu\text{m}$ from the images in Fig. 10, so the technique is unlikely to resolve an individual crack. However, X-ray CT may detect groups of cracks or other flaws that may affect the strength of the joints.

Status of Milestones

Current ANL milestones are on or ahead of schedule.

Communications/Visits/Travel

Visit:

1. Dr. S. K. Lee of Caterpillar Inc. visited Argonne on May 12, 2000 to discuss project details.

Communication:

1. Discussions have been taking place with Eaton Corporation and St. Gobain Industrial Ceramics to obtain additional machined specimens with carefully controlled machining conditions.

Problems Encountered

None this period.

Publications

None this period.

INTERMETALLIC-BONDED CERMETS

P. F. Becher, C. G. Westmoreland, and S. B. Waters
Oak Ridge National Laboratory
Oak Ridge, TN 37831-6068

Objective /Scope

The goal of this task is to develop materials for diesel engine applications, specifically for fuel delivery systems and wear components (e.g., valve seats and turbocharger components). This will require materials which have a minimum hardness of 11 GPa and a thermal expansion coefficient of between 10 to $15 \times 10^{-6}/^{\circ}\text{C}$ over the temperature range of 25° to 300° C. The material should also have excellent corrosion resistance in a diesel engine environment, flexure strength in excess of 700 MPa, and fracture toughness greater than $10 \text{ MPa}\sqrt{\text{m}}$ to ensure long term reliability. The material should also be compatible with steels and not cause excessive wear of the steel counter face. The upper temperature limit for fuel delivery systems applications is 540° C, and for the other wear applications, the limit is 815° C. Finally, the total material processing costs for these advanced materials should be competitive with competing technologies such as TiN or other ceramic coatings on high-speed tool steels.

Technical Highlights

Additional processing studies were conducted to refine the reaction sintering process which employs a mixture of submicron TiC with 2 wt. % Mo powder combined with a mixture of two parts Ni plus one part NiAl. This reaction sintering process has been shown to result in a very uniform distribution of the resultant Ni_3Al binder phase, as well as an average TiC grain size ≤ 1 micron. Previous fabrication studies using Ni_3Al powders consistently showed that large Ni_3Al -rich regions and/or large pores were introduced, which is not the case with the reaction sintering approach. Using the reaction sintering approach, dense cermets consisting of submicron grain sized TiC with 60 vol. % Ni_3Al have now been fabricated.

The mechanical properties of TiC- Ni_3Al cermets with an average TiC grain size of 0.6 to 0.8 microns are comparable to those obtained earlier with the cermets where the TiC grain size of 3 – 5 μm . An example is seen in the comparable fracture toughness values in Figure 1, which compares results for materials produced by normal sintering, reaction sintering, and melt-infiltration sintering. Note that the toughness values represent the plateau values from R-curve measurements obtained with a rigorous fracture mechanics specimen (i.e., the applied moment double cantilever beam specimen). The increase in toughness with increased Ni_3Al content is consistent with the observations of the toughening contribution obtained from plastic flow of the Ni_3Al ligaments spanning the cracks.

The linear thermal expansion coefficients (20° to 620°C) of the cermets also increase as the Ni₃Al content is raised, Figure 2. This is expected as the expansion coefficient of the Ni₃Al is about double that of the TiC. Based on the current thermal expansion data for the TiC-Ni₃Al cermets, coefficients in excess of $10 \times 10^{-6}/^{\circ}\text{C}$ can be achieved in this system with Ni₃Al additions of ≥ 40 vol. %.

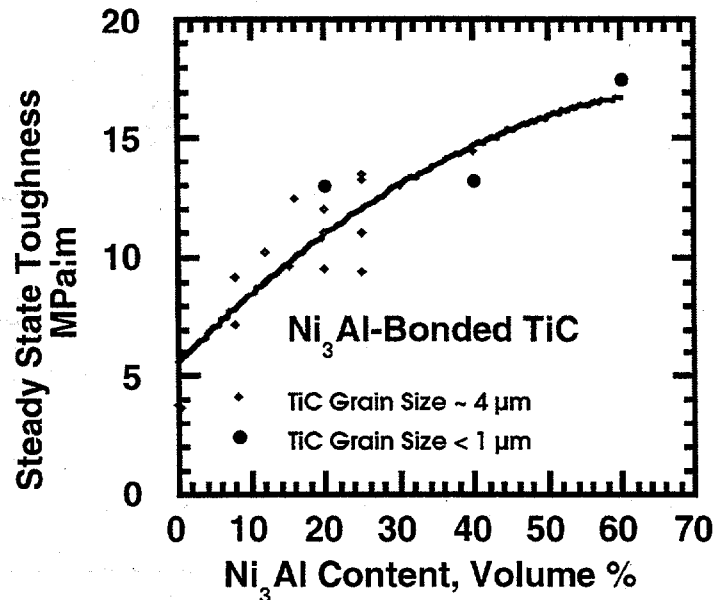


Figure 1. The fracture toughness of the TiC-Ni₃Al cermets increases with Ni₃Al content and is virtually independent of the TiC grain size.

Aside from the TiC-Ni₃Al cermets from reduction of the TiC grain size to eliminate cleavage of the TiC grains, earlier studies at SIU (Wittmer et al.) and at ORNL (Tiegs et al.) showed that modifying the TiC grain morphology to achieve very rounded grains improved the cleavage resistance. In these studies, separate minor chemical additions or modifications to the intermetallic composition were used. By substituting iron for both the Ni and Al constituents to form an intermetallic of Ni_{1.5}Fe_{2.0}Al_{0.5} was found to result in both rounded TiC grains and quite promising mechanical properties at 30 vol. % Ni_{1.5}Fe_{2.0}Al_{0.5}. The linear thermal expansion of this same material was measured to be $9.71 \times 10^{-6}/^{\circ}\text{C}$.

In the current task, samples of submicron TiC-40 vol. % Ni_{1.5}Fe_{2.0}Al_{0.5} were prepared by pressureless sintering by sintering at 1400°C for 1 h in vacuum. The intermetallic phase exhibits a face-centered cubic type structure as does Ni₃Al and the sintered cermets exhibited a porosity of ~ 5 %. The pore ranged in size from < 1 micron to ≤ 100 microns. The fracture strength of this cermet in four point flexure was found to be 917 ± 116 MPa (8 breaks) with the large scatter attributed to the large pores present. Improvements in the processing are expected to reduce the porosity and improve the strength of this material.

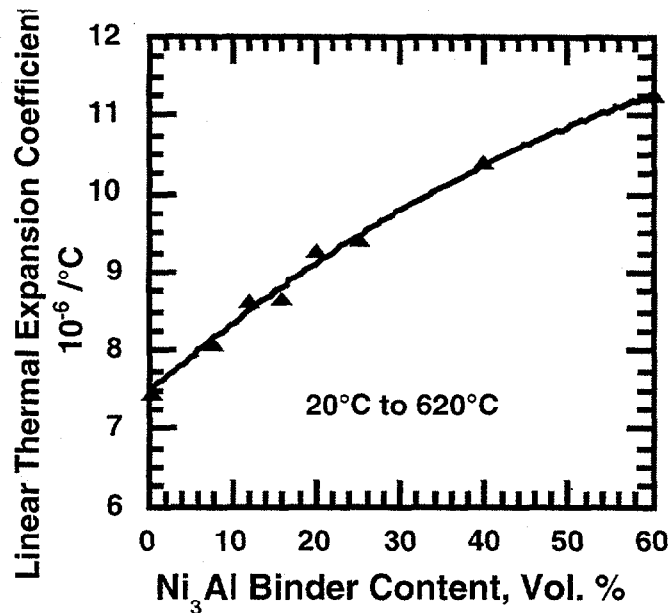


Figure 2. The thermal expansion coefficients steadily increase with Ni_3Al content.

Status of Milestones

On Schedule

Communication/Visits/Travel

Additional samples of TiC-40 vol. % Ni_3Al cermets prepared and shipped to Cummins Engine for evaluation. Review of cermet efforts was held at ORNL on September 8, 2000 to discuss future directions with Tom Yonushonis, Randy Stafford, and Malcolm Naylor of Cummins Engine, Kevin McNerney and Jim Stephen of CoorsTek, Dale Wittmer of Southern Illinois University, Al Weimer of the University of Colorado, and Ray Johnson and Paul Becher of ORNL.

Problem Encountered

None

Publications

K.P. Plucknett and P.F. Becher, "TiC/ Ni_3Al Composites Prepared by Melt-infiltration Sintering: Processing and Microstructure Development," J. Am. Ceram. Soc., accepted for publication.

TESTING AND CHARACTERIZATION

Task Title: NDE/C Technology for Heavy Duty Diesel Engines:
Fuel Delivery and Insulating Materials

Principle Investigator: W. A. Ellingson
Argonne National Laboratory

Objective/Scope

The objective of the work in this task, part of the Testing and Characterization research area of the Heavy Vehicle Propulsion System Materials Program, is to develop enabling nondestructive evaluation/characterization (NDE/C) technology. Specifically, this project addresses development of advanced NDE/C technology for: (a) advanced fuel delivery systems (including injector nozzles), and (b) insulating materials for reduced heat loss in the combustion zone. Fuel delivery systems for heavy-duty diesel engines are complex, very expensive and represent a significant portion of the cost of a heavy vehicle diesel engine. High pressures inside these fuel delivery systems contribute to poor fuel delivery and hence poor emissions. Materials development is part of Goal 3 of the heavy vehicle propulsion materials program. Insulating materials are also a significant materials development area because of the improvement in efficiency obtained if reduced heat losses can be obtained. NDE/C technology that could provide information for cost reduction as part of production as well as provide information as part of engine component surveillance, would be a significant contribution to the goals.

Technical Highlights

NDE/C technology developments continued to focus on fuel delivery systems and insulating materials, with an emphasis on ceramic materials.

NDE for Fuel Delivery Systems

We reported last period that we had begun discussions with Cummins Engines regarding ceramic fuel injector components. This period we are reporting on the initial NDE results from these injector pins. We received 6 injector pins for study. There were 3 sets of 2 pins each of: (a) Ceria stabilized Zirconia (CSZ), (b) Magnesia (MgO) stabilized Zirconia from Australia (Carpenters), and (c) Magnesia (MgO) stabilized Zirconia from Coors. The test specimens (see Figs.1 and 2) are stepped right circular cylinders. These are machined to critical dimensions and any defects in the material or caused by machining could cause severe engine problems.

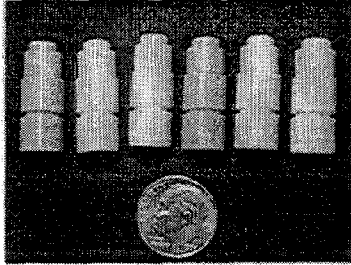


Fig. 1
Photograph of 6 ceramic fuel injector
pins supplied by Cummins Engine

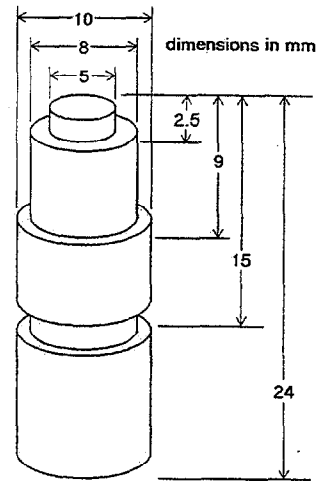


Fig. 2
Schematic diagram of fuel
injector pins

In order to evaluate these fuel pins for machining-induced damage, the ANL developed elastic optical scatter system (see Fig.3) was utilized. In this system, a low power polarized laser is used to provide incident, focused light onto the test sample. Since the ceramic materials are known to be optically translucent as a function of wavelength, the laser light will penetrate below the surface of the material and scatter back to a set of special detectors. Analyzing the output of the special detectors allows determination of variations within the materials. In order to assess this technology, it is necessary to systematically assess the optical transmission characteristics of the various materials. The approach is to use well-defined step wedges of known thickness to establish the penetration and scatter characteristics as a function of wavelength. Cummins prepared step wedges of the various materials as shown in the photograph in Fig. 4 below. The optical transmission data are now being acquired. We decided to scan the cylinder anyway to obtain preliminary data. These ceramic fuel injector pins were scanned on the outer surfaces just below the first shoulder as noted in the diagram shown in Fig.5. The pins were mounted on a rotation stage such that the outer surface of each pin was vertical. The data were obtained by stepping each pin through 1 degree steps thus providing 360 individual steps around the surface. This results in each step being about 60um. In the vertical direction, data were acquired in a 1mm band just below the shoulder. These were acquired in 100 individual 10um steps. Fig.6 below shows the image scan data from each of the specimens. Note that the non-uniformity in the gray scales of the images, horizontally, is caused by poor center of rotation of the test samples and not caused by material non-uniformities. If careful attention is paid to some of the detail in the image data, there appear to be differences among the materials. It is not clear at this time that these differences be quantified until we are able to precisely align to a more exact center of rotation. Next period we plan to obtain precision centering stages, using precision machine tool chucks, to allow more exact centering. A precision dial indicator will also be used for alignment. In addition, next period we plan to try to obtain data on the top of the shoulder. Currently we could not do this because of issues with mechanical stages

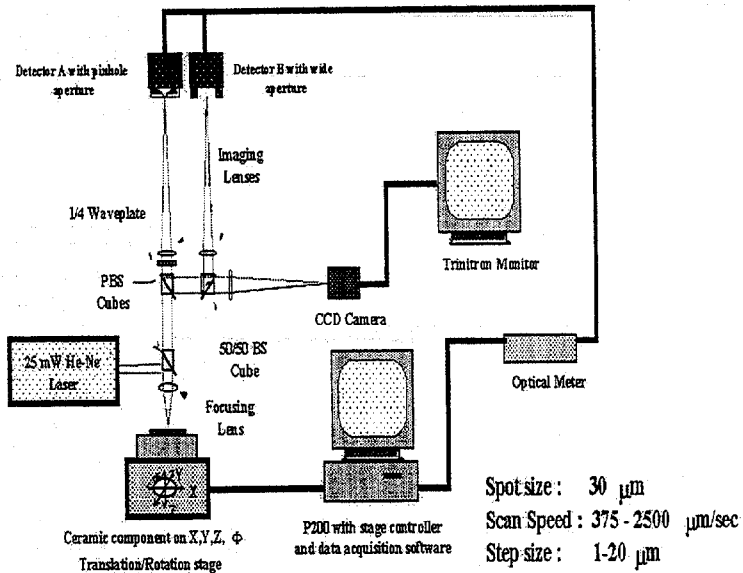


Fig. 3

Schematic diagram of laser-based elastic optical scatter system used to study subsurfaces and surfaces of ceramics

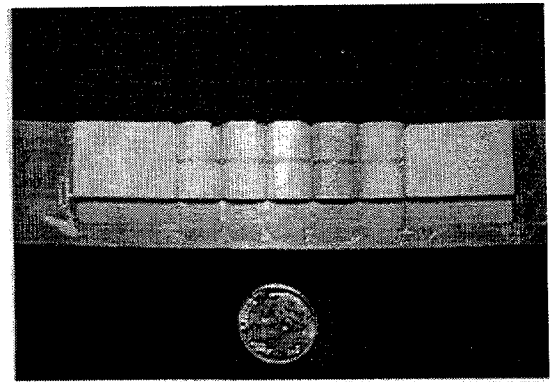


Fig. 4

Photograph of step wedges of various ceramic materials. Note the wedges are shown still mounted to the steel bar used

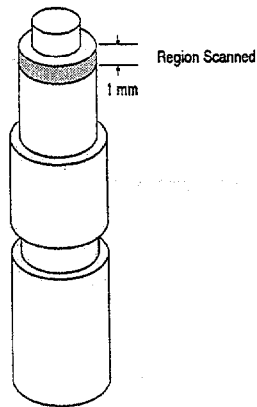


Fig. 5

Diagram showing location of NDE data acquisition

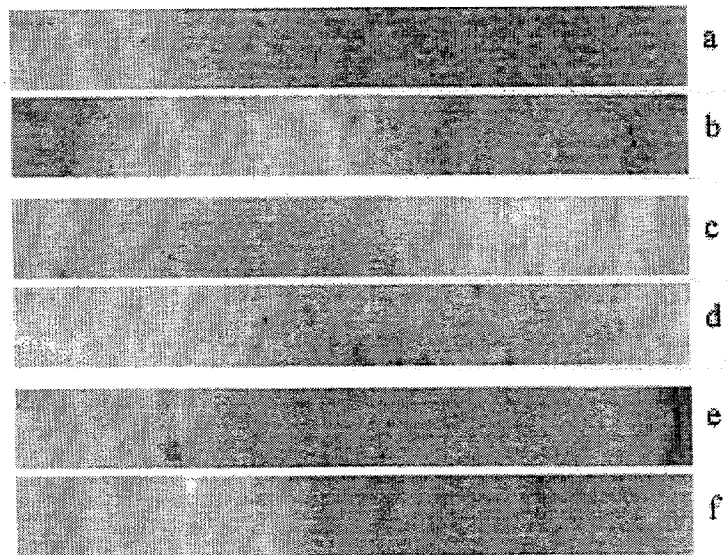


Fig.6

Elastic Optical Scatter Image Data from Each of the Fuel Pins: a),b) Ceria Stabilized Zirconia, c),d) Ytria Stabilized Zirconia, e),f) Australian Zirconia

NDE for Insulating materials

Discussions continue with staff at Caterpillar Inc., about use of ceramics as insulating materials. As now planned, the NDE/C efforts will begin in FY 2001 to be consistent with the work plan at Caterpillar Inc.

Testing and Evaluation of Advanced Ceramics at High Temperature

J. Sankar, A.D. Kelkar, D.E. Klett, Q. Wei and S. Yarmolenko

NSF Center for Advanced Materials and Smart Structures
Department of Mechanical Engineering,
North Carolina A & T State University, Greensboro, NC 27406

Objective/Scope

Use of advanced ceramics in heavy vehicle propulsion systems can significantly increase the operation temperature, and consequently improve the efficiency, and reduce pollution. Among ceramics for this application, silicon nitride has been considered to be one of the most promising candidates. Silicon nitride has high strength at elevated temperatures; it has very small thermal expansion coefficient, and therefore, good thermal shock resistance; it is chemically inert and can be used under hostile working conditions. However, like all ceramic materials, silicon nitride suffers from poor fracture toughness. In the last two decades, tremendous effort has been practiced to improve the fracture toughness of silicon nitride ceramics. Presently, silicon nitride ceramics with moderate to high fracture toughness can be produced through gas sintering, hot isostatic pressing (HIPing), etc. Since no external reinforcement is added to enhance the fracture toughness of this kind of material, it has been called self-reinforced silicon nitride.

In addition, heavy vehicle propulsion application needs both newer and innovative materials for various applications and as well as innovative interdisciplinary approaches to understand their behavior.

We have been participating in this research project to study the high temperature behavior of gas sintered silicon nitride and other ceramic systems in an interdisciplinary way in the recent years.

The tasks of our work includes the following:

- To understand the high temperature mechanical performance (creep, fatigue) of self-reinforced silicon nitride ceramics;
- To understand the environmental effect on the high temperature mechanical behavior of self-reinforced silicon nitride ceramics;
- To understand the microstructures of the silicon nitride ceramics, and
- To understand the effect of surface engineering (coating) on the mechanical properties of silicon nitride and environmental effect on ceramic systems performance.
- To investigate the effect of Partially Stabilized Zirconia (PSZ) thermal barrier coating on diesel engine performance.
- To use Finite Element Methods (FEM) to understand the behavior of the various materials systems under investigation through modeling.

Technical Highlights

Introduction

In mid 80s, Si₃N₄ ceramics with high fracture toughness had been produced through composition and microstructure design such that the fracture toughness reached ~10 MPa.m^{1/2}. One of the newer Si₃N₄ ceramics, GS44, has been developed by AlliedSignal with yttria, alumina and magnesia as sintering aids. This material has moderate to high fracture toughness (>8.0 MPa.m^{1/2}) and quite high room-temperature strength. The elongated grains work in such a way that crack bridging, pull-out of these grains and crack deflection mechanisms effect the reinforcement and lead to much improved fracture toughness. However, it was found that the creep resistance of this material is remarkably decreased at temperatures greater than 1100°C.

It is well recognized that the amorphous grain boundary and multiple junction phases in silicon nitride ceramics lead to creep processes via solution-precipitation, grain boundary sliding and cavitation at high temperatures. A recent theoretical consideration on the tensile creep of silicon nitride has even correlated the creep strain rate with the amount of amorphous second phase, which showed that the creep strain rate increases dramatically with the fraction of the amorphous second phase. According to the model, it is desirable to minimize the amount of amorphous second phases, or to re-crystallize these phases by any means possible.

Liu *et al.* at Oak Ridge National Laboratory have studied the effect of heat-treatment on the creep behavior of GS44. They conducted conventional furnace annealing and microwave annealing on the materials and carried out tensile creep tests on specimens machined out of the as-received and heat-treated ceramic tiles. Improvement in creep behavior by microwave annealing has been reported. They did not provide microstructural analysis. In order to understand the high temperature creep resistance of this material upon heat-treatment, we studied microstructural changes on the samples after conventional furnace and microwave annealing. Therefore, this work is a follow-up of the work by Liu *et al.* Tensile creep tests were conducted by Liu *et al.* on as-sintered, furnace and microwave annealed GS44 samples. The creep-tested samples were then analyzed in this work for microstructural changes. This is one of the few reports on the microstructural changes associated with microwave annealing of silicon nitride ceramics.

Results and Discussion

Silicon Nitride Ceramics

In this reporting period, we performed detailed transmission electron microscopy (TEM) and X-ray diffraction analysis on the GS44 samples under as-received condition, and after heat-treatment. Samples for (TEM) observations were cut from the as-sintered and creep tested specimens close to the fracture surface. The samples were polished to 50-80 µm and then a crater was made using a dimple grinder, with the center of the crater only about 10 µm or less. The samples were then ion milled to electron transparency. High-resolution TEM observations were performed on TOPCON-002B

with 1.8Å point-to-point resolution at the first Scherzer focus. We also performed analytical TEM observations on the samples to study the triple-junction phases, especially their changes upon heat-treatment. Samples for X-ray analysis were polished to obtain a flat surface, and the X-ray diffraction measurements were performed on a Rigaku X-ray diffractometer.

The complete information on the chemical composition of GS44 is proprietary to AlliedSignal and is not available to the public. However, energy dispersive spectroscopy of the specimens indicated that the sintering aids consist of a combination of yttria, magnesia and alumina. Fig. 1 is the X-ray diffraction result of the as-sintered GS44. It consists of X-ray diffraction peaks exclusively from the β - Si_3N_4 phase. No peaks from α - Si_3N_4 or from other phases than Si_3N_4 are detected. Fig. 2 (a) is a TEM micrograph of the as-sintered GS44 showing a typical triple junction phase. The inset in Fig. 2 (a) is a selected area diffraction (SAD) pattern from the triple junction phase. This SAD pattern exhibits diffuse rings only, indicating fully amorphous state of the triple junction phase. In order to obtain composition information of the triple junction phase, energy dispersive X-ray (EDX) spectroscopy was performed on the triple junction phase, with the result given in Fig. 2 (b). We refrained from quantitative analysis of chemical composition of the triple junction phase due to the difficulty in acquiring precise data for oxygen and nitrogen.

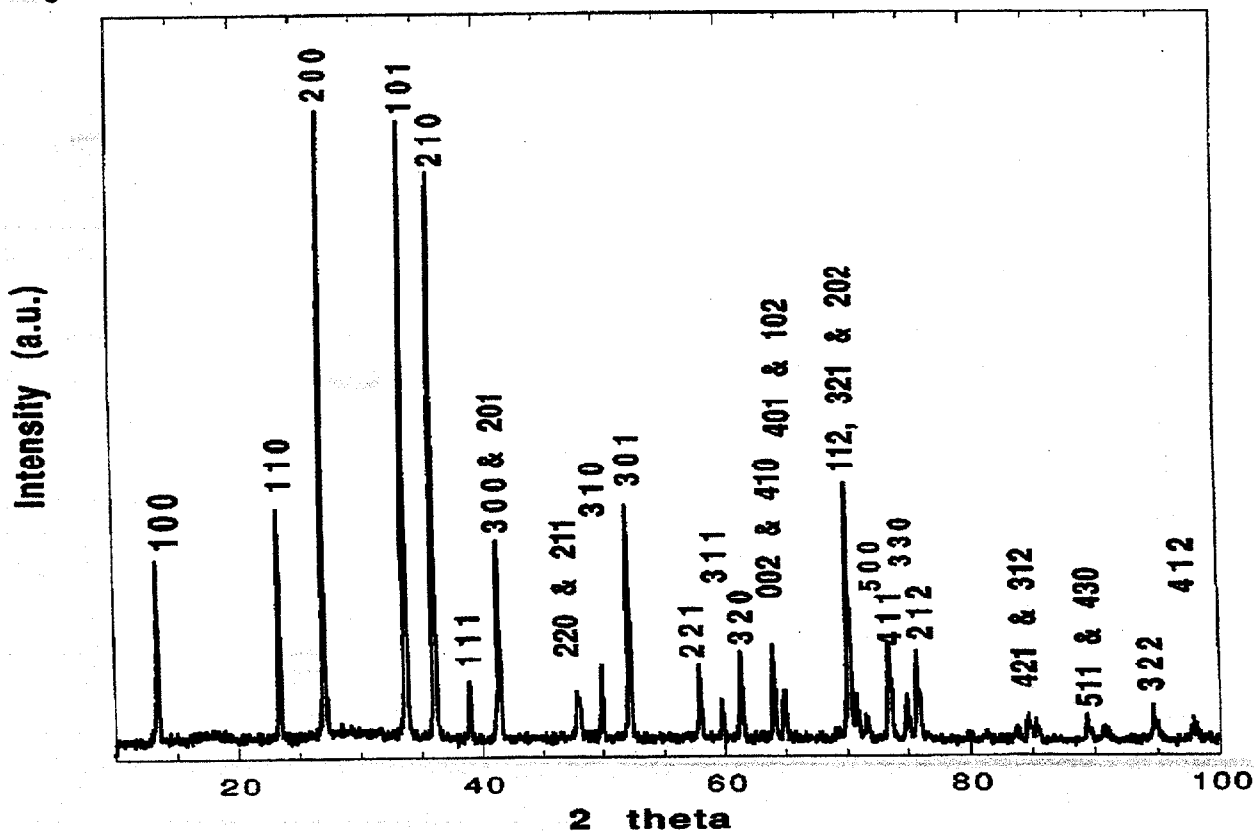


Fig. 1 X-ray diffraction of as-sintered GS44 showing peaks from β - Si_3N_4 only.

Apart from multiple junction amorphous phases, there are still grain boundary phases with varied thickness, from the "equilibrium thickness" of about 1.0~1.5 nm to 3.0~5.0 nm. Fig. 2 (c) shows a high resolution TEM lattice image of two Si_3N_4 grains separated by the amorphous grain boundary phase of ~3.0 nm in thickness.

Detailed TEM observations on the creep-tested as-sintered GS44 specimens have been reported elsewhere. Briefly, a large amount of strain whorls, large dislocation densities in certain silicon nitride grains, multiple junction cavities, grain boundary sliding, and so on, were observed in the creep-tested as-sintered GS44 specimens. It was concluded that for the as-sintered GS44, the dominant creep deformation mechanism is cavitation assisted by grain boundary sliding, which might also be assisted by dislocation generation at the contact locations between two silicon nitride grains.

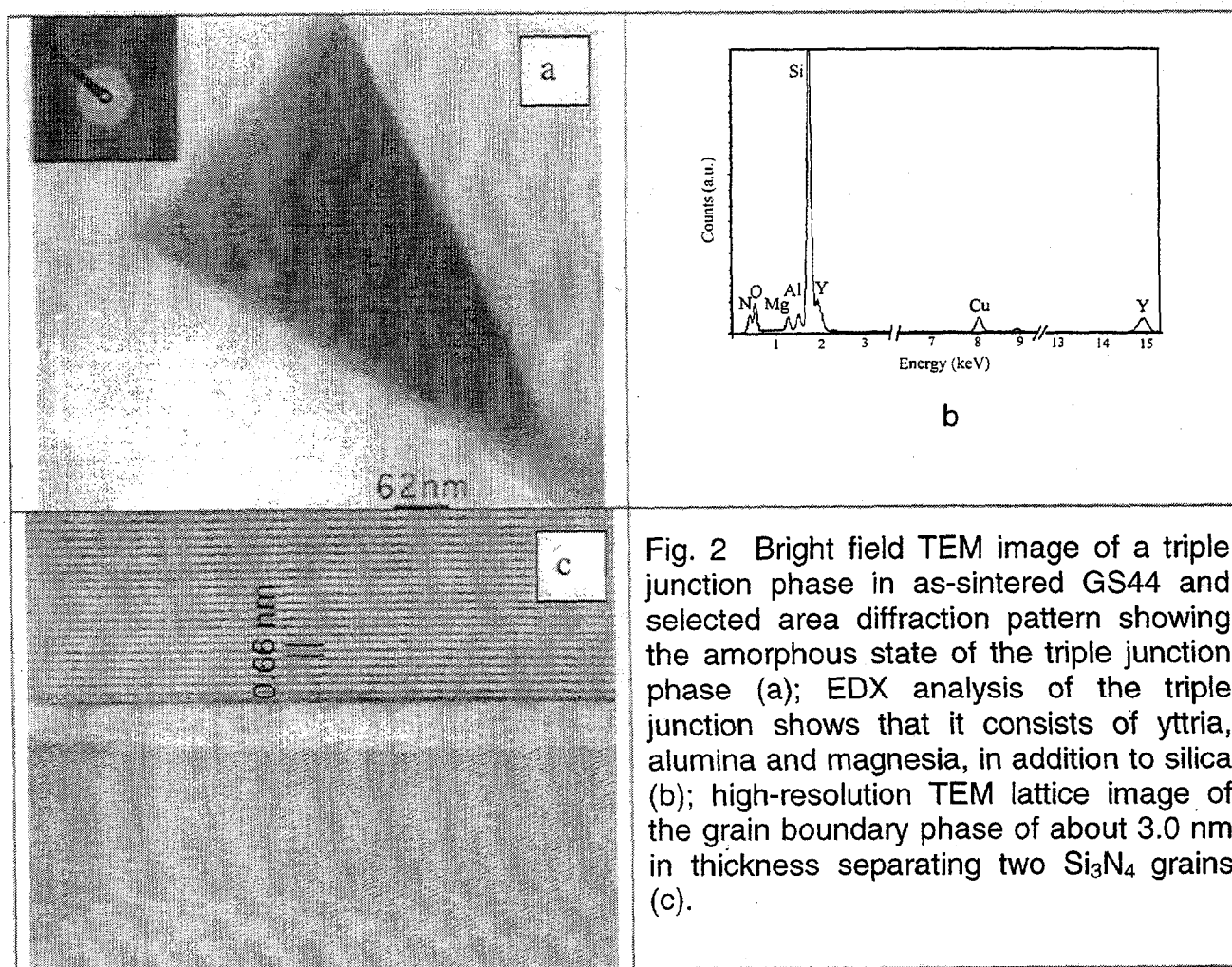


Fig. 2 Bright field TEM image of a triple junction phase in as-sintered GS44 and selected area diffraction pattern showing the amorphous state of the triple junction phase (a); EDX analysis of the triple junction shows that it consists of yttria, alumina and magnesia, in addition to silica (b); high-resolution TEM lattice image of the grain boundary phase of about 3.0 nm in thickness separating two Si_3N_4 grains (c).

Detailed analysis on the triple junction phases given below shows significant changes in the annealed specimens. Fig. 3 (a) is a bright field TEM image of a microwave annealed (1200°C) GS44 sample showing silicon nitride grains and triple junction phases, with the triple junction phases indicated by arrows. Fig. 3 (b) is a micro-

diffraction (μ -diffraction) pattern taken from the triple junction phase. It can be clearly seen that this pattern shows spots, which is typical of crystalline structure. The small tilt range of the goniometer of our TEM prohibits us from obtaining an in-zone diffraction pattern of this phase. However, the crystallinity can be clearly established from the spot pattern. In other words, the triple junction phase in Fig. 3 (a) has been devitrified during the annealing process. Fig. 3 (c) gives another example of the devitrified triple junction phases, with the micro-diffraction pattern given in Fig. 3 (d).

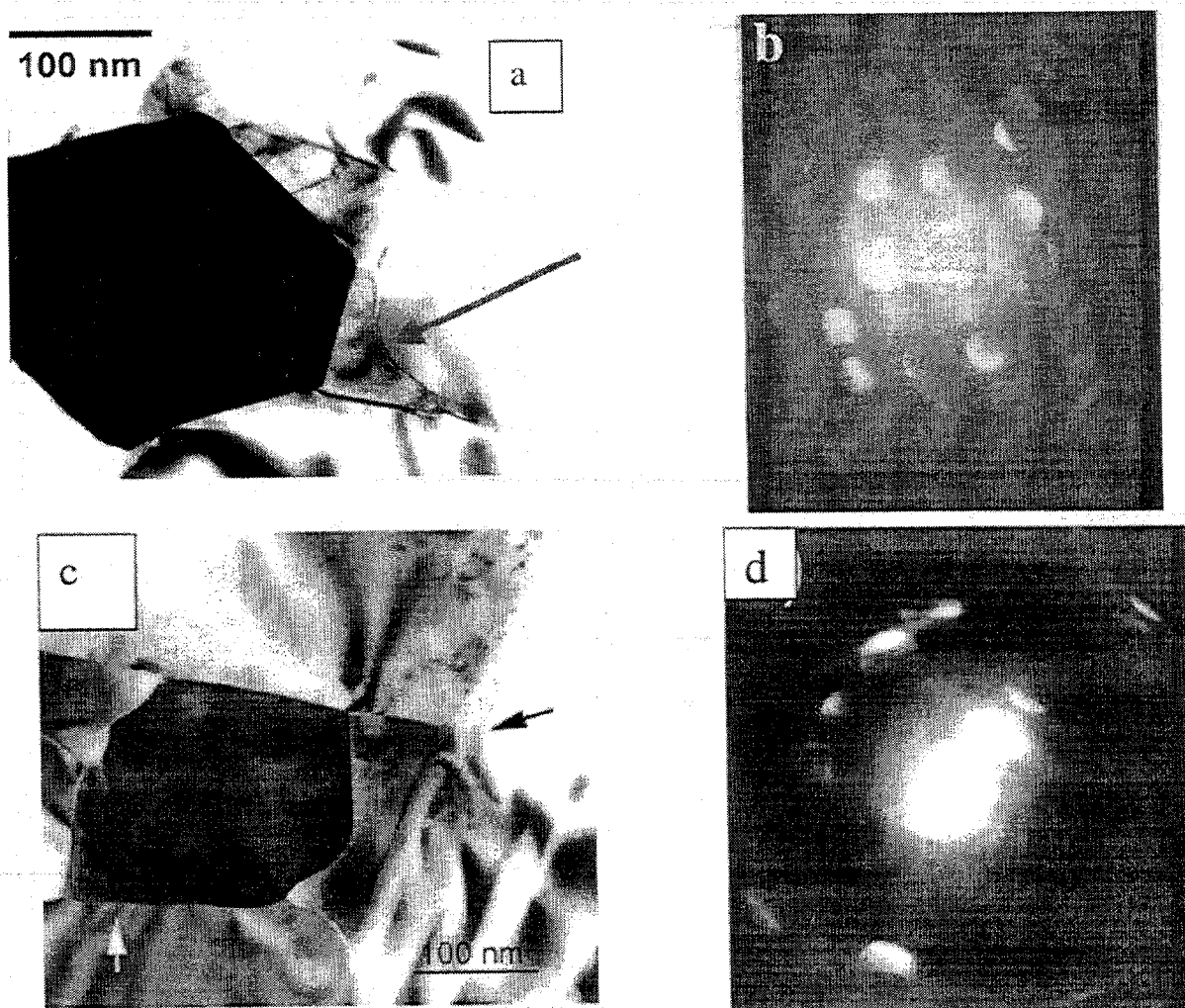


Fig. 3 Bright field TEM micrograph of GS44 microwave annealed at 1200°C, the arrow indicates the triple junction phase (a); microdiffraction from the triple junction phase shows that the triple junction phase has been devitrified (b). In (c) is another TEM image of Si_3N_4 grains and the multiple junction phases indicated by arrows, and μ -diffraction pattern shows that the multiple junction phases have been devitrified (d). Notice no diffuse scattering is visible from the μ -diffraction pattern.

In order to confirm the TEM observations that annealing treatment devitrified the previously amorphous triple junction phases, we performed X-ray diffraction on the annealed specimen. Fig. 4 (a) is the X-ray diffraction result from a GS44 specimen microwave annealed at 1200°C (specimen MA12-5). As compared to the as-sintered specimen (Fig. 1), small peaks that are not from β -Si₃N₄ can be observed. These small peaks are located at 2 theta values of ~30, ~57, ~66, and ~68 degrees. In order to see these peaks more clearly, we conducted fine scan with smaller step-size and larger count rate around these peaks. Fig. 4 (b) shows such a fine scan from 2 theta angle 25 to 35 degrees. A peak at 29 can be observed clearly. Even though we could not establish the crystal structure producing these extra peaks due to lack of detailed information on the chemical composition of the material, we verify again by X-ray diffraction that crystallization occurred in amorphous sintering aids during annealing treatments.

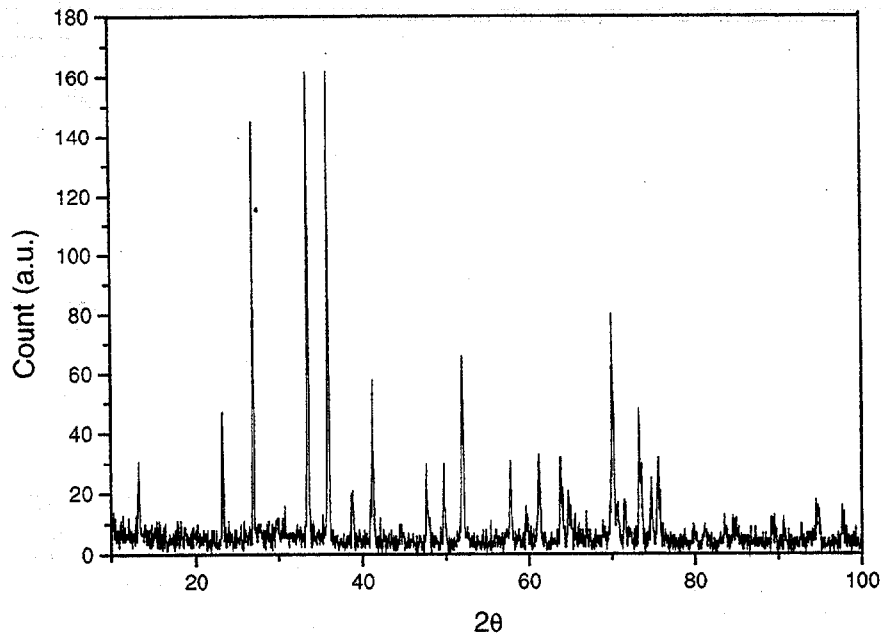
As pointed out in the Introduction, amorphous residues in the grain boundaries and multiple junctions in silicon nitride ceramics decreases its creep resistance at high temperature. A review of experimental data by Luecke and Wiederhorn suggests that the rate of formation and growth of cavities in the second phase controls creep in most commercial grades of Si₃N₄ ceramics. They proposed a simple phenomenological model to correlate the creep rate to the applied stress, the Si₃N₄ grain size, the effective viscosity of the deformable phase, and the volume fraction of the deformable phase. The creep strain rate can be expressed as

$$\dot{\epsilon}_s = A\sigma \exp\left(-\frac{\Delta H}{RT}\right) \frac{\Phi^3}{(1-\Phi)^2} \exp(\alpha\sigma), \quad (1)$$

where A is a constant, σ the applied stress, ΔH the activation energy, R the gas constant, T the absolute temperature, α some constant, and Φ is the volume fraction of the amorphous phase. From Equation (1), it is seen that the steady state creep strain rate is proportional to the cube of the volume fraction of the deformation amorphous phase. Therefore, devitrification of the amorphous grain boundary phase or triple junction phase of silicon nitride ceramics explains the enhancement of the creep resistance at high temperature. When the amorphous phases are devitrified through approaches such as heat-treatment, the detrimental effect of these phases on the high temperature creep performance can be alleviated or even eliminated, resulting in much improved creep resistance.

Therefore, the creep test results, X-ray diffraction studies and microstructural observations of the present work demonstrate that microwave annealing can be an efficient route to improve the creep resistance of sintered Si₃N₄ through devitrification of the glass phases.

a)



b)

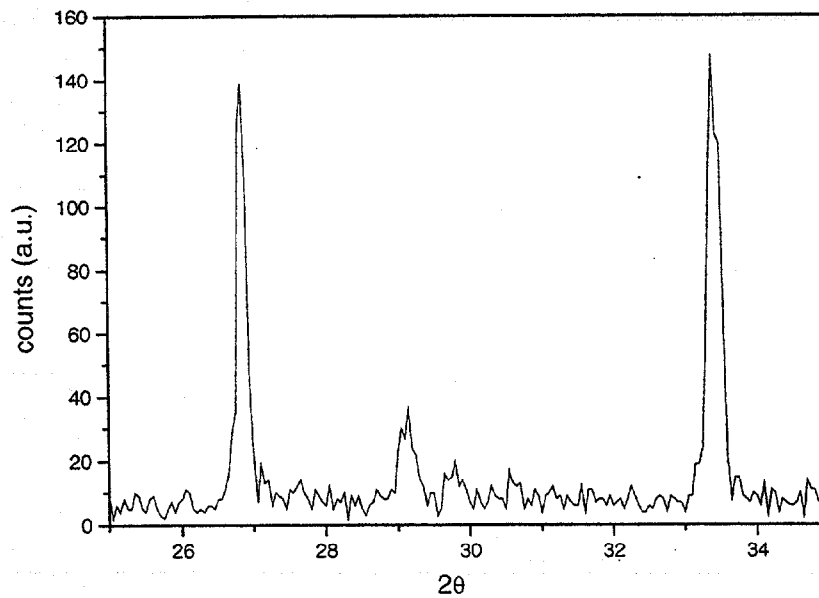


Fig. 4 X-ray diffraction of a GS44 specimen microwave annealed at 1200°C (MA12-5) (a). Compared to Fig.1, small extra peaks which can not be attributed to β - Si_3N_4 appear. Fine XRD scan established more clearly the existence of these peaks (b).

Effect of PSZ thermal barrier coating on diesel engine performance

Investigation of the effect of Partially Stabilized Zirconia (PSZ) thermal barrier coating on diesel engine performance requires plasma sprayed PSZ coating on the aluminum alloy piston face. Coating thickness will range from 0.1 to 2.0 mm. However the cost of individual pistons prohibits application of thermal barrier coating on each piston. Therefore we modified the piston for using different piston caps with the same base. Analytical model of modified piston has been developed.

The piston, shown in Figure 5a is made of aluminum alloy HG 413 (BS 1490 LM 13 TF). The piston was cut above the top ring to remove a cup. Figure 5b shows the bottom part of the piston without the cup and Figure 6 shows the cup. A single cylinder direct injection diesel engine test cell is in place for the experimental work.

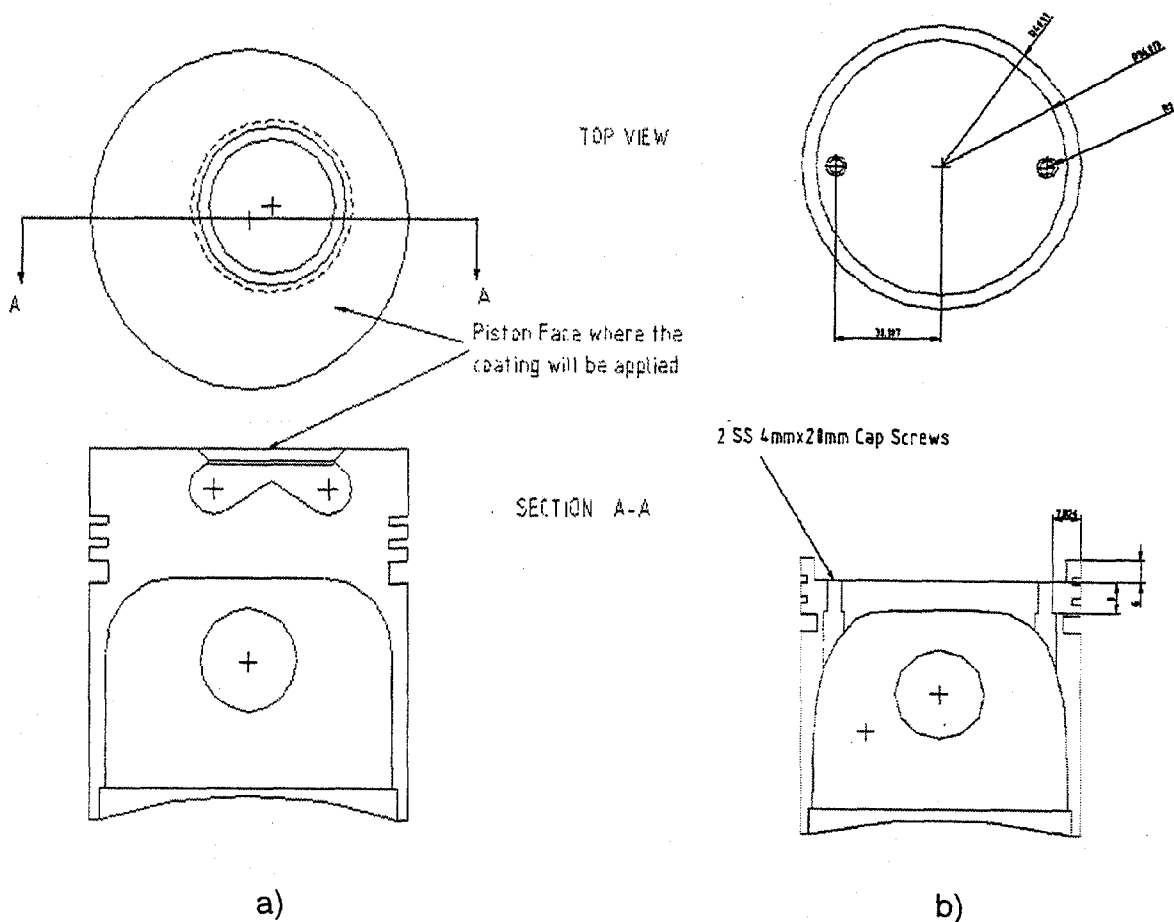


Figure 5. Piston for the Ricardo Hydra single cylinder DI diesel engine (a), Piston without the cup (b)

Several piston cups (Figure 6) will be made from the stock material HG 413 (BS 1490 LM 13 TF). Each cup will be coated with plasma sprayed PSZ thermal barrier coating. It will be performed when plasma spray coating setup at North Carolina A&T State University will be completed.

The cup and the piston will be fastened together with two 2mm stainless steel screws. Each coating will be individually tested. Expected results include, combustion temperature, pressure data and emissions data. Performance comparison will be made against the baseline engine.

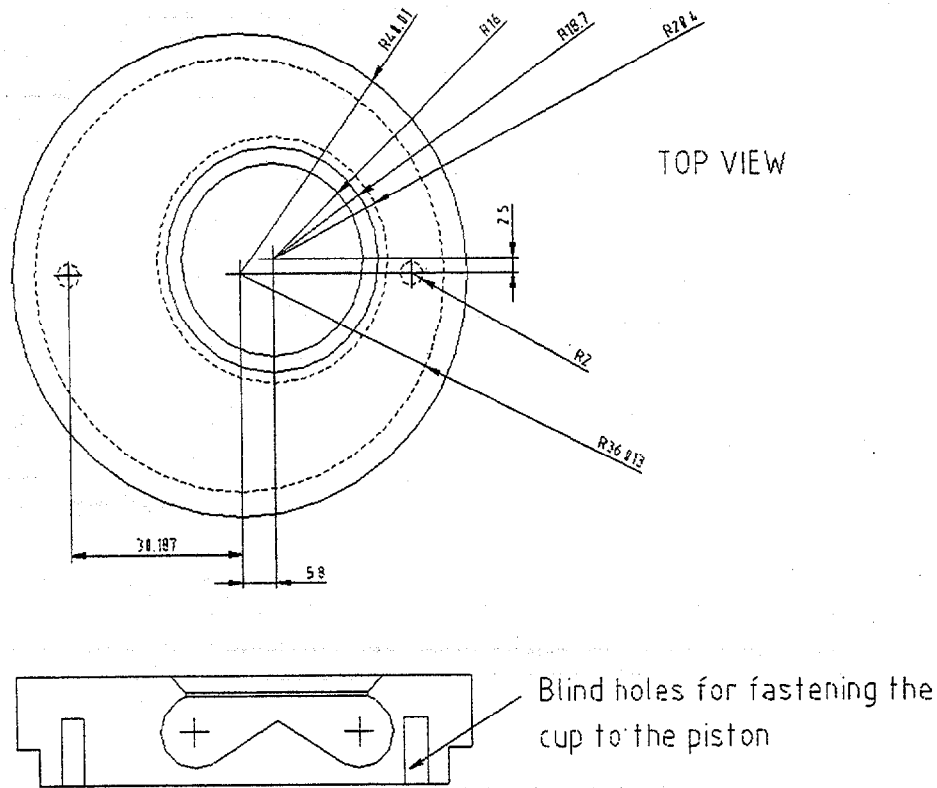


Figure 6. Piston cup

Analytical Model

Finite Element Analysis (FEA) using ANSYS will be used to systematically evaluate thermal and structural effect of the coating thickness on the piston. Figure 7 shows the piston model used for the FEA analysis and Figure 8 shows a 1.5mm thick PSZ thermal barrier coating to be applied on the piston. The piston and coating model have a total of 66,000 elements. Due to the different PSZ and aluminum alloy material properties, a nanoindentation technique will be used to characterize the interfacial properties between the PSZ coating and the aluminum alloy piston.

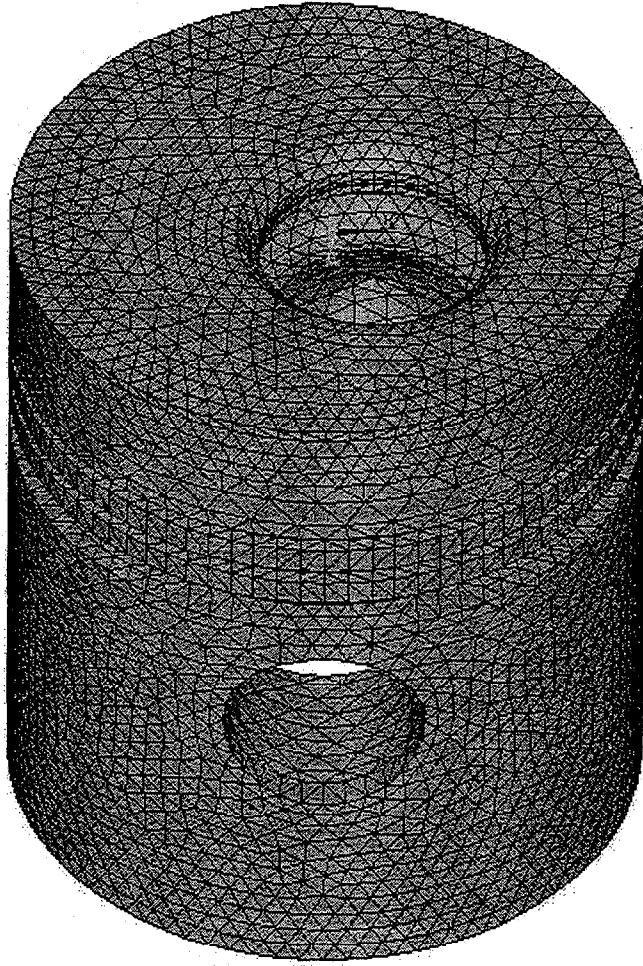


Figure 7. FEA Piston model for the Ricardo Hydra single cylinder DI diesel engine

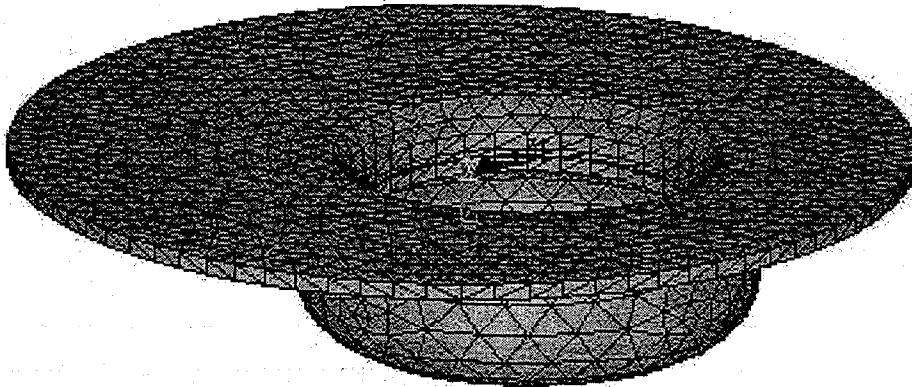


Figure 8. 1.5 mm thick FEA Thermal Barrier Coating model

Status of Milestones:

On schedule.

Communications/Visitors/Travel

None

Publications:

1. Q. Wei, S. Yarmolenko, J. Sankar, A.K. Sharma, Y. Yamagata and J. Narayan, "Microstructure and Nanomechanical Properties of DLC Thin Films Prepared by Pulsed Laser Deposition in Various Atmospheres", in "New Methods, Mechanisms and Models of Vapor Deposition", edited by H.N.G. Wadley, G. Gilmer and W. Barker, Materials Research Society Proc., 2000, Vol. 616.
2. Q. Wei, R. J. Narayan, A. K. Sharma, J. Sankar, S. Oktyabrsky, J. Narayan, "Micro- and nano-mechanical behavior of diamondlike carbon containing foreign atoms prepared by pulsed laser deposition", Mater. Res. Soc. Symp. Proc., 1999, Vol. 555, 303-308.
3. Q. Wei, S. Yarmolenko, J. Sankar, A. K. Sharma, Y. Yamagata and J. Narayan, "Microstructure and nano-mechanical properties of diamondlike carbon thin films prepared by pulsed laser deposition in various atmospheres", MRS 2000 Spring Meeting, April, 2000, San Francisco, CA.
4. Q. Wei, S. Yarmolenko, J. Sankar, A. K. Sharma and J. Narayan, "Preparation of superhard functionally graded tetrahedral amorphous carbon coatings by pulsed laser deposition", MRS 2000 Spring Meeting, April, 2000, San Francisco, CA.
5. Q. Wei, J. Sankar, J. Narayan and K. Liu, "Microstructure and creep behavior of self-sintered silicon nitride ceramics heat-treated by furnace and microwave annealing", 41st AIAA/ASME/ASCE/AHS/ASC SDM Conf., paper number 2000-1603, April 2000, Atlanta, GA.

Problems encountered:

None.

Life Prediction of Ceramic Diesel Engine Components

C. R. Brinkman (ORNL), T. P. Kirkland (ORNL), H. - T. Lin (ORNL),
R. A. Ott (ORNL), S. K. Lee (Caterpillar), and J. Thiele (Caterpillar)

Objective/Scope

The valid prediction of mechanical reliability and service life is a prerequisite for the successful implementation of structural ceramics as internal combustion engine components. There are three primary goals of this research project which contribute toward that implementation: the generation of mechanical engineering data from ambient to high temperatures of candidate structural ceramics; the microstructural characterization of failure phenomena in these ceramics and components fabricated from them; and the application and verification of probabilistic life prediction methods using diesel engine components as test cases. For all three stages, results are provided to both the material suppliers and component end-users.

The systematic study of candidate structural ceramics (primarily silicon nitride) for internal combustion engine components is undertaken as a function of temperature (< 900°C), environment, time, and machining conditions. Properties such as strength and fatigue will be characterized via flexure and rotary bend testing.

The second goal of the program is to characterize the evolution and role of damage mechanisms, and changes in microstructure linked to the ceramic's mechanical performance, at representative engine component service conditions. These will be examined using several analytical techniques including optical and scanning electron microscopy. Specifically, several microstructural aspects of failure will be characterized:

- (1) strength-limiting flaw-type identification;
- (2) edge, surface, and volume effects on strength and fatigue size-scaling
- (3) changes in failure mechanism as a function of temperature;
- (4) the nature of slow crack growth; and
- (5) what role residual stresses may have in these processes.

Lastly, numerical probabilistic models (*i.e.*, life prediction codes) will be used in conjunction with the generated strength and fatigue data to predict the failure probability and reliability of complex-shaped components subjected to mechanical loading, such as a silicon nitride diesel engine valve. The predicted results will then be compared to actual component performance measured experimentally or from field service data. As a consequence of these efforts, the data generated in this program will not only provide a critically needed base for component utilization in internal combustion engines, but will also facilitate the maturation of candidate ceramic materials and a design algorithm for ceramic components subjected to mechanical loading in general.

Technical Progress

Flexure testing of eight lots of silicon nitride in support of Caterpillar, Inc's test program was completed. This involved determining the strength distributions as a

function of temperature, grinding orientation, and time (fatigue). Four-point bend flexure strengths were evaluated using ASTM-B bars (dimensions 3 x 4 x 50 mm). Table 1 presents an overview of the test plan followed, and indicates that testing generally occurred at two temperatures i.e. 20 and 850°C, and two stressing rates i.e. 0.003 and 30 MPa/s, and that grinding orientation on the test bars was either transverse or longitudinal. Material manufacturer is also given. All specimens were commercially finish ground with 320 diamond grit grinding for both transverse and longitudinal machining orientations according to recommended practices described in ASTM C 1161. Further, all specimens were longitudinally beveled. Table 1 also indicates that limited testing was performed on test bars that had previously been exposed for 1000 h at 850°C to an oil ash environment by Caterpillar. This was done on two types of silicon nitride i.e. GS44 and SN235. The upper temperature of 850°C was selected since it is in the approximate operating temperature range of the diesel engine.

Data generated to date are given in Tables 1-5. These data show that both SN235 and SN235P exhibit excellent strength and outstanding fatigue resistance. For example, the fatigue exponent for SN235 was 164 while that of SN235P was 140 (transversely machined specimens). The next most fatigue-resistant silicon nitride was KYON3000 with an exponent of 68 as shown in Table 4. Tables 3 and 5 indicate that limited testing was performed at 1200°C on SN235 and SN235P; however, strengths at the lower stressing rate (0.003 MPa/s) and the fatigue exponents are questionable because of the creep observed in these specimens.

Figures 1 and 2 compare strengths of the engine exposed GS44 and SN235 to these same materials and other unexposed silicon nitrides tested under these same conditions. Note that there was essentially no change in strength level of the engine-exposed materials. Other types of silicon nitride were similarly exposed to the oil ash/air environment and both SEM and X-ray analysis studies are planned of the fracture surfaces. Several of the bars of the SN235 and GS44 have been characterized to date. In the case of the SN235, the non-protective oxide scale was found to contain Zn-Ca-P-Si-O while the similarly appearing GS44 oxide scale consisted of Zn-Ca-P-S-Si-Al-Mg-O.

Figures 3 and 4 compare the fracture surfaces of these two materials and indicate that the SN235 exhibited approximately a 3 micron while the GS44 showed a 15 micron environmentally affected zone. These studies are expected to continue.

Status of Milestones

All milestones are on schedule.

Communications / Visitors / Travel

Nothing to report.

Problems Encountered

None.

Publications

"High Temperature Inert Strength and Dynamic Fatigue of Candidate Silicon Nitrides for Diesel Exhaust Valves," A. A. Wereszczak, T. P. Kirkland, H. -T. Lin, and S. K. Lee, to appear in *Ceramic Engineering and Science Proceedings*, Vol. 21, 2000.

"Strength and its Dependence on Secondary Phase Softening in Silicon Nitrides," A. A. Wereszczak, H. -T. Lin, and T. P. Kirkland, and S. K. Lee, to be presented at the 102nd Annual Meeting and Exhibition of the American Ceramic Society, St. Louis, MO, April 30-May 3, 2000.

"Comparison of Strength and Thermal Properties of Silicon Nitride Ceramics Up To 850C," A. A. Wereszczak, T. P. Kirkland, H. -T. Lin, and S. K. Lee, to be presented at the ASM Materials Solutions 2000 Conference, St. Louis, MO, October 9-12, 2000.

"Strength and Dynamic Fatigue of Silicon Nitride at Intermediate Temperatures," A. A. Wereszczak, H. -T. Lin, T. P. Kirkland, M. J. Andrews, and S. K. Lee, in preparation.

Table 1. Silicon nitride test matrix to compare inert strength, high temperature fatigue performance, effect of machining orientation, and oil ash environmental exposure. ASTM C1161B specimens were 4-pt flexure strength tested.

Test Condition	KYON KYON							
	AS800	GS44	3000	3500	N7202	NT154	SN235	SN235P
20°C 30 MPa/s Longitudinal	Completed (30)	Completed (30)	Completed (27)		Completed (30)	Completed (30)	Completed (9)	Completed (9)
20°C 30 MPa/s Transverse	Completed (30)	Completed (42*)	Completed (27)	Completed (21)	Completed (30)		Completed (15)	Completed (15)
20°C 30 Mpa Transverse		Completed (10#)					Completed (10#)	
850°C 30 MPa/s Longitudinal	Completed (30)	Completed (30)	Completed (27)		Completed (30)	Completed (30)	Completed (9)	Completed (8)
850°C 30 Mpa/s Transverse	Completed (30)	Completed (41*)	Completed (27)	Completed (21)	Completed (30)		Completed (15)	Completed (15)
850°C 0.003 MPa/s Longitudinal	Completed (23)	Completed (21)	Completed (27)		Completed (31)	Completed (27)		Completed (9)
850°C 0.003 MPa/s Transverse	Completed (24)	Completed (37*)	Completed (27)	Completed (21)	Completed (22)		Completed (14)	Completed (15)
850°C 0.003 Mpa/s Transverse		Completed (10#)					Completed (9#)	
Material's Manufacturer	ASCC	ASCC	Kennametal	Kennametal	CFI	Norton	Kyocera	Kyocera

*two lots tested

() indicates number of specimens tested

#tested after 1000 h/850°C oil ash exposure in air

Table 2. Summary of uncensored Weibull strength distributions for silicon nitride specimens longitudinally machined per ASTM C1161.

Material	# of Spmns. Tested	Stressing Rate (MPa/s)	Temp. (°C)	± 95%		Uncens. Chrcstic Strength (MPa)	± 95% Uncens. Chrcstic Strength (MPa)
				Uncens. Weibull Modulus	Uncens. Weibull Modulus		
AS800	30	30	20	23.2	17.1, 30.3	707	695, 719
GS44	30	30	20	22.2	16.3, 29.0	959	941, 975
KYON 3000	27	30	20	10.4	7.7, 13.6	847	814, 881
N7202	30	30	20	22.0	16.2, 28.9	775	761, 788
NT154	30	30	20	9.0	6.7, 11.7	706	675, 736
NT551	32	30	20	12.7	9.2, 16.9	1040	1009, 1070
SN235	9	30	20	12.8	6.8, 21.2	999	937, 1061
SN235P	9	30	20	32.6	18.8, 49.6	792	773, 810
AS800	30	30	850	15.1	11.6, 18.8	623	607, 639
GS44	30	30	850	19.1	14.5, 24.2	776	759, 791
KYON 3000	27	30	850	11.9	8.7, 15.7	801	773, 828
N7202	30	30	850	15.6	11.8, 20.0	689	672, 706
NT154	30	30	850	9.3	6.9, 11.9	685	656, 714
NT551	27	30	850	6.3	4.6, 8.2	558	521, 595
SN235	9	30	850	17.0	9.2, 27.5	866	826, 906
SN235P	8	30	850	30.3	16.5, 48.1	673	643, 691
AS800	23	0.003	850	6.2	4.4, 8.4	440	408, 472
GS44	21	0.003	850	20.5	13.8, 29.0	590	576, 603
KYON 3000	27	0.003	850	11.7	8.5, 15.4	640	616, 663
N7202	31	0.003	850	10.2	7.6, 13.3	538	518, 558
NT154	27	0.003	850	5.9	4.5, 7.4	618	576, 662
SN235P	9	0.003	850	23.6	12.7, 38.8	641	662, 641

Table 3. Summary of uncensored Weibull strength distributions for silicon nitride specimens transversely machined per ASTM C1161.

Material	# of Spmns. Tested	Stressing Rate (MPa/s)	Temp. (°C)	Uncens. Weibull Modulus	± 95%	Uncens.	± 95%
					Uncens. Weibull Modulus	Chrcstic Strength (MPa)	Uncens. Chrcstic Strength (MPa)
AS800	30	30	20	19.4	14.4, 25.1	669	656, 683
GS44	30	30	20	17.4	13.1, 22.0	830	812, 849
GS44 (Oil Ash**)	10	30	20	39	21.8, 63.5	786	771, 800
KYON 3000	27	30	20	14.4	10.4, 19.0	702	682, 722
KYON 3500	21	30	20	14.2	9.8, 19.7	654	632, 675
N7202	30	30	20	18.7	14.3, 23.6	682	667, 696
NT551	30	30	20	9.4	7.0, 12.3	806	772, 839
SN235	15	30	20	23.8	15.4, 33.9	901	879, 923
SN235 (Oil Ash**)	10	30	20	18.6	10.2, 30.0	894	858, 829
SN235P	15	30	20	38.1	24.0, 55.8	666	656, 676
AS800	30	30	850	19.1	14.4, 24.4	608	595, 620
GS44	30	30	850	20.2	14.6, 26.8	747	733, 761
KYON 3000	27	30	850	13.2	9.7, 17.2	643	623, 663
KYON 3500	21	30	850	15.0	10.4, 20.4	674	653, 695
N7202	30	30	850	23.7	17.7, 30.5	687	676, 699
NT551	29	30	850	9.8	7.4, 12.5	582	558, 606
SN235	15	30	850	26.7	18.0, 36.7	777	760, 793
SN235P	15	30	850	19.3	12.5, 27.6	631	612, 649
AS800	24	0.003	850	7.8	5.5, 10.6	429	405, 453
GS44	22	0.003	850	22.6	15.7, 30.8	572	560, 583
GS44 (Oil Ash**)	10	0.003	850	23.1	13.8, 35.8	488	472, 503
KYON	27	0.003	850	8.9	6.7,	569	543,

3000					11.4		595
KYON 3500	21	0.003	850	12.7	8.9, 17.2	442	426, 459
N7202	22	0.003	850	9.2	6.6, 12.2	516	490, 542
NT551	30	0.003	850	4.0	3.0, 5.1	374	338, 411
SN235	14	0.003	850	18.5	11.8, 26.8	744	720, 767
SN235 (Oil ASH**)	9	0.003	850	13.0	6.9 21.5	827	777 877
SN235# (Oil Ash**)	10	0.003	850	7.4	4.0 12.3	803	725 887
SN235P	15	0.003	850	18.2	11.5, 26.8	594	575, 612
SN235	9	30	1200	22.4	12.6, 34.8	442	427, 457
SN235	9	30	1200	61.3	34.5, 96.2	338	334, 342
SN235	6	0.003	1200	10.3	5.6, 16.7	247*	229*, 266*
SN235P	6	0.003	1200	18.5	9.0, 31.5	137*	130*, 145*

*Specimens crept-Shown rates/strengths uncorrected.

#Same data as immediately above, but includes one specimen with large grain size plus a processing flaw.

**After 1000h/850°C oil ash exposure in air.

Table 4. Summary of uncensored dynamic fatigue exponents at 850°C.

Material	Machining Orientation	Fatigue Exponent
AS800	Longitudinal	22
GS44	Longitudinal	32
KYON 3000	Longitudinal	40
N7202	Longitudinal	33
NT154	Longitudinal	75
SN235P	Longitudinal	158
AS800	Transverse	22
GS44	Transverse	34
KYON 3000	Transverse	68
KYON 3500	Transverse	20
N7202	Transverse	28
NT551	Transverse	19
SN235	Transverse	164
SN235P	Transverse	140

Table 5. Summary of uncensored dynamic fatigue exponents at 1200°C.

Material	Machining Orientation	Fatigue Exponent
SN235	Transverse	14#
SN235P	Transverse	9#

Because of creep observed in specimens tested at 0.003 Mpa/s, it is suspected these tests did not meet the criteria of ASTM C 1465, "Test Method for Determination of Slow Crack Growth Parameters of Advanced Ceramics by Consultant Stress-Rate Flexural Testing at Elevated Temperatures."

Figure 2. Comparison of the strengths of several types of silicon nitride tested at 850°C.

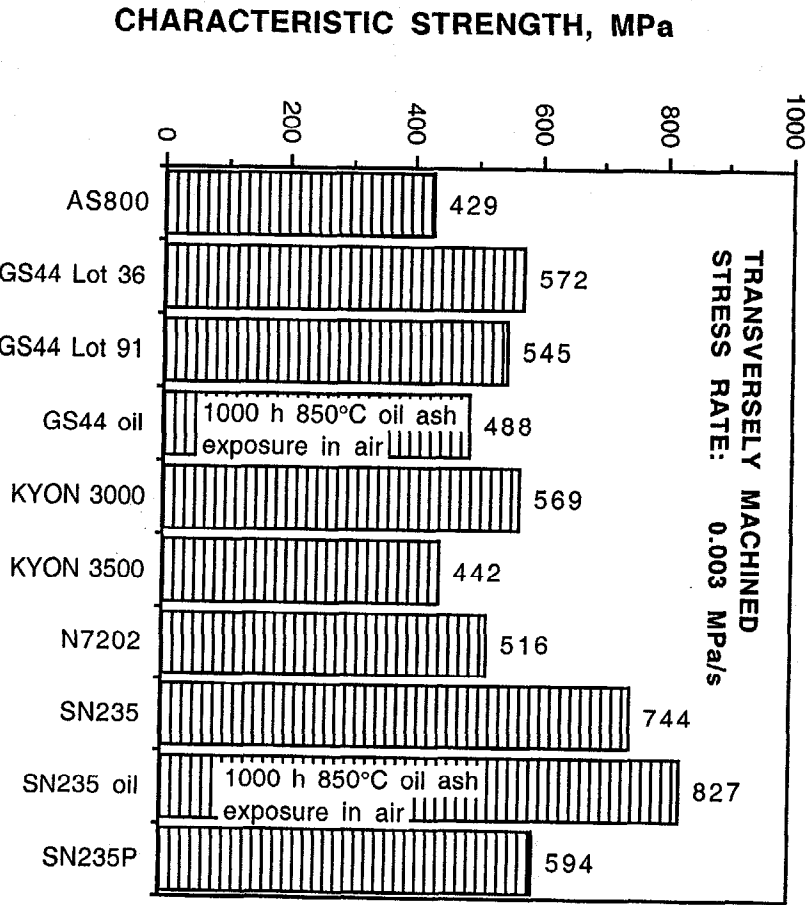


Figure 1. Comparison of the strengths of several types of silicon nitride tested at 20°C.

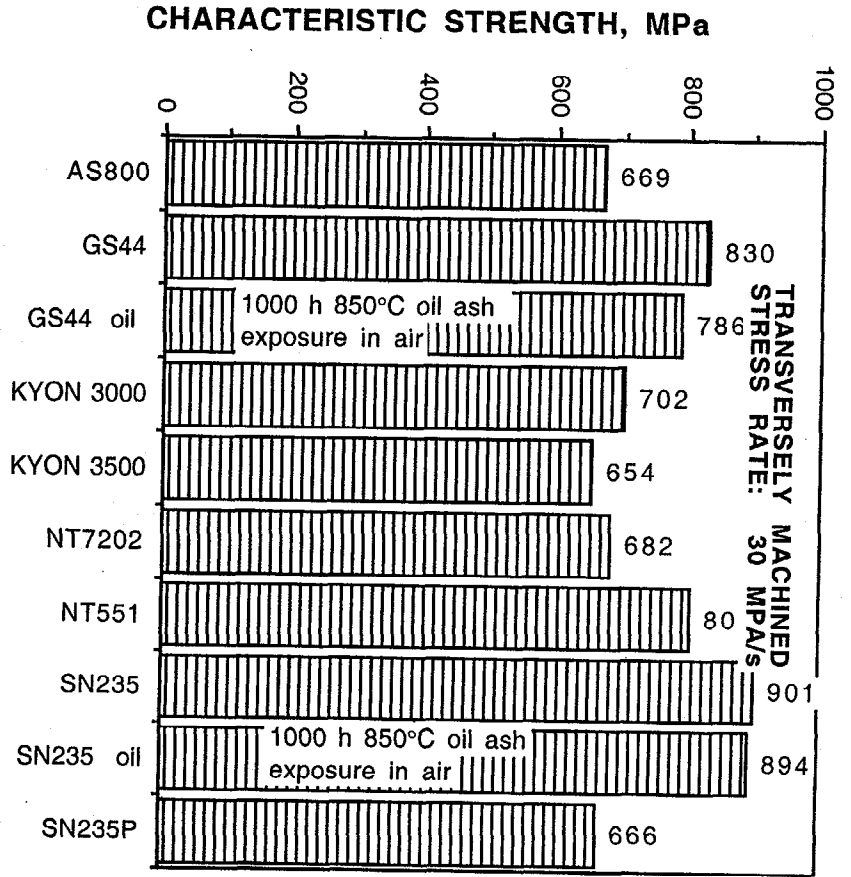


Figure 3. Fracture Surface of Kyocera SN235 After 850°C/1000 h Exposure in Oil Ash Environment

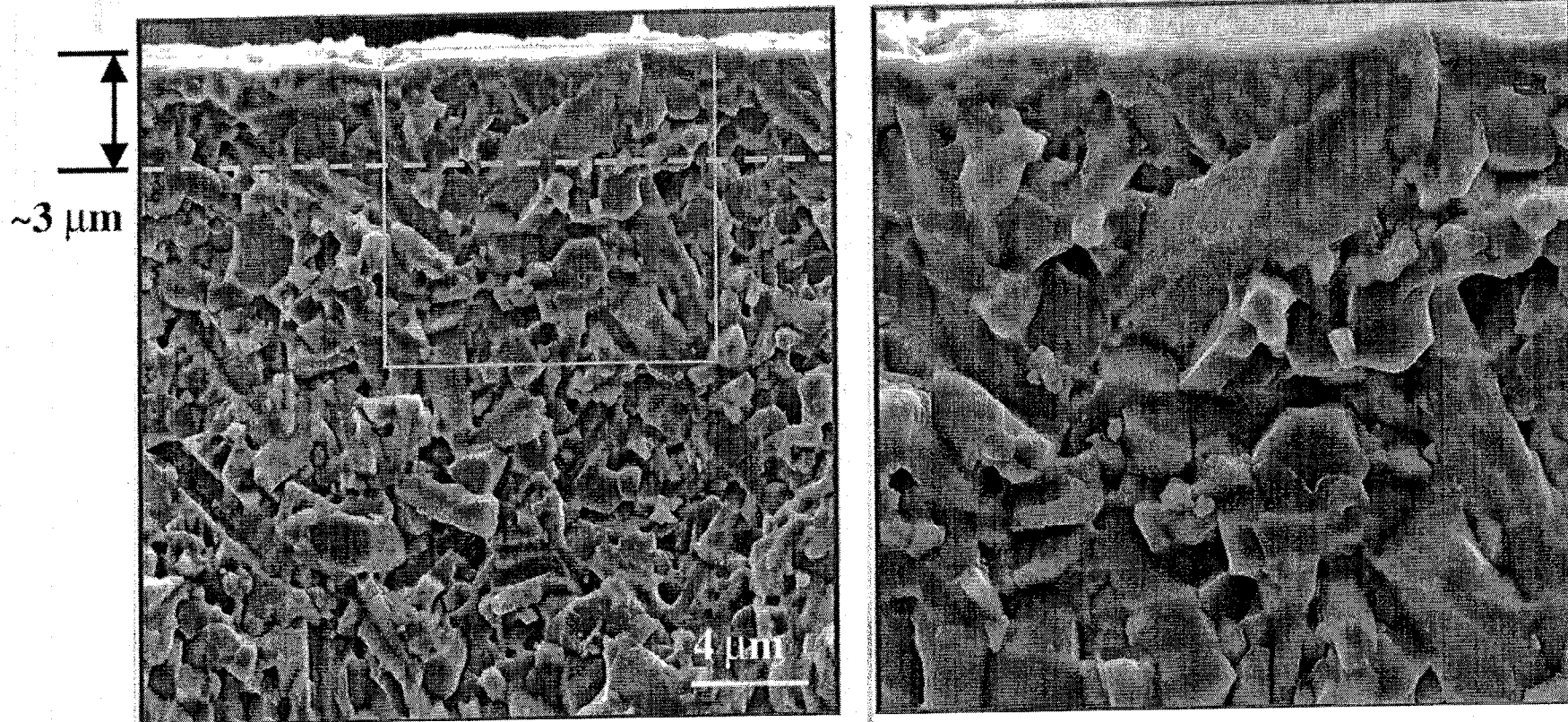
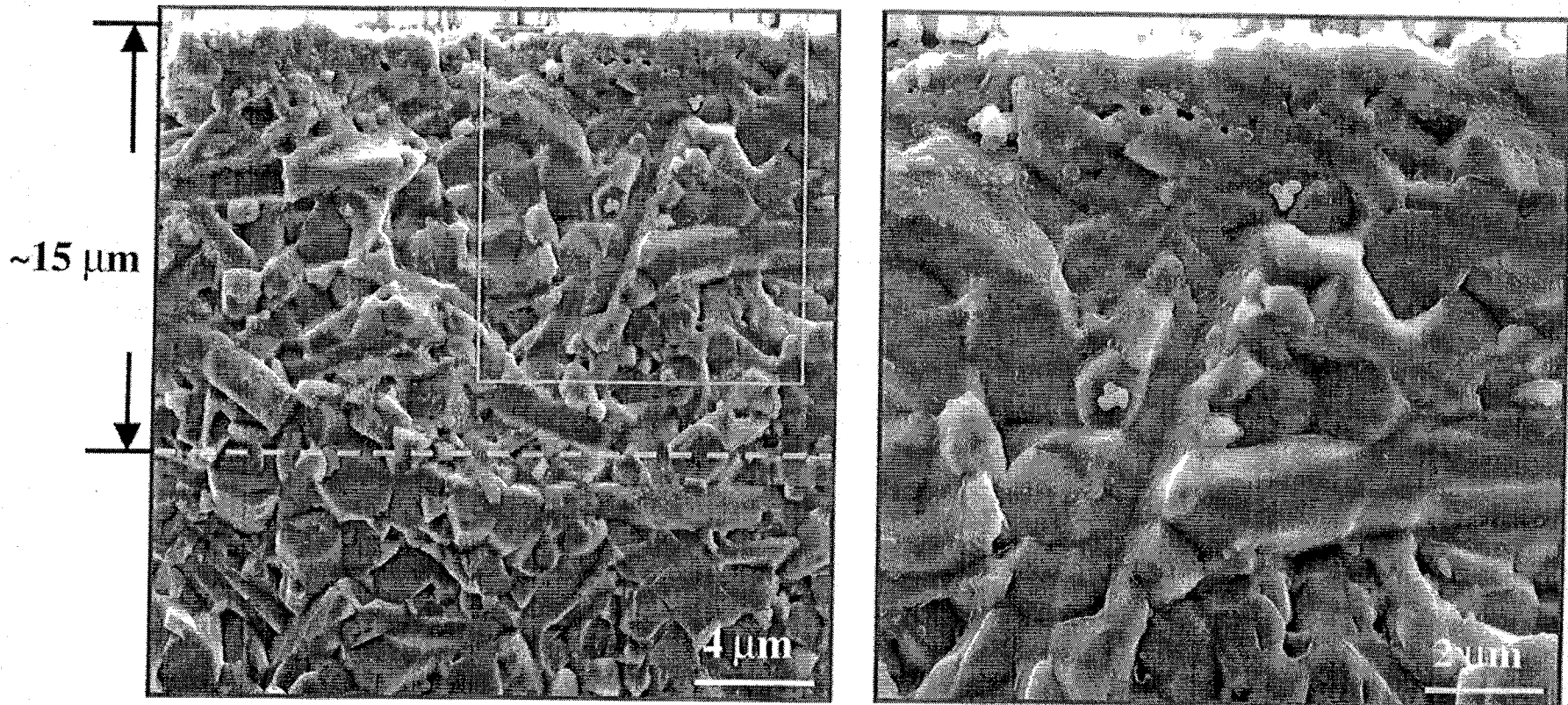


Figure 4. Fracture Surface of Honeywell GS44 After 850°C/1000 h Exposure in Oil Ash Environment



Field Emission Analytical Electron Microscopy for Characterization of Catalyst Microstructures

L. F. Allard, D. A. Blom, and T. A. Nolan

Objective/Scope

The objective of the research is to use analytical and high resolution transmission electron microscopy (TEM) and scanning transmission electron microscopy (STEM) to characterize the microstructures of emission control catalysts. Catalyst research places emphasis on relating microstructural changes to performance of diesel NO_x reduction catalysts. This research is focussed on understanding these changes through TEM and dedicated STEM studies of experimental catalyst materials reacted in an ex-situ catalyst reactor system especially constructed to allow appropriate control of the reaction conditions and the transfer of the sample between reactor and microscope. The focus of particulate studies is to determine particulate structure, composition and morphology. Of particular interest is the comparison of gasoline to diesel particulates.

Technical Progress

Several catalyst materials have been reported in the open literature to show promising catalytic performance for the de-NO_x reaction with hydrocarbon as a reductant. In a major new program of research underway with Caterpillar Inc. (Dr. Paul Park), work is being conducted to investigate the nature of the active sites of promising metal oxide materials so that the catalytic performance can be improved further through a proper design of catalyst preparation processes or an addition of necessary catalytic promoters. Catalyst systems that are being studied include Sn/alumina, Ga/alumina and In/alumina. TEM and STEM techniques are being used to determine the effect of aging on the surface structure and dispersion of metal oxide phases supported on alumina. Hydrothermal stability (sintering), carbon deposition (coking) and SO₂ tolerance (poisoning) will be examined by characterizing samples that are treated in a bulk reactor at Caterpillar Inc. under simulated diesel operating conditions. At the HTML, TEM samples are being reacted in the special catalyst reactor system. This system has recently been re-conditioned and modified to accept a gas composition to simulate diesel exhausts.

A new capability for characterization of the distribution of elements with high spatial resolution in catalyst specimens having dispersions of heavy metal clusters on particulate support materials such as alumina and titania has been introduced in the High Temperature Materials Laboratory, Materials Analysis Group. The Hitachi HD-2000 dedicated scanning transmission electron microscope (STEM) has had installed an EMiSPEC Company beam control and analysis system, which permits "spectrum images" to be obtained. With this technique, images of a catalyst specimen can be acquired in several imaging modes such as bright-field STEM, high-angle annular dark-field STEM, or secondary imaging. Then, a spectrum image map can be recorded, in which an individual spectrum is recorded and saved for each point in the image, by allowing the EMiSPEC system to control the scanning electron beam during the acquisition time. The spectra are acquired typically for times in the 0.3 to 0.5 sec/pixel range, and for an array of, e.g. 150 x 150 pixels. This means the spectrum image takes 1-2 hours to acquire, but it then permits a number of elemental maps to be displayed showing the distribution of each of the elements present in the sample. Even with such short acquisition times, because of the high current density

in the STEM's electron probe, excellent maps of elemental distributions can be obtained, and some idea on relative quantities of each element, point-by-point, can be obtained.

This capability has demonstrated with the analysis of Caterpillar samples of the experimental NO_x-reduction catalyst system comprising indium clusters on alumina. Samples loaded with In at the 2.5 wt%, 5 wt% and 10wt% level have been characterized. The ability to correlate Z-contrast images with spectrum images showing the distribution of In clusters (on the 2.5 wt% samples) and larger particles (on the 5 and 10 wt% samples) has been a valuable technique for unambiguously characterizing these novel catalytic materials. Spectrum imaging is a powerful new tool for analytical microscopy of multi-element specimens, and promises to provide both new and more reliable information in our further studies of NO_x reduction catalyst systems.

MATERIALS AND TESTING STANDARDS

IEA Annex II Management (April 1, 2000-September 30, 2000)
 M. K. Ferber (Oak Ridge National Laboratory)

Objective/Scope

The purpose of this task is to organize, assist, and facilitate international research cooperation on the characterization of advanced structural ceramic materials. A major objective of this research is the evolution of measurement standards. This task, which is managed in the United States by ORNL, now includes a formal IEA Annex agreement identified as Annex II between the United States, Germany, Sweden, Japan, and Belgium. The original annex included four subtasks: (1) information exchange, (2) ceramic powder characterization, (3) ceramic chemical and physical characterization, and (4) ceramic mechanical property measurements. In the United States, a total of 13 industrial and government laboratories have participated and contributed their resources to this research. The research in Subtasks 2, 3, and 4 is now complete. In 1990, research in two new subtasks was initiated, including Subtask 5, Tensile and Flexural Properties of Ceramics, and Subtask 6, Advanced Ceramic Powder Characterization. The research in Subtasks 5 and 6 was completed in 1993 and the reports were distributed. Two new tasks (Subtask 7 on Ceramic Machining and Subtask 8 on Ceramic Powder Characterization) were proposed in late FY 1993 and the research is completed (1996). Subtask 7 in the United States included eight companies and three federal laboratories. The report on the results from research performed in the United States on Subtask 7 is complete (the final report has been compiled of all the international research and distributed). Subtask 8 included six companies. The final report for Subtask 8 is complete. In 1996, research in two new subtasks was initiated, including Subtask 9 - Thermal Shock and Subtask 10 - Ceramic Powder Characterization. The final reports are complete (Subtask 9 - March 2000 and Subtask 10 - February 2000). Subtasks 11 (Techniques for the Measurement of Thermal and Mechanical Fatigue) and 12 (Characterizing Ceramic Powders) were initiated (October 1999). Subtask 12 research performed by NIST has been transferred to Versailles Project on Advanced Materials and Standards (VAMAS) and will no longer be part of this Annex (August 2000).

Recent Developments

A working group meeting was held in conjunction with the annual meeting of the American Ceramic Society. The following workscope was defined for Subtask 11:

(1) Measurement:

Thermal fatigue test. *[by Germany]*

Cyclic up-shock and cooling of a disk specimen by laser method.

Development of Mechanical fatigue evaluation methods. *[by USA and Japan]*

Mechanical bending in air (The same stress as that for the maximum thermal stress in disk specimens for thermal fatigue test should be included between the maximum and minimum stresses. The same temperature as that at the fracture point of disk specimens for thermal fatigue test.)

(2) Fractography of specimens above. *[by Sweden]*

(3) Issue of the country report. *[by each country]*

(4) Issue of the international report. *[by USA]*

(5) Material: One kind of advanced silicon nitride ceramics. (SN282 manufactured by Kyocera)

The International Energy Agency (IEA) Executive Committee (EC) Meeting, which was hosted by Erik Skog of Sycon (formally Sydkraft Konsult AB) was held at Sycon in Malmö, Sweden, on June 22. Attending the meeting were (1) Sidney Diamond - Department of Energy (DOE), Office of Transportation Technologies (United States Executive Committee Chairman), (2) Matt Ferber - Oak Ridge National Laboratory (ORNL) (United States Alternate Executive Committee Member),

(3) Ir. Willy Vandermeulen – Vlaamse Instelling voor Technologisch Onderzoek (VITO) (representing Belgium), (4) Rolf Wäsche – Bundesanstalt für Materialforschung und –prüfung (BAM) (German Executive Committee Member), (5) Masaru Yamashita – New Energy & Industrial Technology Development Organization (NEDO) (Japanese Alternate Executive Committee Member), (6) Mineo Mizuno – Japan Fine Ceramics Center (JFCC) (Japan National Technical Leader), (7) Erik Skog – Sycon (Swedish Executive Committee Member), and (8) Robert Pompe – Swedish Ceramic Institute (Swedish National Coordinator). The traveler represented the DOE, the current Operating Agent for Annex II, by chairing the meeting.

The major objectives of this meeting were to (1) conduct a technical information exchange between the participating countries, (2) review the status of the active Subtasks (11 and 12), (3) discuss proposed changes to our Implementing Agreement (IA) and modification to Annex II, and (4) discuss the future activities of the group. Concerning future activities, the possibility of focusing on diesel engine materials was discussed in detail. Dr. Ferber suggested that the development and verification of advanced characterization methods for these materials would be an appropriate topic.

Subtask 9, Thermal Shock

This Subtask is complete (March 2000).

Subtask 10, Characterizing Ceramic Powders

This Subtask is complete (February 2000).

Subtask 11, Techniques for the Measurement of Thermal and Mechanical Fatigue

In Subtask 11, techniques for the measurement of thermal and mechanical fatigue will be examined. The United States will supply the silicon nitride specimens to be used for the international exchange (SN282 manufactured by Kyocera Corp., Vancouver, Washington). National efforts in Japan and the United States will focus on the development of procedures for evaluating the mechanical fatigue behaviour of silicon nitride ceramics using either uniaxial flexure or biaxial test specimens. The national effort in Germany will consist of the development of thermal fatigue procedures using the laser thermal shock equipment evaluated in Subtask 9. The national effort in Sweden will focus on the evaluation of the fracture surfaces of specimens tested in Japan, the United States, and Germany. Subtask 11 will also include an international effort in which the thermal fatigue behaviour of a single silicon nitride will be compared with the mechanical fatigue data generated at a temperature which is the same as that at the fracture point in thermal fatigue test. Germany will be responsible for the thermal fatigue testing while both Japan and the United States will conduct mechanical fatigue testing. Sweden will perform fractographic analysis of the specimens. The schedule for Subtask 11 is as follows:

- Interim Report-June 22, 2000, Malmö, Sweden
- Interim Country Results-January, 2001 Cocoa Beach
- Final Country Results-April, 2001 TBD
- Final International Results and Final Report-October 2001, Pacific Rim 4

Rotary bend specimens (GS44 material) have been machined for fatigue testing. Testing of these specimens will be conducted at ORNL and Caterpillar.

Subtask 12, Characterizing Ceramic Powders – [See last paragraph – Transition to Versailles Project on Advanced Materials and Standards (VAMAS) (August 2000)]

At the recent IEA Executive Committee meeting, Dr. Wäsche reviewed the proposed effort for Subtask 12. The objectives of Subtask 12, as a follow-on to the work conducted under Subtask 10, will be to (1) tighten and finalize procedures for characterization of secondary properties of selected powders and granules; (2) initiate measurements directed towards characterization of green (pre-sintered) ceramics; and (3) unify IEA efforts with those of the American Society for Testing and Materials (ASTM), the Comité Européen de Normalisation (CEN), and the Japanese Industrial Standard (JIS), leading to International Organization for Standardization (ISO) adaptation. Subtask 12 will place more emphasis on green ceramics. As before, a thorough robustness testing of procedures will be performed prior to round-robin testing. The results that will be obtained through this international collaboration will benefit the international community by providing a basis for pre-standards and standards development and a foundation for improved powder processing and ceramic manufacturing technology.

Laboratories from Belgium, Germany, Japan, Sweden, and the United States representing industrial, academic, and government research organizations will participate in this project. Due to the interest in the Heavy Vehicle Propulsion System Materials Program on the development of international test methods for characterization and testing of advance materials for diesel engines, the powder characterization project will be transitioned to VAMAS – Versailles Project on Advanced Materials and Standards – during FY 2000. Plans will be established to initiate a new IEA activity focused on test methods and standards for the assessment of reliability of advanced materials used for diesel powered heavy vehicles.

The following measurement methods constitute a preliminary list that will be reviewed, finalized, and approved by the Participants prior to initiation of the measurements:

- (1) Density of green ceramics: This task is considered to be important, especially to establish measurement procedure for complex shapes, i.e., by the wax imbedding method or by the evacuation/intrusion method. A prestandard is necessary but it seems to be feasible.
- (2) Strength of green ceramics: This item seems feasible and fits in a way to the density measurements, i.e., strength of green ceramics and dependence of relative humidity.
- (3) Moisture content of granules: Fits into the schedule with green density and density gradients.
- (4) Density gradients in green ceramics: Standardisation seems to be difficult. Prestandard not yet possible. Information exchange is recommended. Round Robin seems to be an adequate measure with the aim of evaluation of methods which are used on international level.
- (5) Distribution of binders: First step necessary. Screening of methods necessary. Which methods are used and who is able to do this.

NOTE: During the past several years NIST has lead several IEA activities to establish the repeatability and reproducibility of test methods used for the characterization of ceramic powders through international round robin studies. This effort has lead to the establishment of several standard tests methods both in the U. S. and the IEA collaborating countries. As a direct result of these efforts and other DOE funded projects, advanced ceramics are now being used in diesel engines and many other applications requiring resistance to wear and corrosion. Due to the interest in the Heavy Vehicle Propulsion System Materials Program on the development of international standard methods for characterization and testing of advance materials for diesel engines, the powder characterization

project (Subtask 12) will be transitioned to Versailles Project on Advanced Materials and Standards (VAMAS). The transfer of this project to VAMAS is a natural step towards development of internationally agreed standard test methods for advanced materials. Upon transfer of the powder characterization project, plans will be established to initiate a new IEA activity focused on test methods and standards for the assessment of reliability of advanced materials used for diesel powered heavy vehicles.

Status of Milestones - Milestone.411531 [Publish Thermal Shock (Subtask 9) Final Report] due June 30, 2000 was completed this period. Milestone 411532 [Publish Powder Characterization (Subtask 10) Final Report] due June 30, 2000 was completed. Both reports were sent to the countries either electronically or on a CD disk. It was the consensus that electronic or CD disks would be provided rather than hard copies unless specifically requested. Milestone 411533 (Provide reports to ASTM) due July 31, 2000 which was changed to September 30, 2000 (need more information on whom to distribute these reports) has been changed to December 31, 2000.

New Milestones (Subtask 11) - 411534 (Interim Report-June 22, 2000, Malmö, Sweden, Executive Committee Meeting) Completed, June 22, 2000. 411535 (Interim Country Results-January, 2001 Cocoa Beach, Florida, meeting). 411536 (Final Country Results-April, 2001 TBD). 411537 (Final International Results and Final Report - October 2001, Pacific Rim 4 meeting, Hawaii).

Communications/Visits/Travel - Said Jahanmir visited with Ray Johnson and Matt Ferber on April 3 to discuss Subtask 12. Mineo Mizuno, Japan Fine Ceramics Center, visited ORNL on April 28 to discuss Subtask 11. Matt Ferber attended the annual AcerS meeting in St. Louis and also held a Subtask 11 Working Group Meeting (May 1, 2000).

Matt Ferber and Sid Diamond visited the following: 06/16/2000—Paris, France (site visit to IEA Headquarters); 06/18-06/21/2000—Goslar, Germany (attend the 7th International Symposium on Ceramic Materials and Components for Engines as United States representative of the International Advisory Committee); 06/22/2000—Malmo, Sweden (attend the International Energy Agency Executive Committee Meeting of the Implementing Agreement for a Programme of Research and Development on High Temperature Materials For Automotive Engines); 06/26/2000—Göteborg, Sweden (site visit to Volvo); 06/27/2000—Mölnlycke, Sweden (site visit to Daros Piston Rings).

Sid Diamond visited ORNL September 21, 2000.

Publications and Presentations -- Ferber, M. K., Kirchhoff, G., Hollstein, T., Westerheide, R., Bast, U., Rettit, U., and Mizuno, M., "Thermal Shock Testing of Advanced Ceramics - Subtask 9 (Final Report)," Oak Ridge National Laboratory, Oak Ridge, Tennessee, Report No. M00-107208, March 2000.

Lum, L. H., Gilissen, R., Meyer, K., Naito, M., Abe, H., Pompe, R., and Jahanmir, S., "Assessment of Powder Characterization Methods for Advanced Ceramics - Subtask 10 (Final Report)," prepared by National Institute of Standards and Technology, Report No. M00-107229 printed at Oak Ridge National Laboratory, Oak Ridge, Tennessee, February 2000.

Ceramic Mechanical Property Test Method Development

George D. Quinn (National Institute of Standards and Technology)

Objective/Scope

This task is to develop mechanical test method standards in support of the Propulsion Systems Materials Program. The test methods should meet the needs of the DOE engine community but should also consider the general USA structural ceramics community as well as foreign laboratories and companies. Draft recommendations for practices or procedures shall be developed based upon the needs identified above and circulated within the DOE ceramics engine community for review and modification. Round-robins will be conducted as necessary, but shall be well-focused, limited in scope, and complementary to IEA round-robins. Procedures developed in this program will be standardized by ASTM and/or ISO.

Technical Highlights and Results

1. Summary

In this semiannual period, progress continued on refining the flexure strength test for cylindrical test specimens. Extensive fractographic analysis on Ceradyne SRBSN was completed. We now have an excellent understanding of the nature of machining damage that can be introduced by various treatments in this material. General guidelines on how to detect machining damage have been prepared.

This work is in conjunction with the NIST Ceramics Machining Consortium.

In this semiannual period, the following draft standards were being developed:

- | | | |
|----|-----------------|--|
| 1. | ISO DIS 14704 | Advanced (Fine) Ceramics - Determination of Flexural Strength at Room Temperature (NIST-USA convenes) |
| 2. | ISO WD 15765 | Advanced (Fine) Ceramics - Determination of Flexural Strength at Elevated Temperature (NIST-USA convenes) |
| 3. | ISO draft 18766 | Fine (Advanced) Ceramics - Determination of Fracture Toughness at Room Temperature by the Surface Crack in Flexure (SCF) Method (convened by USA-NIST) |
| 4. | REBG-draft | Specification for Silicon Nitride Bearing Balls |
| 5. | ASTM C 1161 | Revisions to Flexural Strength Revisions |
| 6. | ASTM C-xxxx | Standard Test Method for Flexural Strength of Advanced Ceramics at Ambient Temperature - Cylindrical Rod Strength |
| 7. | ASTM C 1198 | Revisions to: Standard Test Method- Dynamic Elastic Modulus |
- (DIS = Draft International Standard; FDIS = Final Draft International Standard, WD = Working Draft)

Earlier work in this project has contributed to thirteen completed standards:

- | | | |
|-----|----------------|---|
| 1. | ASTM C 1161-90 | Standard Test Method for Flexural Strength of Advanced Ceramics at Ambient Temperature |
| 2. | ASTM C 1198-91 | Dynamic Young's Modulus, Shear Modulus, and Poisson's Ratio for Advanced Ceramics by Sonic Resonance |
| 3. | ASTM C 1211-92 | Standard Test Method for Flexural Strength of Advanced Ceramic at Elevated Temperature |
| 4. | MIL HDBK 790 | Fractography and Characterization of Fracture Origins in Advanced Structural Ceramics |
| 5. | ASTM C 1239-94 | Standard Practice for Reporting Strength Data and Estimating Weibull Distribution Parameters |
| 6. | ASTM C 1322-96 | Standard Practice for Fractography and Characterization of Fracture Origins in Advanced Ceramics |
| 7. | ASTM C 1326-96 | Standard Test Method for Knoop Indentation Hardness of Advanced Ceramics. |
| 8. | ASTM C 1327-96 | Standard Test Method for Vickers Indentation Hardness of Advanced Ceramics. |
| 9. | ASTM PS 070-97 | Standard Test Methods for the Determination of Fracture Toughness of Advanced Ceramics |
| 10. | ASTM E-1875-98 | Standard Test Method for Dynamic Young's Modulus, Shear Modulus, and Poisson's Ratio by Sonic Resonance |

- | | | |
|-----|----------------|---|
| 11. | ASTM E-1876-98 | Standard Test Method for Dynamic Young's Modulus, Shear Modulus, and Poisson's Ratio by Impulse Excitation |
| 12. | ASTM C 1421-99 | Standard Test Methods for Determination of Fracture Toughness of Advanced Ceramics |
| 13. | ISO 14705-2000 | Fine Ceramics (Advanced Ceramics, Advanced Technical Ceramics) - Test Method for Hardness for Monolithic Ceramics at Room Temperature |

2. Fracture Toughness

2a. ASTM Standard C 1421-99

The November, 2000 ASTM symposium on fracture resistance testing has been organized by Mr. Quinn in cooperation with Jon Salem at NASA-Glenn and Mike Jenkins at the University of Washington. This symposium will be a good opportunity to inform the ceramic and engineering community about the new fracture toughness standards.

A scheduled talk on the fracture toughness standards was presented at American Ceramic Society Conference in St. Louis in April, and paper on C 1421 and the associated SRM 2100 were presented at an ASTM E-08 Fracture and Fatigue symposium in ASTM headquarters in June 2000. Our goal with all these papers and presentations is to spread the word about the new ASTM standard.

2b. Draft International Standard 18766, SCF Method, ISO Technical Committee TC 206

During this period we learned that the ISO TC 206 secretariat had completely retyped the "Working Draft" document so that it could be formally advanced to "Committee Draft" stage. The latest "Working Draft" included major changes and incorporated the first language in any draft standard in the world on the topic of estimating R-curves in Ceramics. Mr. Quinn strongly recommended that the document be withdrawn from CD review and the secretariat agreed. The document was withdrawn as Committee Draft. It is easier to refine the document and make substantive changes when it is in a working draft status. In July, it was decided to hold the document back for 6 months to a year in order to pursue the following loose ends:

1. There is some resistance to inclusion of R-curve provisions, even in an appendix, by some members of the US delegation. The extra time may be used to conduct some corroborative experiments at NIST to verify that the procedures in the draft standards are reasonable.
2. Jon Salem at NASA-Glenn had requested NIST to conduct some extra experiments by the SCF method to try to clarify some results obtained on sintered alpha silicon carbide.
3. The matter of possible interferences from lateral cracks needs to be investigated further. At the Fractography of Glasses and Ceramic Conference in Alfred University in July 2000, Ms. Monica Hangl of the University of Leoben, Austria presented some fascinating results on the presence of secondary lateral cracks that extend very deeply below the surface in some ceramics. Such deep laterals could interfere with the fracture toughness type tests, which presume that only a median crack is present.

3. Flexure Strength at Room Temperature - New Semi articulating Fixture Design

No activity this period. All work is complete, but a report and engineering drawings must be prepared.

4. Diametral Compression

No activity this period. This work is on hold pending further intensive fractographic analysis to determine why our earlier test specimens did not fracture from volume flaws in the middle of the

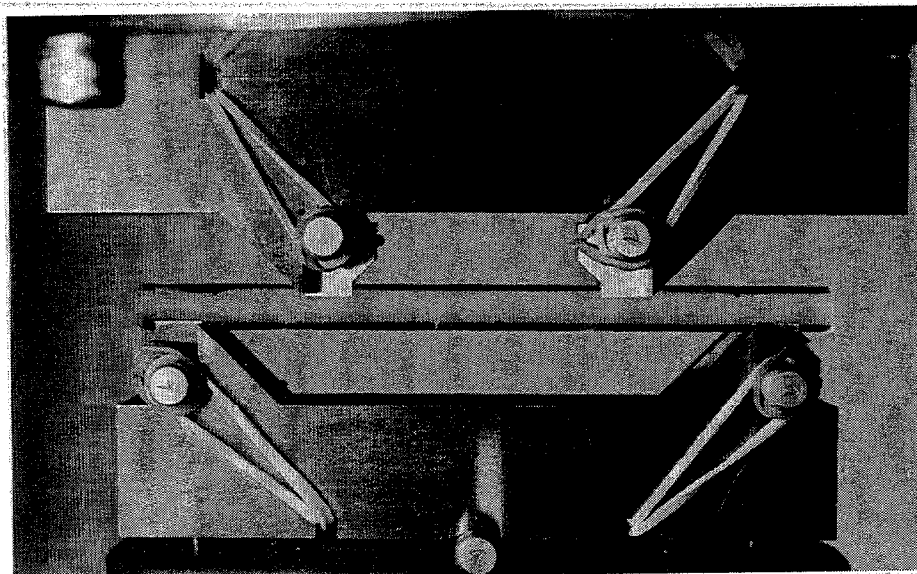


Figure 1 The flexure fixtures for rod specimens.

specimens. We remain optimistic that this method can be refined and made into a user friendly, standardized test.

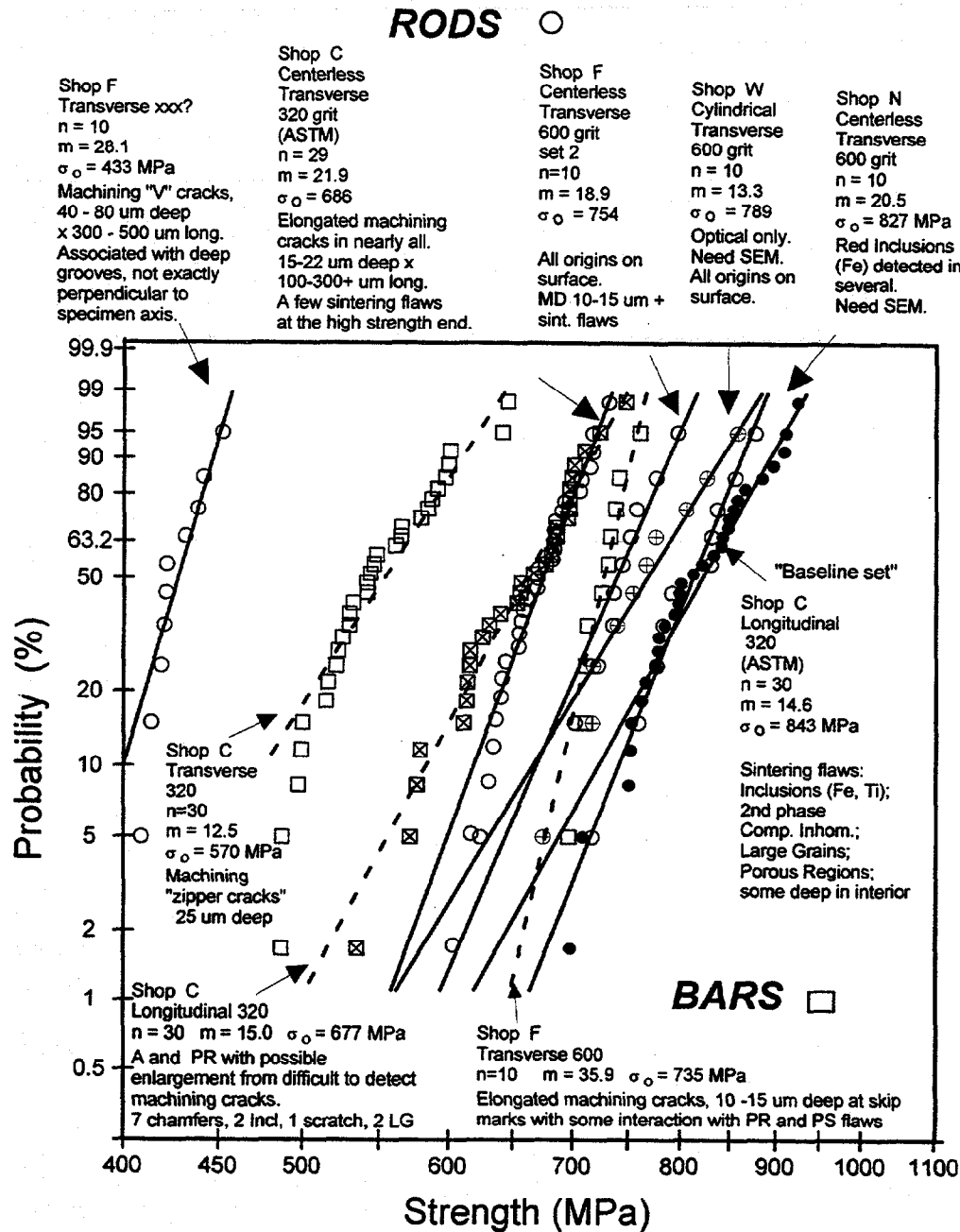
5. Flexure Testing of Cylindrical Ceramic Specimens

Figure 1 shows the new fixture design developed as part of the NIST Machining of Ceramics Consortium. Since there is interest within the DOE Heavy Duty Diesel community for such testing, we accelerated the development of this testing methodology in this program. At the ASTM Committee C-28 meeting in St. Louis in May, 2000 Mr. Quinn made a 15 minute presentation about this project. We presented a draft outline of an ASTM standard test method for flexural strength testing of cylindrical rods. A master review paper on cylindrical flexure strength testing is about half finished.

During this semiannual period we completed a thorough fractographic analysis of fractured Ceradyne sintered reaction-bonded silicon nitride rods. This work was performed in conjunction with the NIST Machining of Ceramics Consortium program. Almost 200 rods and matching bend bars have now been tested and examined carefully with optical microscopy. Over one third were scrutinized with scanning electron microscopy. A very detailed correlation of fractographic and strength and machining procedures was documented in a key paper presented at the July 2000 Alfred University Conference on the Fractography of Glasses and Ceramics. The results of all this analysis are too voluminous to recount here, so we cover only a few primary findings.

Figure 2 shows the final outcomes of the comprehensive analysis for silicon nitride 6 mm diameter rods tested on the new NIST four-point flexure fixture with 40 mm x 80 mm spans. The **inherent strength** (fracture from the material's inherent flaws) was measured with rods ground longitudinally with a 320 grit wheel by Shop C. Many of the origins were located well into the interior and machining damage *was not a factor*. Three batches of rods ground with 600 grit transverse grinding had strengths that either matched the inherent strength level or had only a minor strength reduction (10% or less). That 600 grit transverse grinding is not very deleterious is a very positive outcome. Transverse grinding is

Figure 2 Flexural strengths of rods and rectangular bars of Ceradyne SRBSN prepared by a variety of machining procedures. The Shop C longitudinally-ground rods furnished a baseline strength since nearly every specimens fractured from the material's inherent flaws. Several 600 grit transversely-ground rod data sets match or come close to matching the baseline strength distribution. Note also that the Shop F 600 grit rods and bars have almost identical strengths.



certainly easier to apply to rods than longitudinal grinding. Many components must be transversely ground.

Other more aggressive grinding procedures, e.g. 320 grit transverse, had more deleterious effects upon strength, both for rods and bars. Machining cracks were obvious in these specimens. We were able to measure the size, shape, and severity of the machining flaws. They are not all identical and there are different types of machining cracks. There was a direct correlation between the size and severity of the flaws and the strengths. This is exactly as predicted from fracture mechanics, but comprehensive, detailed corroborations such as we have achieved are very rare. Initially, we thought it would be difficult to detect the machining flaws in this particular toughened silicon nitride, but patience and persistence paid off. Eventually we learned that machining cracks have telltale features that make them easy to spot in many cases. For example, fingerlets at the origin such as shown in Figure 3 are a dead giveaway that a machining crack or a scratch is at the origin. Another telltale feature is a *flattened fracture mirror*. Fracture mirrors that are *wider along the tensile surface* than they are deep, are very indicative of a long shallow crack or scratch on the surface. The widening can be pronounced and has been quantified as shown in Figure 4. What is remarkable about this is that we have a telltale feature that is indicative of machining damage and *does not even require the flaw itself to be seen!* Low power ~20X microscopy is sufficient. Indeed, some photocopies of fracture mirrors in the Oak Ridge Report: "Strength and Fatigue of NT 551 Silicon Nitride and NT 551 Diesel Exhaust Valves," by Andrews, Wereszczak, Kirkland and Breder show elongated fracture mirrors with the transversely-ground Norton NT 551 bars!

A general users guide on how to detect machining damage has been prepared in an effort to enable general engineers and non-expert fractographers to detect machining cracks. Figures 5 and 6 show a few key illustrations that can be consulted for assistance. We envision that these illustrations can be added to the ASTM C 1322 fractographic analysis standard and can also be included in Lew Ive's new Standard Practice for the Effect of Machining on Strength Standard.

Matching rectangular bend bars were also prepared in several cases. In one instance, Shop F's 600 grit transversely ground rods and bars had nearly identical strengths, and it was confirmed that the fracture origins were nearly identical: 10 – 15 μm deep machining cracks that intersected natural inherent flaws in the material. It is very reassuring that rods and bars of the same material would have the same strengths and same flaws.

In contrast, another set of rectangular bars prepared by Shop C with 320 grit longitudinal machining did not match the rod strengths. In each case, the dominant flaws were material inherent flaws and machining damage was inconsequential. The specific nature of the inherent flaws varied, however. The rods had a greater fraction of inclusions, compositional inhomogeneities and pore type flaws, whereas the bend bars had pores and collapsed spray dry powder agglomerates. Although the material flaws did not quite match between the bars and rods, it was nonetheless gratifying to observe that the 320 grit longitudinal-grinding in both rods and bars was *not deleterious* to strength. Strength-limiting machining flaws were rare.

6. Flexure Testing of Segmented Cylindrical Ceramic Specimens

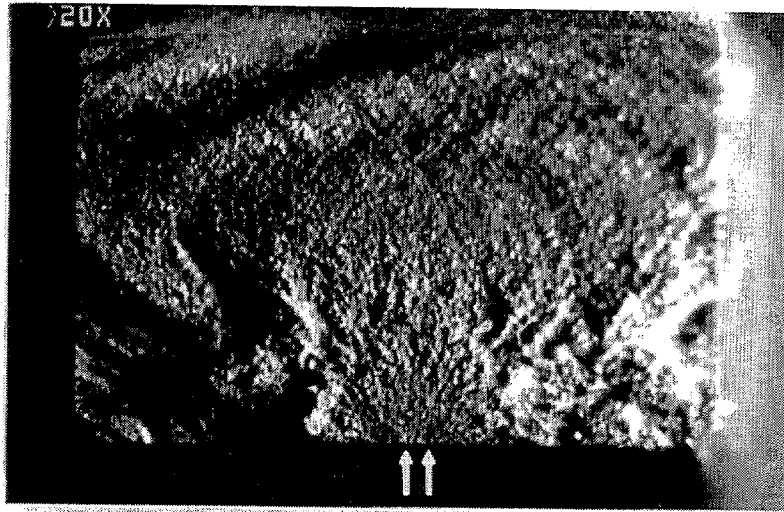
No progress this period.

7. Rolling Element Bearing Group (REBG) Silicon Nitride Bearing Ball Specification

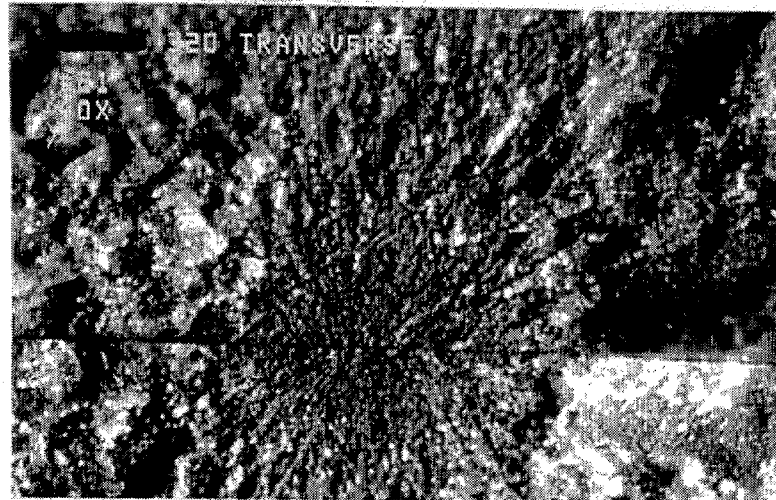
The REBG dissolved and reestablished itself as a formal ASTM Committee. Their first meeting was in April and much of the meeting was evidently spent getting organized and learning how ASTM

Figure 3 Examples of a “Zipper” machining crack SRBSN. 320 grit transverse ground. 487 MPa.

20X
Optical



40X
Optical



150X
SEM

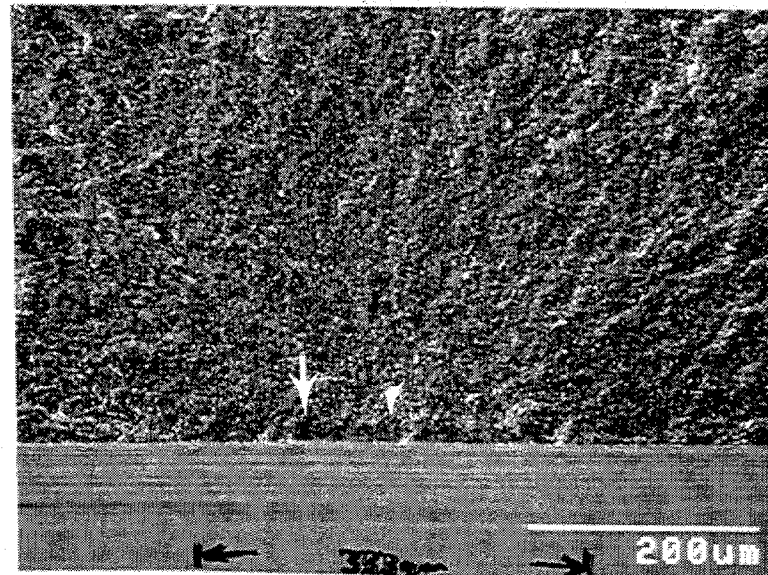


Figure 4 Elongated fracture mirrors are telltale signs of surface machining damage or scratches. Ellipticity is the ratio of mirror depth to width. The data below are for 320 grit transversely-ground silicon nitride rectangular bars. Ellipticity is directly related to the flaw severity. The weaker the specimen, the severer the flaw, and the more elongated the mirror. It is easy to discern the flattened mirrors with low power optical microscopy when the ellipticities are less than 0.85.

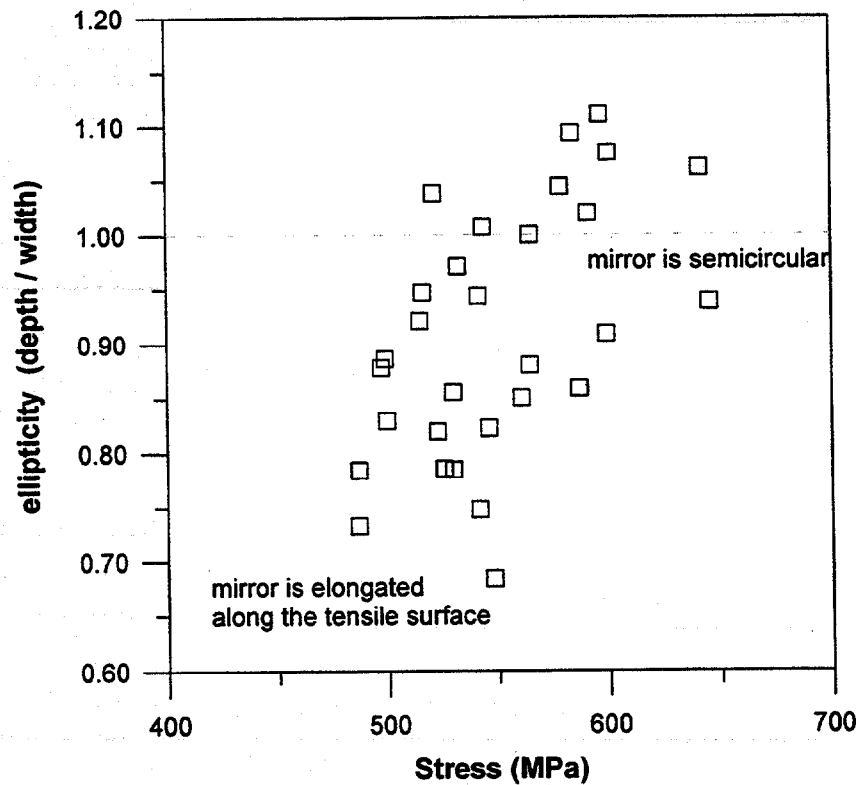
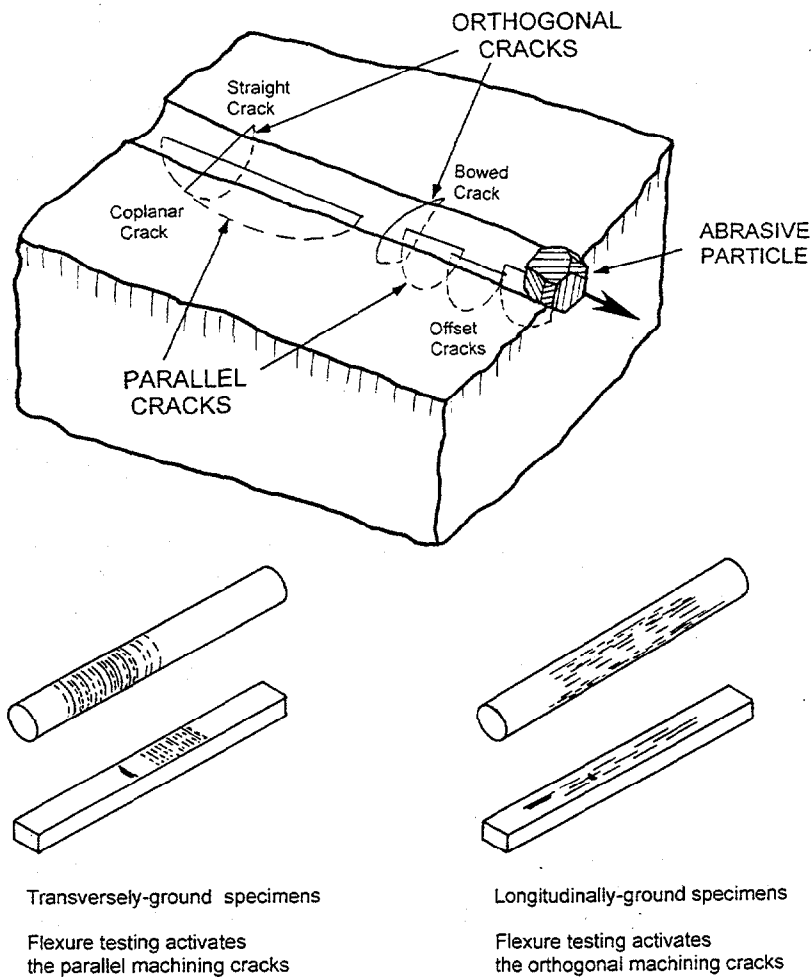


Figure 5. Schematic of flaws introduced by machining or scratching a ceramic or glass surface. An abrasive grit particle moves from left to right. Lengthy coplanar or shorter overlapping semi-elliptical *parallel cracks* form in the direction of abrasive motion. Short *orthogonal cracks* form perpendicular to the abrasive motion direction. Although the *parallel* and *orthogonal* cracks have similar depths, the former are severer due to their greater length and stress intensity shape factor. This often causes a dependence of specimen strength on the direction of machining, if machining cracks are strength limiting. Adapted from Rice and Mecholsky.¹



¹ There are two primary changes to their figure. First, the bowed orthogonal cracks are corrected to bow in the *direction of the abrasive motion*. Secondly, Rice and Mecholsky used the terms "longitudinal" and "transverse" in a manner which caused some confusion. They used the terms to describe the cracks with respect to the grinding direction. The long cracks parallel to the machining direction were called "longitudinal cracks", and the shorter orthogonal cracks were called "transverse cracks." Using their nomenclature, flexure testing of *longitudinally*-ground bend bars would activate *transverse* cracks and vice versa. The new nomenclature shown in the Figure above eliminates this confusion.

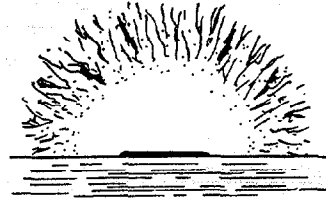
Figure 6 Telltale signs of machining cracks. These flaws are common in biaxial disks and transversely-ground uniaxial flexure or tension strength specimens.

Fractographic Manifestations of Machining Damage

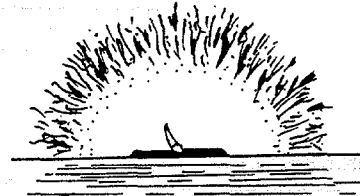
GROUND SURFACES

Common in biaxial disks and transversely-ground uniaxial flexural or tension strength specimens.

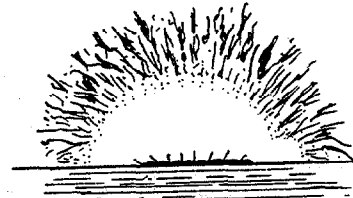
(a) **elongated "coplanar parallel crack"**
(or coplanar linked semi-elliptical cracks).
A deep striation may or may not necessarily be present.
The fracture mirror may be elongated along the outer specimen surface.



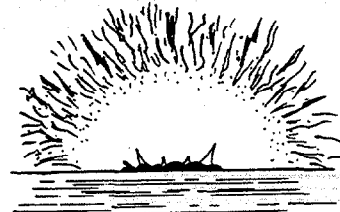
(b) **elongated "coplanar parallel crack"**
linked with a **natural flaw**.
A step in the fracture origin emanates from the discontinuity.



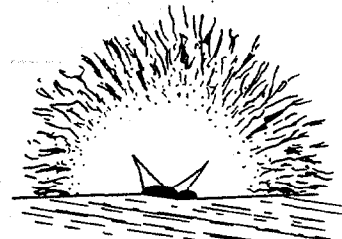
(c) **"zipper crack"**
This is a series of short semi elliptical cracks, which have linked. A series of short tails, or "**machining crack hackle,**" emanate from the links or overlaps of the flaws and extend up into the fracture mirror. These tails may be tilted to the left or right and help confirm that fracture originated in the central region of the set. The short tails are telltale features of slightly misaligned or overlapping transverse machining cracks (or a scratch) and are often easier to see with an optical microscope with low angle lighting than with a scanning electron microscope. The fracture mirror may be elongated along the specimen outer surface or it may have one or two prominent **side lobes**. This origin type is common in transversely-ground rectangular flexure specimens or scratched biaxial disk specimens.



(d) **coarse "zipper crack"**
This is made up of a series of irregular, less coplanar semi-elliptical cracks. Larger tails than in (c) are created. In severe cases, the tail may extend all the way to the mirror boundary. The fracture mirror may be elongated. This origin is common in transversely ground or scratched specimens and the markings are sometimes termed "**shark's teeth.**"



(e) **"V machining crack"**
The crack(s) that intersects the fracture surface at an angle. Only a portion of the machining crack series is exposed. A pronounced step occurs in the fracture mirror. One or two (shown) tails extend well up into the fracture mirror. The machining direction is not quite perpendicular to the specimen length and uniaxial stress axis due to grinding wheel cross feed. This origin is common in cylindrical specimens prepared by centerless or transverse grinding wherein the wheel and work piece displace axially relative to each other.



functions. A few minor changes to the specification were made. Mr. Quinn plans to attend their next meeting in November in Orlando.

8. Review ASTM C 1161 Flexural Strength "Standard Procedure" for machining specimens

A presentation was made in the ASTM Subcommittee C28.01 meeting in St. Louis about possible changes to the machining specifications in the ASTM flexure standards C 1161 and C 1211. These procedures trace their roots back to the MIL STD 1942(MR) in 1983. It is felt that after 17 years, we may wish to reconsider some of the tolerances and requirements. The last bimonthly listed the specifications and some suggested changes. Much of the work performed in the NIST Machining of Ceramics Consortium program has shed new light on machining cracks, their size, morphology and depth. Some of these results were reviewed at the ASTM meeting, but there really was not sufficient time to discuss them all in detail.

Following the meeting, Mr. Quinn met with Ron Chand who suggested some useful improvements to the C 1161 specifications. Hopefully, a major revision to C 1161 in general, and the machining specifications in particular, can be prepared before the next C 128 meeting in November 2000

9. Elastic Modulus by Resonance, Revise ASTM C 1198 and C 1259

Mr. Quinn and Jeff Swab will refine ASTM standards C 1198 and C 1259 for the influence of chamfers. Years ago as part of this project, we helped write ASTM standard C 1198 for the determination of elastic modulus of ceramics by resonance of prism specimens. This standard was adapted to more modern impulse excitation methods which also use beam resonance and standard C 1259 also was prepared. The resonance method of elastic modulus determination entails measuring the resonant frequency of vibration of a prismatic beam specimen. Elastic modulus is calculated from the beam mass, dimensions, and the resonant frequency. This is a well established, simple methodology which has been codified in the two C-28 standards. The standards require nearly perfect rectangular beam specimens, however, since the equations which relate elastic modulus to the beam dimensions, beam mass, and the resonant frequency assume that the beam has a perfect rectangular geometry. C 1198 and C 1259 recommended against using chamfered bars. A paper on how to extend the applicability of C 1198 and C 1259 to ordinary chamfered ceramic strength specimens was written and published by the Journal of the American Ceramic Society in February, 2000.

A proposed revision to C 1198 and C 1259 will be presented at the ASTM Committee C-28 meeting in November 2000 in Orlando for consideration for a subcommittee ballot in winter of 2000/2001.

10. ISO Technical Committee TC 206 (Fine Ceramics)

WG 2 Flexure Strength at Room Temperature

The draft standard passed the Final Draft International Standard ballot. Japan voted negative on the grounds that as-fired specimens and fully-articulated fixtures needed to be reconsidered. The United Kingdom voted negative on the grounds that they already had a CEN standard for Europe and the ISO standard was not compatible. Nine other countries voted affirmative. The document is ready for its final worldwide ballot

WG 3 Hardness

This document, ISO 14705, was approved in 2000 and now is a formal ISO standard. It is harmonious with ASTM C 1326 and C 1327.

WG 8 Flexural Strength at Elevated Temperature

A VAMAS Technical Working Area 3 international round robin was completed. This project was organized by the Japan Fine Ceramic Center. The draft final report, written by Drs. Okada and Mizuno, was thoroughly reviewed and we recommended many refinements. It was published in September as:

“VAMAS Round Robin on Flexural Strength of Silicon Nitride at High Temperature,” Versailles Advanced Materials and Standards Report #39 ISSN 1016-2186, Japan Fine Ceramic Center, Nagoya, Japan, September 2000.

The project was organized as a direct challenge to the United States and Europe on the matter of the best requirements for flexural strength fixtures. The Japanese felt that the USA and European standards (with their recommendations for using fully-articulating fixtures with rolling-pin loading points) were too restrictive. Much to our gratification, the results of the round robin show that the best results were obtained with fully-articulating fixtures with rolling-pin loading points. The positive outcome will hopefully alleviate many of the concerns the Japanese have had about such issues for the last 20 years.

This TWA 3 project was a logical follow on to the International Energy Agency Subtask 5 round robin project of 1989-1993. We are grateful to Kristin Breder at ORNL and Sung Choi who contributed a lot of help to the 1999-200 VAMAS TWA 3 program.

As a result of the VAMAS round robin, a new annex to the ISO draft standard was written by Mr. Quinn. The annex is attached to this semiannual report.

12. Other Activities*12a. Review of biaxial creep data*

We recently no feedback from NASA-Glenn after we sent them a complete set of biaxial disl creep data collected I 1987 and 1988. This topic was discussed in the last semiannual report.

12b. VAMAS round robins relevant to this project.

The round robin on elevated temperature flexural strength was completed and valuable lessons learned will be applied to the ISO Working Group 8 draft standards as described above. During this period, Mr. Quinn resigned as chairman of VAMAS Technical Working Area 3, Ceramics. Mr. Quinn nominated Dr. Kristin Breder of the Higgins Grinding Center, Norton Company as the new TWA 3 chairperson. The VAMAS Steering Committee approved the nomination.

Problems encountered

None this period.

Publications/Presentations

There was a lot of writing and presenting this semiannual period!

1. G. Quinn and J. Swab, “Elastic Modulus by Resonance of Rectangular Prisms: Corrections for Chamfers,” *J. Am. Ceram. Soc.*, 83 [2] 317-320 (2000).
2. G. D. Quinn, L. Ives, P. Koshy, and S. Jahanmir, “Flexural Strength of Cylindrical Test Specimens,” presented at the Annual Meeting of the American Ceramic Society, May 1, 2000, St. Louis.
3. G. Quinn, “Fracture Toughness Standard Test Methods,” presented at the Annual Meeting of the American Ceramic Society, May 2, 2000, St. Louis.
4. I. Bar-On, G. D. Quinn, J. Salem, and M. J. Jenkins, “Fracture Toughness Standard Test Method C 1421-99 for Advanced Ceramics,” presented at the 32nd National Symposium on Fatigue and Fracture, ASTM, June 16, 2000, *to be publ. in ASTM STP 1406*, 2001.

5. G. D. Quinn, K. Xu, R. Gettings, J. A. Salem, and J. Swab, "Standard Reference Material 2100: Ceramic Fracture Toughness," presented at the 32nd National Symposium on Fatigue and Fracture, ASTM, June 16, 2000, *to be publ. in ASTM STP 1406*, 2001.
6. G. D. Quinn and J. J. Swab, "Comparisons of Calculated and Measured Flaw Sizes," presented at the 4th International Conference on the Fractography of Glasses and Ceramics, Alfred University, July 2000, *to be publ. in Ceramic Transactions*, eds, J. Varner, G. Quinn, V. Frechette, American Ceramic Society, Westerville, OH, 2001.
7. G. D. Quinn, L. K. Ives, S. Jahanmir, and P. Koshy, "Fractographic Analysis of Machining Cracks in Silicon Nitride Rods and Bars," presented at the 4th International Conference on the Fractography of Glasses and Ceramics, Alfred University, July 2000, *to be publ. in Ceramic Transactions*, eds, J. Varner, G. Quinn, V. Frechette, American Ceramic Society, Westerville, OH, 2001.
8. G. Quinn, "Special Mechanical Testing Methods for Ceramics," Chapter 4-9-7n in *Encyclopedia of Materials Science and Technology*, Elsevier, *to be publ. 2001*
9. M. Jenkins, G. D. Quinn, J. A. Salem, I. Bar-On, "Development, Verification and Implementation of a National Full-Consensus Fracture Toughness Test Method Standard for Advanced Ceramics," , " to be presented at and published in the proceedings of the November, 2000 Symposium on *Fracture Resistance Testing of Monolithic and Composite Brittle Materials*, ASTM STP 1409, J. A. Salem, M. G. Jenkins, and G. D. Quinn, eds., ASTM, West Conshohocken, PA 2001.
10. G. D. Quinn, "The Fracture Toughness Round Robins in VAMAS: What We Have Learned," to be presented at and published in the proceedings of the November, 2000 Symposium on *Fracture Resistance Testing of Monolithic and Composite Brittle Materials*, ASTM STP 1409, J. A. Salem, M. G. Jenkins, and G. D. Quinn, eds., ASTM, West Conshohocken, PA 2001.
11. G. D. Quinn, K. Xu, R. J. Gettings, J. A. Salem, and J. J. Swab, "Does Anyone Know the Real Fracture Toughness? SRM 2100: the World's First Ceramic Fracture Toughness Reference Material," , " to be presented at and published in the proceedings of the November, 2000 Symposium on *Fracture Resistance Testing of Monolithic and Composite Brittle Materials*, ASTM STP 1409, J. A. Salem, M. G. Jenkins, and G. D. Quinn, eds., ASTM, West Conshohocken, PA 2001.

Communications/Visits

Mr. Quinn attended the meeting of ASTM Committee C-28 as well as the American Ceramic Society in St Louis in May, 2000. Mr. Quinn also attended the Fourth International Conference on Fractography of Glasses and Ceramics, Alfred University, July, 2000.

The following has been proposed as a new annex to the draft International Standards Organization standard for elevated temperature flexural strength testing of ceramics.

ANNEX F

VAMAS Round Robin

A round robin project on elevated temperature flexure strength was conducted under the auspices of the Versailles Advanced Materials and Standards (VAMAS) program in 1999 – 2000. Thirteen laboratories in six countries measured the strength of silicon nitride at 1200°C in air. Semi- and fully-articulating fixtures were used. All testing was in four-point flexure, with either 10 mm x 30 mm or 20 mm x 40 mm spans. Most laboratories tested 10 or 12 specimens.

Some of the conclusions from this project are:

- a. The strengths of specimens tested with the 10 mm x 30 mm spans were slightly greater (6.3%) than the strengths of specimens tested with 20 mm x 40 mm spans. The difference in average strengths was primarily due to the difference in Weibull effective volumes or effective areas. (The Weibull modulus was approximately 10.)
- b. Specimens tested on fully-articulated fixtures were slightly stronger (5.1%) than specimens tested on semi-articulated fixtures.
- c. The limited number of specimens tested by each laboratory led to a large reproducibility uncertainty (between-laboratory strength variations). Much of the difference can be attributed to small sample size statistical effects and the differences are within the confidence intervals predicted by Weibull statistics.
- d. Supplemental experiments confirmed that friction constraints may affect load-displacement curve data (and presumably the measured flexure strength) with fixtures having rollers that are not completely free to roll. Fixtures with rollers in square slots of insufficient clearance may inhibit roller motion.
- e. Additional testing in inert nitrogen environment was performed by two laboratories. Nitrogen-tested specimens were weaker than air-tested specimens, presumably due to oxidative crack healing in the latter.
- f. Load-displacement curves were valuable in interpreting the performance of the test fixtures and for confirming that the material has linearly-elastic behavior up to fracture.

Reference

[F1] A. Okada and M. Mizuno, "VAMAS Round Robin on Flexural Strength of Silicon Nitride at High Temperature," Versailles Advanced Materials and Standards Report #39 ISSN 1016-2186, Japan Fine Ceramic Center, Nagoya, Japan, September 2000.

INTERNAL DISTRIBUTION

L. F. Allard, Jr.
P. F. Becher
T. M. Besmann
P. J. Blau
R. A. Bradley
T. D. Burchell
A. Choudhury
S. A. David
M. K. Ferber
R. L. Graves
C. R. Hubbard
M. A. Janney
D. R. Johnson (5)
R. R. Judkins
M. A. Karnitz
J. O. Kiggans

E. Lara-Curzio
R. J. Lauf
H. T. Lin
K. C. Liu
R. A. Lowden
W. D. Manly
S. B. McSpadden
A. E. Pasto
M. H. Rawlins
A. C. Schaffhauser
D. P. Stinton
T. N. Tiegs
S. G. Winslow
R. E. Ziegler
Laboratory Records - RC

Jeffrey Abboud
Gas Turbine Association
1050 Thomas Jefferson St., NW, 5th Floor
Washington DC 20007

B. P. Bandyopadhyay
University of North Dakota
Box 8359 University Station
Grand Forks ND 58202-8359

Donald F. Baxter, Jr.
Advanced Materials & Processes
ASM International
9639 Kinsman Road
Materials Park OH 44073-0002

M. Brad Beardsley
Caterpillar Inc.
Technical Center Bldg. E
P.O. Box 1875
Peoria IL 61656-1875

Ramakrishna T. Bhatt
NASA Glenn Research Center
MS-106-1
21000 Brookpark Road
Cleveland, OH 44135

Bruce Boardman
Deere & Company, Technical Ctr.
3300 River Drive
Moline IL 61265-1792

Donald J. Bray
Advanced Refractory Technologies
699 Hertel Avenue
Buffalo NY 14207

Jeff Bougher
Caterpillar Inc.
Technical Center, Bldg. E
P.O. Box 1875
Peoria IL 61656-1875

Mike Bowling
Cummins Engine Company, Inc.
1900 McKinley Avenue
P.O. Box 3005
Columbus IN 47202-3005

Walter Bryzik
U.S. Army Tank Automotive
Command
R&D Center, Propulsion Systems
Warren MI 48397-5000

David Carruthers
Kyocera Industrial Ceramics
5713 East Fourth Plain Blvd.
Vancouver WA 98661

Ronald H. Chand
Morton Advanced Materials
185 New Boston Street
Woburn MA 01801

William J. Chmura
Torrington Company
59 Field Street, P.O. Box 1008
Torrington CT 06790-1008

William S. Coblenz
Defense Adv. Research Projects Agency
3701 N. Fairfax Drive
Arlington VA 22203-1714

Gloria M. Collins
ASTM
100 Barr Harbor Drive
West Conshohocken PA 19428-2959

Shawn Cooper
FEV Engine Technology
4554 Glenmeade Lane
Auburn Hills MI 48326-1766

Douglas Corey
Honeywell
2525 West 190th Street, MS:T52
Torrance CA 90504

Keith P. Costello
Chand/Kare Technical Ceramics
2 Coppage Drive
Worcester MA 01603-1252

Gary M. Crosbie
Ford Motor Company
P.O. Box 2053, 20000 Rotunda Drive
MD-3182, SRL Building
Dearborn MI 48121-2053

Pamela Cunningham
WETO Technical Library
MSE, Inc.
Industrial Park, P. O. Box 4078
Butte MT 59702

S. Keoni Denison
Norton Company
1 New Bond Street
Worcester MA 01615-0008

Sidney Diamond
U.S. Department of Energy
Office of Transportation Technologies
EE-33, Forrestal Building
Washington DC 28505

Michael Easley
Honeywell
P. O. Box 52181
MS 551-11
Phoenix AZ 85072-2181

James J. Eberhardt
U.S. Department of Energy
Office of Transportation Technologies
EE-33, Forrestal Building
Washington DC 20585

Jim Edler
Eaton Corporation
26201 Northwestern Highway
P.O. Box 766
Southfield MI 48037

William A. Ellingson
Argonne National Laboratory
Energy Technology Division, Bldg. 212
9700 S. Cass Avenue
Argonne IL 60439-3848

John W. Fairbanks
U.S. Department of Energy
Office of Transportation Technologies
EE-33, Forrestal Building
Washington DC 20585

Ho Fang
Applied Materials
2695 Augustine Drive, MS-0962
Santa Clara CA 95054

Dan Foley
Honeywell
MS:1/5-1, 26000
2525 West 190th Street
Torrance CA 90504

Douglas Freitag
DuPont Lanxide Composites
21150 New Hampshire Avenue
Brookeville MD 20833

Richard Gates
NIST
Bldg. 223, Rm. A-256
Rt. 270 & Quince Orchard Road
Gaithersburg MD 20899

Ludwig J. Gauckler
ETH Zurich
Nonmetallic Materials
Sonneggstr. 5
CH-8092 Zurich, SWITZERLAND

Robert J. Gottschall
 U.S. Department of Energy
 Metal & Ceramic Sciences, ER-131
 19901 Germantown Road
 Germantown MD 20874-1290

Thomas J. Gross
 U.S. Department of Energy
 Office of Transportation Technologies
 EE-30, Forrestal Building
 Washington DC 20585

Changsheng Guo
 United Technologies Research Center
 Machining Systems, MS 129-46
 East Hartford CT 06108

Darryl Gust
 Cummins Engine Company, Inc.
 1900 McKinley Avenue
 P.O. Box 3005
 Columbus IN 47202-3005

Nabil S. Hakim
 Detroit Diesel Corporation
 13400 Outer Drive West, A08
 Detroit MI 48239-4001

Alan M. Hart
 Dow Chemical Company
 1776 Building
 Midland MI 48674

Deborah A. Haught
 U.S. Department of Energy
 Office of Power Technologies
 EE-23, Forrestal Bldg.
 Washington DC 20585

Daniel Hauser
 Edison Welding Institute
 Microjoinint & Plastics Tech. Team
 1250 Arthur E. Adams Drive
 Columbus OH 43221-3585

John Haygarth
 Wah Chang
 P.O. Box 460
 Albany OR 97321-0460

Gene Huber
 Precision Ferrites & Ceramics
 5432 Production Drive
 Huntington Beach CA 92649-1525

Adam Jostsons
 ANSTO
 PMB1
 Menai, NSW, Australia 2234

Yury Kalish
 Detroit Diesel Corporation
 Mechanical Systems
 13400 Outer Drive West
 Detroit MI 48239-4001

Roy Kamo
 Adiabatics, Inc.
 3385 Commerce Park Drive
 Columbus IN 47201

Ralph Kelly
 Cincinnati Milacron
 P.O. Box 9013
 Cincinnati OH 45209

W. C. King
 Mack Truck, Z-41
 1999 Pennsylvania Avenue
 Hagerstown MD 21740

Tony Kirn
 Caterpillar Inc.
 Defense Products Dept., JB7
 Peoria IL 61629

Joseph A. Kovach
Parker Hannifin Corporation
6035 Parkland Boulevard
Cleveland OH 44124-4141

Edwin H. Kraft
Kyocera Industrial Ceramics
5713 E. Fourth Plain Boulevard
Vancouver WA 98661

Oh-Hun Kwon
Norton Company
Saint Gobain Industrial Ceramics
1 Goddard Road
Northboro MA 01532-1545

S. K. Lau
B. F. Goodrich Aerospace R&D
9921 Brecksville Road
Brecksville OH 44141

Elaine Lentini
Saint-Gobain Industrial Ceramics
Goddard Road
Northboro MA 01532

Stan Levine
NASA Glenn Research Center
21000 Brookpark Road, MS:106/5
Cleveland OH 44135

Robert H. Licht
Norton Company
Saint Gobain Industrial Ceramics
1 Goddard Road
Northboro MA 01532-1545

E. Lilley
Norton Company
Saint Gobain Industrial Ceramics
1 Goddard Road
Northboro MA 01532-1545

B. J. McEntire
Applied Materials Corporation
3050 Bowers Avenue
Santa Clara, CA 95054

James McLaughlin
Sundstrand Power Systems
4400 Ruffin Road
P.O. Box 85757
San Diego CA 92186-5757

Biljana Mikijelj
Ceradyne, Inc.
3169 Red Hill Avenue
Costa Mesa CA 92626

Carl E. Miller
Delphi Energy & Engine Mgmt. Systems
4800 S. Saginaw Street, MC 485-301-150
P. O. Box 1360
Flint MI 48501-1360

Malcolm Naylor
Cummins Engine Company, Inc.
P.O. Box 3005, Mail Code 50183
Columbus IN 47202-3005

Dale E. Niesz
Ceramic & Materials Engineering
607 Taylor Road, Rm. 204
Piscataway, NJ 08854-8065

Thomas J. Paglia
Coors/ACI
3315 Boone Road
Benton AR 72015

Richard Palicka
CERCOM, Inc.
1960 Watson Way
Vista CA 92083

Vijay M. Parthasarathy
Solar Turbines
2200 Pacific Highway, M.Z. R-1
San Diego CA 92186

Magan Patel
Cummins Engine Company, Inc.
Mail Code 50183
Box 3005
Columbus IN 47202-3005

James W. Patten
 Battelle
 Vehicle and Emissions Systems
 Org. 7749, Rm. 11-4-04
 505 King Avenue
 Columbus, OH 43201-2693

Joe Picone
 Norton Company
 1 New Bond Street
 Box 15008
 Worcester MA 01615-0008

Stephen C. Pred
 Pred Materials International, Inc.
 60 East 42nd Street, Suite 1456
 New York NY 10165

Vimal K. Pujari
 Norton Company
 Saint Gobain Industrial Ceramics
 1 Goddard Road
 Northboro MA 01532-1545

Fred Quan
 Corning Inc.
 Sullivan Park, FR-2-8
 Corning NY 14831

George Quinn
 NIST
 I-270 & Clopper Road
 Ceramics Division, Bldg. 223
 Gaithersburg MD 20899

Mike Readey
 Caterpillar, Inc.
 Technical Center, Bldg. E
 P.O. Box 1875
 Peoria IL 61656-1875

Jack A. Rubin
 CERCOM, Inc.
 1960 Watson Way
 Vista CA 92083

Robert J. Russell
 Riverdale Consulting, Inc.
 24 Micah Hamlin Road
 Centerville MA 02632-2107

J. Sankar
 North Carolina A&T State Univ.
 Dept. of Mechanical Engineering
 Greensboro NC 27406

Maxine L. Savitz
 General Manager, Technology/Partnerships
 Honeywell
 2525 West 190th Street, MS:1/5-2
 Torrance CA 90504

Jim Schienle
 Honeywell
 1130 West Warner Road
 M/S 1231-K
 Tempe AZ 85284

Gary Schnittgrund
 Transfer Technology
 16401 Knollwood Drive
 Granada Hills CA 91344

Robert S. Shane
 Shane Associates
 1904 NW 22nd Street
 Stuart FL 34994-9270

Subu Shanmugham
 MicroCoating Technologies
 3901 Green Industrial Way
 Chamblee GA 30341-1913

Albert J. Shih
 North Carolina State University
 Mechanical & Aerospace Engineering
 2217 Broughton Hall, Box 7910
 Raleigh NC 27695

Charles Spuckler
 NASA Glenn Research Center
 21000 Brookpark Road, MS: 5-11
 Cleveland OH 44135-3127

Gordon L. Starr
Cummins Engine Company, Inc.
P.O. Box 3005, Mail Code:50182
Columbus IN 47202-3005

Marian Swirsky
Cambridge Scientific Abstract
Commerce Park, Bldg. 4, Suite 804
23200 Chagrin Blvd.
Beachwood OH 44122

Victor J. Tennery
113 Newell Lane
Oak Ridge TN 37830

Malcolm Thomas
Allison Engine Company
P. O. Box 420 (W06)
Indianapolis IN 46206

Marc Tricard
Norton Company
Superabrasives Division
1 New Bond Street, MS-412-301
P. O. Box 15008
Worcester MA 01615-0008

Marcel H. Van De Voorde
Commission of the European Union
Eeuwigelaan 33
1861 CL Bergen
THE NETHERLANDS

Robert M. Washburn
ASMT
11203 Colima Road
Whittier CA 90604

R. W. Weeks
Argonne National Laboratory
Bldg. 362, E313
9700 S. Cass Avenue
Argonne IL 60439

Sheldon M. Wiederhorn
NIST
Building 223, Room B309
Gaithersburg MD 20899

Matthew F. Winkler
Seaworthy Systems, Inc.
P.O. Box 965
Essex CT 06426

Thomas J. Wissing
Eaton Corporation
26201 Northwestern Highway
P.O. Box 766
Southfield MI 48037

James C. Withers
MER Corporation
7960 S. Kolb Road
Tucson AZ 85706

Dale E. Wittmer
Southern Illinois University
Mechanical Engineering Dept.
Carbondale IL 62901

Egon E. Wolff
Caterpillar Inc.
Technical Center
P.O. Box 1875
Peoria IL 61656-1875

Roy Yamamoto
Ethyl Petroleum Additives, Inc.
500 Spring Street
P. O. Box 2158
Richmond VA 23218-2158

R. L. Yeckley
Kennametal, Inc.
P.O. Box 231
Latrobe, PA 15650

Thomas M. Yonushonis
Cummins Engine Company, Inc.
1900 McKinley Avenue
P.O. Box 3005, Mail Code 50183
Columbus IN 47202-3005

S. Charles Yoon
Cincinnati Milacron, Inc.
P.O. Box 9013
3000 Disney Street
Cincinnati OH 45209-9013

Jong Yung
Sundstrand Aerospace
Dept. 789-6
4747 Harrison Avenue
Rockford IL 61125

Zhenqi Zhu
Stevens Institute of Technology
Department of Mechanical Engineering
Castle Point on Hudson
Hoboken NJ 07030

Department of Energy
Oak Ridge Operations Office
Assistant Manager for Energy
Research and Development
P. O. Box 2001
Oak Ridge TN 37831-8600

For distribution by microfiche
as shown in DOE/OSTI-4500,
Distribution Category UC-332
(Ceramics/Advanced Materials).

